Doctoral Dissertation
Doctoral Program in Metrology (XXXVII cycle)

Accurate Characterization and Modeling of Electric Double-Layer Supercapacitors

By

Melika Hassanzadeh

******

Supervisor:

Dr. Mauro Zucca

INRIM - Istituto Nazionale di Ricerca Metrologica

Doctoral Examination Committee:
Prof. Carlo RAGUSA, Politecnico di Torino
Prof. Vincenzo CIRIMELE , Università di Bologna
Prof. Andrea MARISCOTTI , Università di Genova

Politecnico di Torino
2025

Declaration

I hereby declare that the contents and organization of this dissertation constitute my own original work and does not compromise in any way the rights of third parties, including those relating to the security of personal data.

Melika Hassanzadeh

2025

* This dissertation is presented in partial fulfillment of the requirements for **Ph.D. degree** in the Doctoral School of Politecnico di Torino (ScuDo).

I would like to dedicate this thesis to

my wonderful parents, ***Shahnaz*** *and* ***Parviz****, whose unwavering support has been my guiding light, and I can never fully repay their love and sacrifices,*

my beloved brothers, ***Milad*** *and* ***Moein****, for always standing by my side,*

and the purest loves of my life, ***Panah*** *and* ***Adrian****.*

You may be far from my sight, but you are always closest to my heart.

I share this milestone with you with all my love and gratitude.

Acknowledgment

First and foremost, I would like to express my unlimited gratitude to my supervisor, Dr. Mauro Zucca. His invaluable guidance, professionalism, and support have been pivotal throughout my research journey. I am beyond thankful for his valuable advice, constructive feedback, and continuous motivation, which have shaped both my academic and personal growth.

I am also deeply grateful to Dr. Umberto Pogliano whose insightful scientific suggestions and expertise have significantly contributed to the development of this work, and I truly appreciate his support.

A heartfelt thanks to Dr. Gabriella Crotti and Dr. Domenico Giordano at INRiM for their warm presence and kind words that always brightened my days. Their thoughtful messages meant more to me than words can express.

I would also like to extend my sincere appreciation to the reviewers of this thesis for their valuable time and thoughtful comments.

I am deeply appreciative of my dear family, friends and colleagues who have been part of this journey, offering companionship, collaboration, and encouragement along the way.

This thesis is a reflection of all the support I have received, and I am truly grateful to everyone who has been part of this experience.

Abstract

This thesis concerns the characterization of supercapacitors (SCs), with particular reference to Electric Double-Layer Capacitors (EDLCs). These components have gained significant attention as high-power energy storage devices due to their quick charge-discharge cycles, long cycle life, and high efficiency. These characteristics make them interesting for applications such as power electronics, renewable energy systems, hybrid and electric vehicles.

SCs have a reputation for being a device whose parameters have low repeatability and low reproducibility and so they are considered like unstable components, and difficult to be characterized, where the few parameters provided by manufacturers are affected by a very large uncertainty. On the other hand, when SCs can work in synergy with batteries, for instance smoothing out peaks in power demand like in braking and acceleration in e-mobility, a rather accurate model of the SC parameters is required by the charge control, to work efficiently and safely with batteries.

This thesis aimed to contribute to some aspects of SC characterization and model identification, and the work is organized as follows.

Chapter 1 discusses the SC as a component, including definitions of main quantities, such as capacitance, equivalent series resistance, specific power, and so on. Then a brief history of technology and the general characteristics and the three main families of SCs, are described. We then move to an analysis of SCs essential components such as current collectors, electrodes, electrolytes and separators, by providing an idea of the extensive research in progress, especially on electrode materials, which largely determine the characteristics of the device.

In Chapter 2, a review of existing measurement techniques and international standards governing SCs characterization are presented, highlighting their limitations in providing accurate and repeatable parameter estimation. The analysis focuses on time-domain measurement methods, because these methods are considered by international standards and offer direct insights into the static and

dynamic behavior of EDLCs in the laboratory and under real operating conditions. This thesis work has contributed to introducing an original technique for the measurement of leakage resistance, which allows to determine the behavior of the SC over a long-time span, even days.

Chapter 3 focuses on the measurement repeatability. No measurement has meaning if it is not repeatable, and this depends both on the method, on the measurement instrumentation and on the device under test. In this case the SC is not a repeatable device, but it becomes so if adequate preliminary training is carried out. Repeatability is maintained even after days, and training must be repeated when the SC is left in long phases (weeks) of standby.

Chapter 4 discusses the modeling of the time behavior of a SC. A simple RC circuit is not so accurate for simulating the behavior of the SCs in an electronic system but a multi branch model is needed. In this thesis the three-branch model has been chosen as a compromise between simplicity and accuracy, also introducing the original non-linear leakage resistance identified in Chapter 2. This thesis also contributed to a new method for the accurate identification of the circuit parameters from the measurements, based on state equations and on optimization, which improves the matching between measurements and model over long periods.

Finally, Chapter 5 provides a new general method for the uncertainty assessment of SC equivalent circuit parameters, and here it is applied to a three-branch equivalent circuit.

In summary, this thesis work shows how SC measurements can have good repeatability and limited measurement uncertainties. Moreover, this work highlights how the proposed modified three branch equivalent circuit model, together with the proposed identification procedure, results to be a very good tool for the SC simulation and control. Finally, a new method for the measurement of the non-linear leakage resistance and another new method providing the estimate of the equivalent circuit parameters uncertainty is also proposed in this thesis.

List of Contents

List of Figures

List of Tables

List of Abbreviations

Abbreviation	Meaning
2QCG	Two Quadrant Current Generator
AC	Activated Carbon
BMS	Battery Management System
CMS	Charge Management System
CV	Cyclic Voltammetry
CNT	Carbon Nano Tube
DUT	Device Under Test
DoD	Depth of Discharge
ESR	Equivalent Series Resistance
ECM	Equivalent Circuit Models
EDLC	Electric Double Layer Capacitor
EIS	Electrochemical Impedance Spectroscopy
GO	Graphene Oxide
GCD	Galvanostatic Charging-Discharging
GCSD	Galvanostatic Charging-Self Discharging
RGO	Reduced Graphene Oxide
SC	Supercapacitor
SoC	State of Charge
SMS	Supercapacitor Management System
SoH	State of Health

Preamble

Metrology is very important when it comes to supercapacitors (SCs) for several strong reasons. Firstly, it guarantees the accurate characterization of SCs, enabling researchers and engineers to gain a thorough understanding of their functionality both in laboratory and operating conditions.

Secondly, metrology makes sure that measurements are traceable to the International System of Units (SI), which is the benchmark for measurement. In SC measurements, this traceability ensures consistency and comparability, which is essential for manufacturing, research, and regulatory compliance. Standardized and uniform procedures can be implemented in many laboratories and organizations thanks to SI-traceable measurements.

Thirdly, accurate SC models are needed to fully explain the behavior of SCs. On the other hand, the models require accurate measurements in order to be identified. Models are crucial for predicting and simulating the behavior of SCs in a variety of applications. Accurate models reduce the need for expensive trial-and-error methods in system design and optimization.

Thus, metrology is essential for the advancement of SC technology, standardization, and ensuring successful application of SC technology in many different fields.

Most of the research and tests performed and reported in this Ph.D thesis are done in the framework of the following two European projects.

1. The research project EMPHASIS "Efficient Materials and Processes for High Energy Supercapacitors for Smart Textiles and Electromobility Applications." Financed by the European Union in the Horizon Europe Research and Innovation Programme, grant number 101091997. The project started in January 2023 and is a three-year project. It is coordinated by Pleione Energy S.A and 14 partners from 6 different European countries are participating in this project. EMPHASIS's primary goals are to:
   - Create innovative and environmentally friendly materials for SCs;

- Enhance design procedures and develop energy storage solution design architectures;
- Offer applicable solutions for safe SC devices with high energy and power densities;
- Accelerate the shift to a new energy system that is climate neutral;
- Create consumer-focused next-generation SCs, like smart clothing and electromobility;
- Create high-performance energy storage systems with renewable materials and in accordance with circular economy guidelines;
- Achieve the economic and technical goals outlined in the European Commission's 2030 SET plan.

2. The 23IND04 MetSuperCap project: "Metrology for Static and Dynamic Characterization of Supercapacitors" is a three-year project which started in June 2024 and received funding from European Partnership on Metrology, co-financed from the Horizon Europe program and by the participating states. This project is coordinated by INRIM and has 12 partners from 7 European countries. The following goals have been established by the MetSuperCap project to create a traceable, reliable, and consistent measurement and characterization framework for SCs and SC banks/modules [1], [2].
   - Traceable characterization of SCs and SC banks;
   - To create software models with targeted error below 5 %, in static and dynamic conditions;
   - To define and test fast and accurate techniques for the determination of state of health (*SoH*) and state of charge (*SoC*) of SCs;
   - To create and produce two test benches fitted with the measurement systems for tracking the behavior of SCs and banks under real operating conditions;
   - To facilitate the take up of the measurement infrastructure and technology.

Chapter 1

Introduction

1.1 An introduction to supercapacitor technology

An amount of about $617 \cdot 10^{15}$ J (estimated in 2019 [3]) energy is produced everyday worldwide mainly using fossil-sourced methods and renewable- sourced methods such as wind turbines and solar panels which are more sustainable technologies. To increase the share of renewables a crucial issue to be addressed is the capability of storing energy: batteries represent the main device for this purpose, but supercapacitors (SC) are also interesting since they are faster in terms of charging and discharging times and can be interesting in storage systems and other applications (e.g. grid stability [3]- [5]).

SCs are like a bridge between conventional capacitors and batteries and are another way of storing energy. The main limit of such devices is their low energy density (up to 10 Wh/kg for electric double layer and up to 100 Wh/kg for pseudo and hybrid SCs), which is from 2 to 10 times lower than lithium-ion (Li-ion) batteries (in the range of 200 -1000 Wh/kg). On the other hand, SCs can charge and discharge faster due to the lower internal resistance. The specific energy of SC, like the one of Li-ion batteries, is constantly increasing [4]. The interesting feature of SCs is the higher power density (in the range of 2,000 - 10,000 W/kg), while Li-ion batteries have lower power density (in the range of 50 -200 W/kg). For both devices the research target is to obtain higher energy density and higher power density at the same time [6].

With the advent of hybrid electric vehicles and the quickly expanding market for portable electronic gadgets, there has been an urgent need for ecologically responsible high-power energy sources. Owing to its pulse power supply, long cycle life, and high charge propagation dynamic, SCs have received increasing attention [7].

SCs have some characteristics and parameters which make them different from other storage devices and these parameters should be considered when choosing the appropriate storage system for an application. Some of the main characteristics of SCs and their definitions are as follows.

- **Capacitance and specific capacitance**

SCs capacitance, in farads (F), is a measure of their capacity to hold electric charge. SCs, in contrast to normal capacitors, have a narrow double-layer separation at the electrode-electrolyte interface and high-surface-area electrodes, which allow them to attain very high capacitance values (up to thousands of farads). The capacitance is influenced by the distance between the electrolyte ions and electrode surface, the pore structure, and the electrode surface area.

In electric double layer capacitors (EDLCs) (see Sect. 1.4.1), two porous electrodes are electrically connected with an ionic liquid called electrolyte. When a voltage is applied to EDLCs the negative ions from the electrolyte move towards the positive electrode and similarly the positive ions from the electrolyte are attracted by the negative electrode. As it is making additional layers on the electrodes, it is automatically reducing the distance between the anode and cathode. On the other hand, considering the basic two plates model, the capacitance in both conventional capacitors and SCs is determined according to Eq. (1.1) as follows.

$$C = \frac{\varepsilon A}{d} \tag{1.1}$$

where C is the capacitance in farads (F), ε is the permittivity of the electrolyte (dielectric in conventional capacitors), A is the surface area of the electrodes in square meters (m^2), and d is the distance between the electrodes in meters (m).

According to Eq. (1.1), one can conclude that with higher values of ε, A and lower values of d, the higher values for capacitance can be achieved. In SCs all these three conditions are verified, in comparison to conventional capacitors. These three conditions are achieved by: larger surface area of the electrodes because of their porous materials, higher permittivity of the electrolyte materials than dielectrics, and lower distance between charges in electrode surface and electrolyte ions in comparison to the distance between two electrodes in conventional capacitors.

The measurement techniques, procedures and the equations for computing the capacitance of SC with each measurement technique are described in Chapter 2 and also in Appendix A.

The term "specific capacitance" is also a common term which is defined as capacitance per unit mass (or sometimes per unit area or volume). Specific capacitance defines how well the electrode materials can store charge per their unit mass. So, the electrode material with higher specific capacitance, can lead to a more compact and a lighter SC. Hence, specific capacitance is very important in applications that the portability and low weight of SC is in higher priority (like portable electronic devices, and smart clothing). In Eq. (1.2), the $C_{sp}$is specific capacitance (F/g), C is the capacitance (F), and m is the mass of SC (g).

$$C_{sp} = \frac{C}{m} \tag{1.2}$$

- **Internal resistance**

The internal resistance of a SC that prevents current flow is known as Equivalent Series Resistance (*ESR*). This parameter is not a physical resistor, but a resistance defined in the modeling to represent the real physical phenomena that happens in a SC. Such a phenomenon is determined basically by the effect opposed to the passage of electrical current by electrodes (electrode resistance) and by the ability of the electrolyte to promote the movement of the ions (electrolyte conductance). The sudden voltage drop which happens in SCs after an electrical current is injected is due to this *ESR* [8]. This voltage drop in the physical structure of the SC, besides electrode materials and electrolyte, is due to the contact resistance between internal components (for example the contact between electrodes and current collectors).

The quality of the connections to the cell terminals, temperature, state of charge, and electrochemical aging are some of the factors that affect this internal resistance, which is in the order of mΩ. This parameter's measurement is crucial for two reasons: first, a voltage drop brought on by ohmic phenomena in SCs reduces energy efficiency [9], and second, to prevent overheating, the heat that has been dissipated needs to be eliminated [10]. The measurement technique, procedure, and the equation to compute this parameter is explained further in Chapter 2 and also in Appendix A Sect. A.1.4.

- **Self-discharge phenomena**

The self-discharge phenomena is an electrochemical process that causes the loss of certain amount of energy (or charge) within the cell during rest phases. A leakage current through the ion-conducting membrane that separates the two electrodes serves as a representation of this phenomena. SC voltage drop over time in long rest phase is a sign of the self-discharge process. It is among the primary drawbacks that prohibit the use of SCs for energy storage for long durations [11], [12]. In Chapters 2 and 3, our method to calculate the leakage resistance (R_{lea}) which represents this phenomenon in the SC model is explained in detail.

- **Power density**

SCs power density is the quantity of power that SCs can deliver per mass unit (W/kg). SCs are distinguished by their extraordinarily high-power densities (up to 10,000 W/kg). This characteristic makes them perfect for applications needing quick charge/discharge cycles, which enables them to transmit or absorb energy rapidly. On the other hand, batteries low power density, which means slow energy release makes them suitable for sustainable energy productions. *ESR*, electrode design, and electrolyte characteristics are some of the variables that affect power density of SCs [13], [14].

- **Energy density**

This parameter represents the amount of energy per unit mass that can be stored in a storage system. Normal capacitors have low energy densities because of the straightforward physical separation of charge. In contrast, SCs have a moderate energy density, which is more than that of typical capacitors (0.1–10 Wh/kg). Batteries have a high energy density (usually 200-1000 Wh/kg), because chemical energy is transformed into electrical energy [13].

- **Charge/discharge time**

When a SC is powered by a voltage source, the charge time is the amount of time in seconds that it takes for its terminals to reach their nominal voltage value starting from zero volt. The time it takes for a fully charged SC to be discharged to zero volts is known as the discharge time. Charge and discharge times for SCs are typically relatively quick, ranging from a few seconds to a few minutes [15].

- **Voltage limit**

Single SCs function at low voltages (usually between 2.7 and 5 volts) and they must be coupled in series to achieve greater voltages. Higher voltages can be supported by typical capacitors, but the energy they can store drops exponentially with voltage. Batteries can run at a variety of voltages, depending on their chemical composition (3.7 V for Li-ion cells, for example).

- **State of Charge (*SoC*)**

A SCs State of Charge (*SoC*) is a measurement of the charge or energy that is accessible in SC with respect to its maximum capacity, given in percentage [16]. It shows what proportion of a cell's capacitance is still unused. A cell is considered fully charged when its *SoC* is 100 % and totally drained when the *SoC* is 0 %. Several conditions, including discharge/charge cycles and temperature can affect the *SoC*, which is a crucial parameter that the SC Management Systems (SMS) need to know to manage a SC module [17]. Therefore, to regulate overcharging or over-discharging of SCs, the *SoC* needs to be predicted using an accurate estimation algorithm. According to [16], the equation for computing the *SoC* of a SC is as follows. In Eq. (1.3), $C_{SC\_Residual}$ is the accessible charge of SC (F), and $C_{SC\_Nominal}$ is the cell's nominal capacitance (F).

$$SoC = \frac{C_{SC\_Residual}}{C_{SC\_Nominal}} 100 \tag{1.3}$$

- **Depth of Discharge (*DoD*)**

The percentage of the capacity that has been discharged with respect to the maximum capacity of SC is known as the Depth of Discharge (*DoD*) which serves as the amount of energy that has been used and can be calculated as Eq. (1.4) in which $E_{discharge}$, is the used or discharged energy during operation (Wh) and E_{total} is the total energy that can be stored in SC when it is fully charged (Wh).

$$DoD = \frac{E_{discharge}}{E_{total}} 100 \tag{1.4}$$

Since the sum of the *SoC* and *DoD* values equals the percentage of the total cell capacitance (100 %), Its value can also be computed using the Eq. (1.5) as follows.

$$DoD = 1 - SoC \quad (1.5)$$

For instance, the *DoD* is 70 %, if a SC discharges 70 % of its capacity. Managing the *DoD* is essential, because greater *DoD* levels can lead to quicker aging and a shorter lifetime.

- **State of Health (*SoH*)**

A SC's overall health and remaining lifespan with respect to its initial performance are measured by its State of Health (*SoH*). Usually, it is stated as a percentage, where a new SC's *SoH* is represented 100 %. *DoD*, operating conditions and temperature, and cycling voltage are some of the factors that can cause *SoH* to deteriorate with time [18]. *SoH* is indicated by a degradation of capacitance or an increase in *ESR*. Keeping an eye on *SoH* makes it easier to forecast when a SC needs to be changed since it is no longer meeting performance standards.

In the literature, the methods to estimate *SoH* are based on the degradation model [19], differential voltage analysis [20], and incremental capacitance analysis. *SoH*, can be expressed as Eq. (1.6) based on capacitance degradation. In Eq. (1.6), $C_{current}$ is the measured nominal capacitance of SC after aging (F), and $C_{initial}$ is the initial nominal capacitance of the SC when it is new (F).

$$SoH = \frac{C_{current}}{C_{initial}} 100 \quad (1.6)$$

- **Aging**

SC aging is a parameter to determine the lifetime of SC and is studied in two categories:

1) "Cyclic aging" which is the aging of SC caused by the number of charging/discharging over time. The more it is used, the more aging effects can be seen.
2) "Calendar aging" which refers to the aging that happens when SC is not in use.

Exceeding the limit values of temperature, humidity, charge/discharge current, voltage, can accelerate the aging of SC [21], [22]. *SoH* allows the estimation of the ending life of SC, and it decreases with aging. Aging in SC causes the decrease in the capacitance value and increase in the *ESR* value over time. By the manufacturers, the SC is considered as defective when the *ESR* reaches to the

double of its initial value, or the capacitance reaches 80 % of its initial value or less. These values can vary depending on the application [23].

- **Cycle life**

This parameter represents the number of cycles that a SC can be charged and discharged in its standard lifetime. Aging, the impact of *DoD*, and temperature are some of the many variables that affect this metric. SCs can have a cycle life up to some millions of cycles, which is a very long duration [15].

- **Energy efficiency**

In the same cycle of SC, the ratio of the energy delivered at discharging phase ($Q_{SC\_Discharge}\ in\ Eq.(1.7)$) to the energy supplied during charging phase ($Q_{SC\_Charge}\ in\ Eq.(1.7)$) is known as the SC's energy efficiency, given as a percentage and can be expressed as Eq. (1.7).

$$\eta_E = \frac{Q_{SC\_Discharge}}{Q_{SC\_Charge}} 100 \tag{1.7}$$

Depending on the working conditions, SCs can have energy efficiency up to 98 %. *ESR*, current rates, and temperature are some of the variables that affect efficiency. Efficiency decreases by higher resistive losses caused by higher charge/discharge currents. SCs, as opposed to batteries, can withstand quick cycles of charging and discharging with little energy loss. This great efficiency makes them appropriate for applications needing rapid energy storage and release, particularly in high power and short duration applications [24].

Table 1.1 shows a short comparison between conventional capacitors, SCs, and batteries in terms of the energy storage mechanism, composition, capacitance value, rated voltage, cycle life, energy density, power density, leakage current, charge-discharge time.

Table 1.1. Comparison between capacitors, SCs, and batteries.

	Capacitor	SC	Battery
Energy storage mechanism	electrostatic	electrostatic and electrochemical	electrochemical
Composition	dielectric	electrolyte	chemicals
Capacitance	up to some mF	up to some thousand F	μF to mF
Lifetime (cycle)	millions of cycles	500,000 to 1 million	50-2000
Rated voltage	up to kV	< 5 V	up to tens of volts
Energy density (Wh/kg)	0.1-10	1-100	200-1000
Power density (W/kg)	10,000-100,000	2000-10,000	50-200
Charge/discharge duration	seconds	seconds to tens of minutes	minutes to hours
Leakage current	negligible	high	negligible

1.2 When SCs appeared on the market

Electric double-layer SCs are the most common type of SCs in the market. The concept of storing electrical energy in the electric double layer that is formed at the interface between an electrolyte and a solid has been known since the late 1800s.

In 1966, the US company Standard Oil of Ohio (SOHIO) accidentally discovered the double-layer capacitor while working on fuel cells, but it wasn't until the late 1970's that the Japanese company, NEC, began commercially offering the first SC (NEC's Supercapacitor TM), under license from SOHIO [4], [5]. In 1975, a first SC was created by General Electric, but there were not any known commercial applications. Initially they were used as backup power devices for volatile clock chips and complementary metal-oxide-semiconductor (CMOS) computer memories. Many other applications have emerged over the past 40 years, including wireless communication, power quality, and improved energy efficiency via regenerative energy capture processes, for instance in hybrid electric vehicles. Overall, the unique attributes of SCs often complement the limitations of other power sources like batteries and fuel cells [6], [25].

Early SCs were rated at a few volts and had capacitance values measured from fractions of farads up to several farads. The trend today is for cells ranging in size from small millifarad-size devices with exceptional pulse power performance up to devices rated at some thousand farads [26]. Technology is experiencing increasingly broader use, both replacing batteries in some cases, and in others complementing their performance.

1.3 SCs application and why their diffusion is desirable

Advanced energy storage technologies are now more important than ever with the continued integration of renewable energy sources. While conventional electrochemical batteries have traditionally been the foundation of energy storage, their low power density, slow charging rates, and shorter lifespan have sparked the investigation of alternate options. The SC, which has many benefits over traditional batteries, is one such promising technology [27].

As energy storage devices, SCs fill the gap between batteries and conventional capacitors. When needed, they can supply immediate bursts of energy thanks to their quick storage and power delivery. SCs also have exceptional cycle stability, which allows for a far longer lifespan than conventional batteries [28].

The potential of SCs to improve the integration and exploitation of renewable energy sources, such as solar and wind power, is a major element influencing the necessity of using SCs. These sources are unstable and erratic by nature, which poses problems for the stability and dependability of the grid. SCs can be used in conjunction with renewable energy systems to store extra energy during times of high production and discharge it during times of high demand, reducing intermittent use of batteries and assuring a steady and reliable power generation [29]- [33].

SCs can also play an important role in meeting the growing demand for electric and hybrid vehicles (HEVs), which are on the rise. SCs give electric vehicles a distinct edge by enabling quick charging and discharging cycles, improving the effectiveness of regenerative braking, raising overall performance and complementing batteries by improving their life and shaving power demand and release peaks [34].

The potential of SCs to transform portable electronics and energy harvesting devices is a significant factor driving the demand for SCs. Compact, lightweight, and long-lasting energy storage solutions are becoming more and more in demand as wireless sensors, wearable technology, and Internet of Things (IoT) applications proliferate. SCs with their high-power density can be perfect choices for applications demanding short energy bursts and long operational lifetimes [35].

SCs have a wider temperature range than batteries. While the temperature range for SCs is almost -40° to +85° degrees celsius, this range for batteries is almost -5° to +55° degrees celsius, so preheating techniques are adopted at winter temperatures and cooling techniques during summer. Batteries' safety is highly

dependent on their internal temperature stability. If the temperature inside the battery reaches its limits(either the positive temperature limit or the negative temperature limit), some chemical reactions can occur which create heat, and the resulting higher temperature causes further chemical reactions and produce more heat, and this chain can continue up to destroying the battery or in worse cases exploding by igniting the fire (reaching up to 400 degrees) and gas release. This phenomenon is called “thermal runaway” and can occur in milliseconds [5]. In SCs, on the other hand, the energy is produced electrostatically in electric double layer capacitors (EDLCs) and in pseudocapacitors the faradaic redox reaction takes place at the electrode surface which minimizes the heat generation, also the low internal resistance of SCs helps to have lower heat production in comparison to batteries which eliminate the risk of thermal runaway in SCs. So, from this point of view, SCs are safer than batteries.

As a result, due to their distinct characteristics and inherent advantages over ordinary batteries, the integration of SCs within modern energy systems is of vital importance. SCs are also used in various applications ranging from uninterrupted power supplies (UPSs), cordless screwdrivers, hybrid vehicles requiring stop-and-go driving, buses, trains, agricultural machinery, excavators, cranes, and forklifts, as well as digital cameras that can be used as spotlights. Fast EV charging, sensor networks, flexible and wearable SCs, robotic powering, integrated systems for renewable energy and energy devices, eviction sliding operation (like as in the Airbus A380 airplane) [29]- [36], and other possible applications, SCs can transform the energy industry and open the door for a robust and sustainable future through additional research and development.

1.4 Types of SCs and their energy storage mechanisms

Optimizing the performance of energy storage devices, such as SCs and batteries, requires a thorough understanding of the charge storage mechanism. It makes it possible for scientists to design these devices more efficiently and improve electrode composition, which increases cycle life, power density, energy density, and overall performance of the device.

Gaining insights into the charge storage mechanism provides a deep understanding of the fundamental principles governing energy storage systems. This knowledge serves as a foundation for future research endeavors, facilitating the exploration of innovative materials, new electrode architectures, and the investigation of emerging energy storage technologies.

1.4 Types of SCs and their energy storage mechanisms

Based on their storage mechanism, SCs can be divided into three primary categories: electrochemical double-layer capacitors (EDLCs), pseudocapacitors, and hybrid SCs. Each category and its storage mechanism will be covered in detail in this section.

1.4.1 Electric Double Layer Capacitors (EDLCs)

Among three different types of SCs in terms of storage mechanism, the most common type is the Electric Double Layer Capacitor (EDLC). The core of EDLC is made of two porous electrodes submerged in an electrolyte. These SCs can store energy electrostatically or via non-faradaic process [37], which involves no transfer of charge between electrode and the electrolyte, it means the electrolyte is not absorbed by the electrode material in these SCs (which happens in faradaic storage mechanism) and when a voltage is applied across the electrodes of these SCs, the electrolyte ions moves towards the electrode with opposite polarity. This creates two layers of charged ions forms between the electrode material and the electrolyte. The Helmholtz layer, where strongly bound ions stick to the electrode surface, and the diffuse layer, where less tightly bound ions extend into the electrolyte are the two regions that make up this double layer. The creation of an electric field because of the charge separation at this double layer allows energy to be stored as electrostatic potential [38].
With the creation of this double layer, the distance between the electrode surface and electrolyte ions is about a few nanometers and much less than the distance between the two electrodes in conventional capacitors which leads to having much higher capacitance and energy density in these SCs. However, compared to batteries this is still quite low [7]. The most common applications of EDLCs are backup power systems, energy management, and regenerative braking systems.

1.4.2 Pseudocapacitors

The second type of SCs are called pseudocapacitors. The difference between EDLC and a pseudocapacitor lies in their materials and thus their energy storage mechanism. Electrode materials used in pseudocapacitors (usually metal oxides or conductive polymers) are capable of quick and reversible redox reactions. Like how ions are stored in the electrodes of batteries, these materials can store and release charges by directly allowing ions from the electrolyte into their structure. The oxidation state of the electrode material changes because of the creation and dissolution of surface-bound species [36]. So, the electrode-electrolyte interface of

pseudocapacitors features reversible faradaic redox processes that serve as an energy storage mechanism [39].

In contrast to EDLCs, which primarily store energy through the physical separation of charges at the double layer, pseudocapacitors' energy storage mechanism is essentially based on electrochemical processes [37]. Pseudocapacitors have higher energy densities than EDLCs (up to 10 times higher) and due to the slower kinetics of redox processes compared to the quick charge-discharge cycles of EDLCs, they might have slightly lower power densities, but they still keep the quick charge-discharge characteristics of SCs with respect to batteries which make them suitable for a variety of applications. They combine the benefits of capacitors and batteries [37], [40]. The choice of electrode material, the composition of the electrolyte, and the design of the device all have an impact on the overall performance of this type of SCs [37]. These types of SCs are used mainly in hybrid electric vehicles (HEVs), and portable electronic devices.

1.4.3 Hybrid SCs

The third type of SCs are the hybrid SCs, which aim to provide improved performance characteristics by utilizing the benefits and reducing the drawbacks of EDLCs and pseudocapacitors. Graphene and other carbon-based materials, such as conducting polymers or metal oxides, can be combined with other kinds of materials to create hybrid materials, which are used as SC electrodes. These hybrids make multifunctional electrode structures that enhance charge storage mechanisms, electrical conductivity, and overall energy storage performance by utilizing the beneficial characteristics of each material type [41]. One electrode in these SCs functions as an electrostatic (EDLC) and the other as a faradaic (pseudocapacitor), for this reason these SCs are also called asymmetric. The combination of EDLC and pseudocapacitor storage mechanisms together leads to overshadowing of the limitations of the combining components and they can achieve energy and power densities higher than EDLCs and pseudocapacitors without sacrificing cycling stability or affordability, which has hindered the popularity of pseudocapacitors.[3]. Hybrid SCs have a greater lifespan than batteries, but a shorter lifespan than EDLCs. These SCs are generally employed in backup power systems, power grid balancing, high energy demanding applications, renewable energy storage, and electric vehicles.

SCs with hybrid materials are divided into three categories as follows [41].

- Asymmetric hybrids

1.4 Types of SCs and their energy storage mechanisms

- Battery-type hybrids
- Composite hybrids

1.4.3.1 Asymmetric hybrids

Asymmetric hybrids SCs integrate processes that are both faradaic and non-faradaic through coupling a pseudocapacitive electrode to an EDLC electrode [41], [42]. Generally, carbon-based materials are utilized as the negative electrode while certain pseudocapacitive materials are used as the positive electrode [41], [43].

1.4.3.2 Battery-type hybrids

The two different electrodes coupled in battery-type hybrids, are SC electrode and battery electrode. This setup combines the energy characteristics of batteries with power, cycle life, and recharge durations of SCs to imitate the need for better energy SCs and higher power batteries [41].

Although the few available experimental data shows that these hybrids could potentially fill the gap between batteries and SCs, experts agree that further study is required to fully understand the potential of battery-type hybrids [44].

1.4.3.3 Composite hybrids

The main goal for using composite electrodes is to combine different electrode materials to be used in a single electrode. In this way, both chemical and physical charge storage mechanisms occur in one electrode.

In SC electrodes, composite materials combine different elements, such as metal oxides and carbon-based materials, to produce synergistic effects that improve the overall device performance. These materials take advantage of the distinctive qualities of each component, offering a balanced strategy that balances the advantages of various materials, resulting in improved SC performance [45].

On one hand, materials based on carbon promote a capacitive double layer of charge and offer a high surface area backbone that improves the interaction between the electrolyte and the deposited pseudocapacitive materials. On the other hand, the composite electrode's capacitance can be further increased by the pseudocapacitive materials via faradaic processes [46].

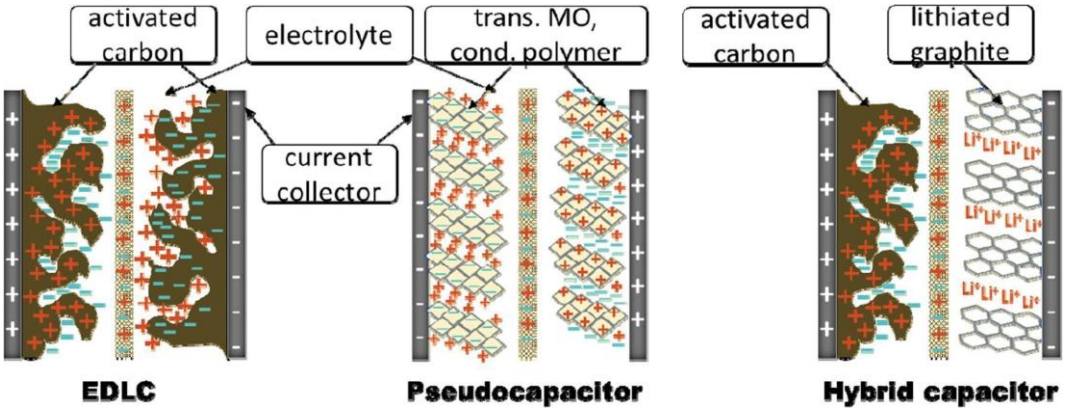

Figure 1.1 Schematic diagram of the storage mechanism of different types of SC [47].

Table 1.2. Advantages and disadvantages of different types of SCs.

	EDLCs	**Pseudocapacitors**	**Hybrid SCs**
Advantages	-Higher energy densities than conventional capacitors -No chemical or structural change during charge storage -Wide temperature window -Have high cycling stability -High dynamic	-Higher energy densities than EDLC -Can achieve extraordinary capacitances	- The most flexible performance characteristics of any SC, it fits the widest range of applications. -Can achieve very high energy and power densities without sacrificing in cycling stability and affordability
Disadvantages	-Can't match energy densities of mid-level batteries because of limited surface area and pore size distribution of conventional electrode materials.	-Lower power density than EDLC -lifetime can be limited by mechanical stress caused during reduction-oxidation reaction -The best metal-oxides electrodes are very expensive and require aqueous electrolytes, which means lower voltage -Average dynamic	-Relatively new and unproven technology. More research is needed to better understand the full potential of hybrid capacitors. -Slow dynamic

The charging mechanisms of EDLCs, pseudocapacitors and hybrid capacitors are illustrated in Fig 1.1, and in Table 1.2 the advantages and disadvantages of these three types of SCs are summarized.

1.5 SCs components and their materials

SCs consist of four core components, which together make the foundation of SC technology: current collectors, electrodes, electrolytes, separators [48]. These four elements can be seen in Fig. 1.2 and are briefly described in the following.

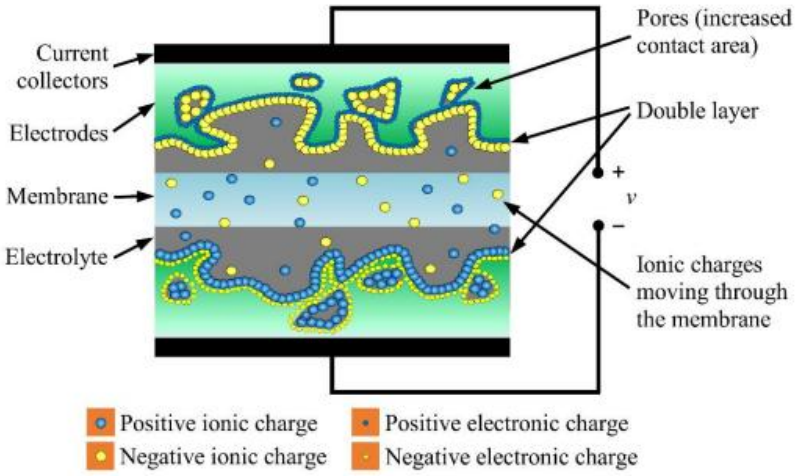

Figure 1.2. Schematic of a SC cell [49].

High power density of SCs requires both high electrical conductivity (thus a quick charge transit) of the electrode materials and the electrolyte solution, while high energy density is largely ensured using high-capacitance materials (high surface area or pseudo-active species). Since these two factors influence the final performance of the SC, optimizing the energy density without sacrificing their high-power density is one of the most important aspects in the development of SCs [50]. So, the materials utilized to build a SC, specifically the electrodes and electrolytes, have a significant impact on how well it performs. In short, for choosing the electrode materials the important factors to consider are long-term stability, high specific surface area, high electric conductivity, resistance to electrochemical oxidation/reduction, high temperature stability and for choosing the electrolyte materials, the most important factors are high ionic conductivity, low viscosity to

access small pores, chemical stability, easy availability and cost effectiveness [38]-[51].

To further enhance the performance of SCs, scientists have been investigating new electrode and electrolyte materials in recent years, and the ongoing development of nanostructured materials can help the advancement of SC technologies [50].

In this section, SCs core components and some of the materials used in electrodes and electrolytes are described.

1.5.1 Current collector

SCs current collectors are crucial parts that allow electrical current to flow to and from the electrode materials efficiently. In other words, the SC and external circuits are electrically connected by current collectors. These collectors, which are often made of conductive metals like copper, aluminum, or other appropriate metals, are attached to the electrode materials directly. They give the electrodes mechanical support and structural integrity in addition to improving the electrical conductivity inside the SC. The SC's high-power density and quick energy storage and release capabilities are largely dependent on the smooth operation of the charge and discharge processes, which are made possible by the current collectors [48].

1.5.2 Electrodes

Another SCs' essential component is the electrode, which is where the energy is stored and released in these high-performance electrochemical devices. Electrodes enable the quick charge and discharge of electrical energy by facilitating the adsorption and desorption of ions at the electrode-electrolyte interface. The electrochemical processes that take place during charge and discharge cycles depend heavily on the electrode material. The electrode material's porosity offers ions a large surface area to attach and detach from, which enhances the SC's effective electrical energy storage. The ion adsorption and desorption processes that control the energy storage capacity are significantly influenced by the specific surface area, pore size distribution, and electrical conductivity of the electrode material. To maximize the performance of SCs in a variety of applications, it is crucial to choose the suitable electrode material [52], [53].

In short, the materials used in the electrode of EDLCs are mostly activated carbons (AC), carbon nanotubes (CNT), graphene, and the materials used in the

electrodes of pseudocapacitors are mostly conductive polymers, metal oxides, conductive polymers, metal sulfides, mixed metal oxides, composite materials, and hybrid materials [54].

It's worth mentioning that there may be some overlaps because certain materials, such as conductive polymers, can exhibit both pseudocapacitive and EDLC behavior depending on their unique properties and how they are used in the electrode design [54].

In the following subsections, each of these materials and their mechanism in SCs are described.

1.5.2.1 Electrode material for EDLCs

Throughout the development of EDLCs, to achieve a satisfactory performance of the SC in terms of both power delivery rate and energy storage capacity, proper control over the specific surface area and the pore size adjusted to a suitable type of electrolyte solution is essential [47]. The most preferred electrodes are made of carbon-based materials, such as activated carbon (AC) and carbon nanotubes (CNTs), due to their physical and chemical characteristics. Low cost, a wide range of form (powders, fibers, aerogels, composites, sheets, monoliths, tubes, etc.), ease of processing, relatively innocuous electrochemistry, controlled porosity, and electro-catalytic active sites for a variety of redox reactions are some of these characteristics [55]. The carbon-based electrode materials of SCs can have three pore sizes which build their porous characteristic. The pore sizes are divided according to the size of the average diameter, as follow:

- micropores (less than 2 nm)
- mesopores (2 to 50 nm)
- macropores (more than 50 nm)

EDLC electrode materials should have a wide surface area for charge accumulation as well as an appropriate pore structure [3]. A combination of all three pore sizes is needed to have the best performance of the SC. Micropores by providing higher surface area makes possible to reach higher capacity for charge storage. Mesopores are suitable for providing fast ionic mobility and ion transport. Macropores facilitate electrolyte accessibility and ion transfer to mesopores and micropores, and therefore in the presence of macropores there is lower ionic resistance. Ionic mobility is hampered by irregular pore connection and blind or

isolated pores may not be wet by electrolytes, so besides pore size, pore structure also plays a role in SC performance [37].

1.5.2.1.1 Activated Carbons (ACs)

Activated carbons are frequently used in the electrodes of EDLCs. Due to its special characteristics. Through a procedure called activation, activated carbon is created from carbonaceous precursors like coconut shells, wood, peat, or other organic materials. The precursor material is heated to high temperatures while being surrounded by gases like steam or carbon dioxide during the activation process. This procedure results in the formation of a very porous structure with a large surface area and a great number of micropores and mesopores [56], [57].

Activated carbon is commonly employed as the active component in both the positive and negative electrodes of an EDLC. To help with the passage of charge, these electrodes are frequently deposited onto a conductive substrate, like a current collector composed of metal foil. Ions from the electrolyte are drawn to the charged surface of the activated carbon electrodes when a voltage is applied across the SC, creating the double layer of separated charges that stores electrical energy [58].

The resulting activated carbon material has several critical characteristics that make it a great option for SC electrodes, including:

- High surface area: the activated carbon's high specific surface area (around 1000-2000 $m^2 g^{-1}$) offers plenty of room for the adsorption of ions from the electrolyte [57], [59]. This raises the SC's total energy storage capacity by enabling a greater amount of charge to be held at the electrode-electrolyte interface.
- Pore structure: the activated carbon structure has micropores and mesopores, which improve ion accessibility and diffusion inside the electrode material. This enables speedy ion movement and effective charge storage, enabling quick charge-discharge cycles [60].
- Electrical conductivity: to enable the quick transfer of electrons between the electrode material and the external circuit, activated carbon must generally have strong electrical conductivity. Fast energy delivery and absorption are made possible by SC's high electrical conductivity [60].
- Chemical stability: since activated carbon is chemically stable, the charge-discharge cycles have little effect on its structure or other

characteristics. The SC's long-term dependability and cycling stability are guaranteed by this stability [60].

In summary, these characteristics of activated carbon when used as SCs' electrode material, result in high power density, rapid charge-discharge cycles, and excellent cycling stability.

1.5.2.1.2 Carbon nanotubes (CNT)

Carbon nanotubes (CNTs) are an example of a nanomaterial having remarkable mechanical, electrical, and thermal capabilities. CNTs have been investigated as a potential material for SC's electrodes in a few studies. The utilization of CNTs in SC's electrodes has demonstrated significant promise for enhancing the energy density, power density, and cycle life of SCs. Because of the special characteristics of CNTs, ions can be transported effectively, producing materials with high capacitance values, quick charge/discharge rates, and exceptional long-term stability [38], [60].

1.5.2.1.3 Graphene

A possible electrode material for SCs is graphene, which is a single layer of carbon atoms organized in a two-dimensional hexagonal lattice. Due to its outstanding qualities, it is ideally suited for improving the overall effectiveness and energy storage performance of various energy storage devices. Here is a summary of how graphene is utilized in SCs as an electrode material [61]. SC's electrodes can incorporate graphene in a variety of ways as follows.

- **Graphene electrodes**

Graphene sheets can be utilized directly as electrodes, frequently serving as both positive and negative electrodes. To promote charge transfer, these sheets are often grown or deposited onto a conductive substrate, such as a metal foil or a carbon cloth [62], [63].

- **Graphene oxide (GO)**

A graphene derivative with functional groups including oxygen is called graphene oxide. GO is simple to synthesize and can be used to create coatings or thin films. By reducing GO,the reduced graphene oxide (RGO) is created, and it keeps some of the special characteristics of graphene. Films made of GO or RGO make superior electrode materials [63].

- **Graphene composites**

To develop composite electrodes that take advantage of synergistic effects, graphene can be mixed with other materials, such as conducting polymers or metal oxides. These composites can provide both high capacitance from the pseudocapacitive component and high power from graphene conductivity [63].

- **Three-dimensional architecture**

An even greater surface area and improved ion accessibility are provided by graphene-based 3D structures like graphene aerogels or foam-like materials, significantly enhancing energy storage capacity and performance [63].

1.5.2.2 Electrode material for pseudocapacitors

The choice of electrode materials for pseudocapacitors, affects its electrochemical performance, energy storage efficiency and response time as well, especially in applications like electric vehicles and portable devices that demand quick charging and discharging. Moreover, the choice of electrode materials is essential for guaranteeing the pseudocapacitors' cycling stability, which enables them to continue functioning for many charge-discharge cycles [64]. The necessity for sustainable electrode materials is highlighted by the growing relevance of pseudocapacitors' environmental sustainability, which is in line with the desire for greener technologies on a worldwide scale [64].

Sustainability in energy storage is enhanced using eco-friendly materials, which reduces the environmental impact of pseudocapacitor manufacturing and disposal. Technological progress in energy storage systems is fostered by pioneering research into new electrode materials, which push the limits of pseudocapacitor performance [65].

Here are some common materials used in the electrodes of pseudocapacitors and their short description and functionality:

1.5.2.2.1 Metal oxides

Metal oxides offer an appealing substitute as an electrode material for SCs, because of their high specific capacitance (Sec.1.1), low resistance, and high conductivity [42].

Due to their pseudocapacitive properties, metal oxides such as ruthenium dioxide (RuO_2), manganese dioxide (MnO_2), and cobalt oxide (Co_3O_4) serve as flexible electrode material in SCs. Metal oxides perform reversible redox reactions

when used in electrode structures, which makes it easier to store charge by allowing ions to move between the oxide materials and the electrolyte. Rapid charge-discharge rates, prolonged cycling stability, and the possibility of customizing properties through material composition are all desirable traits of metal oxide based SCs [63].

1.5.2.2.2 Metal sulfides

Metal sulfides such as Nickel Sulfides (NiS) and molybdenum disulfides (MoS2) are attractive electrode materials for SCs, because of their capacity to undertake reversible redox processes. These materials, when used as SC electrodes, engage in a faradaic process that facilitates charge storage by allowing ions to move back and forth between the sulfide materials and electrolyte in a reversible manner which increases energy storage capacity and electrochemical performance [66].

1.5.2.2.3 Mixed metal oxides

They combine the advantages of various metal oxides, frequently boosting their capacity for energy storage and cycling stability. Mixed metal oxides can display synergistic effects that result in superior charge storage mechanisms and enable higher energy densities and longer device lifespans than their single-metal oxide counterparts by customizing the composition and structure [63].

1.5.2.2.4 Conducting polymers

SCs now use polymers as valuable electrode materials, giving energy storage technology a fresh perspective due to their high conductivity, redox reactive properties, and ease of synthesis. Conducting polymers such as polyaniline, polypyrrole, and polythiophene enables pseudocapacitive behavior when utilized as electrodes [67].

During charging, the polymer goes through an oxidation process that causes the insertion of electrolyte ions into its structure. Greater charge storage capacity is the consequence [67]. The polymer goes through reduction while discharging, releasing the accumulated ions and electrons.

Conducting polymers can fill the gap between batteries' high energy density and SCs' quick charge and discharge capabilities because of their unique charge storage mechanism. Conducting polymers combine the advantages of typical capacitive and pseudocapacitive characteristics in SCs' electrodes, resulting in increased energy storage capacity, greater power density, and prolonged cycling stability [67].

1.5.3 Electrolyte

The electrolyte is another essential component of SCs and acts as the conductive layer between the two electrodes, facilitating the effective flow of ions [48]. The performance of a SC is also significantly influenced by electrolyte selection. As the medium for ion transport between the electrodes, the electrolyte must be stable over several charge-discharge cycles and able to support high ionic conductivity. The precise needs of the SC design, the electrode materials, and the intended application all influence the electrolyte choice [68], [69].

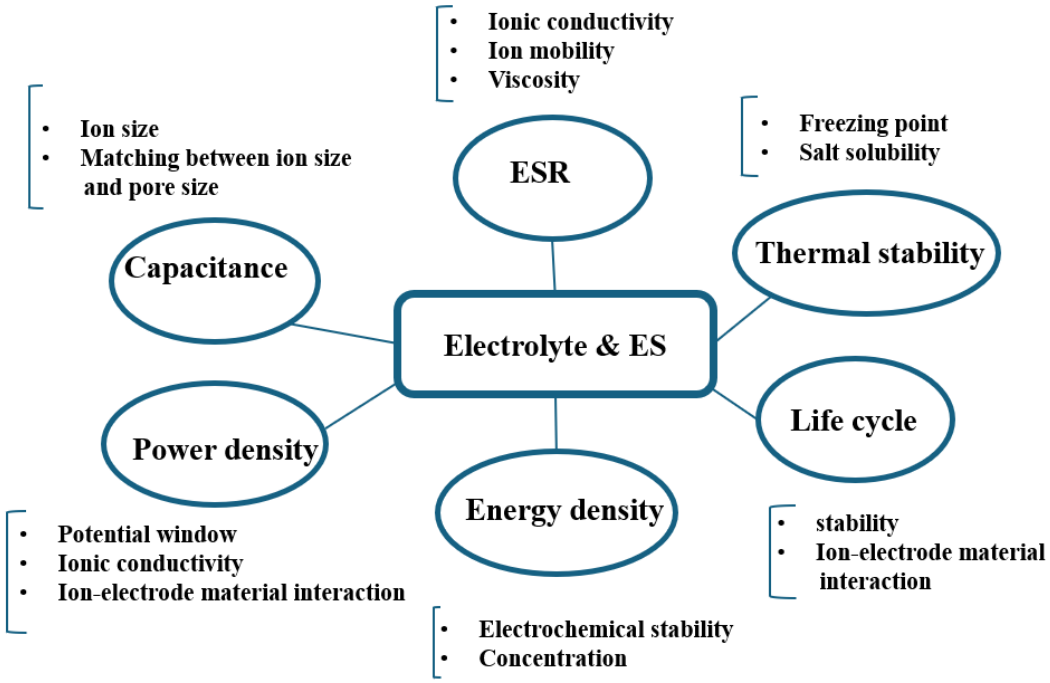

Figure 1.3. effects of electrolyte material on the electrochemical performance of SCs [68].

In Fig. 1.3, the effects of choosing proper electrolyte on enhancing the performance of SC are highlighted. The electrolyte for EDLCs is commonly an aqueous solution with ions like sodium, potassium, or ammonium. Aqueous solutions of sulfuric acid (H_2SO_4) or potassium hydroxide (KOH) are examples of electrolytes that are frequently utilized. The electrode-electrolyte interface's fundamental role in EDLCs is to promote the creation of the electrical double layer, which facilitates charge separation and storage [69].

1.5 SCs components and their materials

Depending on the precise redox processes occurring at the electrode-electrolyte contact, different electrolytes can be used in pseudocapacitors. Electrolytes that can take part in redox reactions and contribute to the charge storage mechanism are frequently needed for pseudocapacitive materials. Utilizing various electrolytes, such as organic electrolytes or aqueous solutions containing metal salts, may be necessary to achieve this [69].

So, while electrolytes are used by both EDLC SCs and pseudocapacitors to promote charge storage, the precise electrolyte composition may vary depending on the electrode materials and charge storage methods involved [50].

Depending on the application and design specifications, SCs can use a variety of electrolytes, either organic (non-aqueous) or aqueous (water-based). SCs that need high power density might benefit from aqueous electrolytes because of their strong ionic conductivity. These electrolytes are often based on chemicals like potassium hydroxide or sulfuric acid [50], [68].

Organic electrolytes, on the other hand, have a higher energy density and a wider voltage range, which makes them suitable for SCs with larger energy storage capacities. They typically consist of organic solvents with dissolved salts [68].

Due to its special qualities and benefits, ionic liquids are a particular family of electrolytes that have drawn interest in the field of SC technology. Ionic liquids are made up of big organic cations and inorganic or organic anions, and they are liquid at room temperature or below. When utilized as electrolytes in SCs, they provide several advantages. SCs can operate across a wider voltage range thanks to the broad electrochemical stability window of ionic liquids, which could result in higher energy densities and improved performance. Ionic liquids are safer substitutes for some organic solvents because they are also non-volatile and non-flammable. The extended operational lifetime of SCs is attributed to their low vapor pressure and thermal stability [50].

Ionic liquids can be used in SCs, but there are drawbacks as well, such as their comparatively high cost and viscosity, which might impair ion movement and lower the device's power density. To maximize their benefits and overcome these drawbacks, scientists are still investigating and developing ionic liquid-based electrolytes. These materials have the potential to greatly enhance the energy and power performance of SCs for a range of applications [69]. In Fig. 1.4, different electrolyte materials used in SCs are classified.

In particular, the kind of electrolyte and electrode material combination affects the thermal and electrical properties of the capacitors as well as their operation. The preferred energy density, power density, cycling stability, and cost are all factors that must be considered when selecting an electrode material. To further improve the functionality and adaptability of SCs, scientists are investigating and developing new electrode materials.

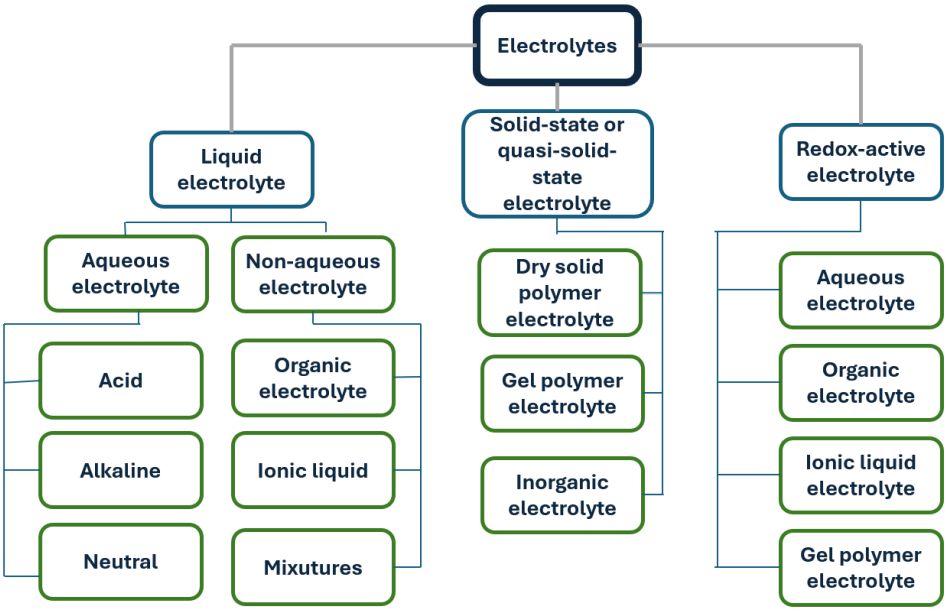

Figure 1.4. Classification of electrolytes for SCs [68].

1.5.4 Separator

The separator effectively keeps the ions flowing between the positive and negative electrodes apart while physically separating them. The separator serves as an insulation barrier to stop direct electrical contact between the electrodes and is often composed of polymeric films or membranes. It also ensures the ionic conductivity required for charge and discharge processes by allowing ion transit in the electrolyte. A key element in the design of SCs systems used in a variety of applications, from electronics to renewable energy storage, is the separator's function in preventing short circuits and preserving the structural integrity of the SC, which is necessary for its safe and dependable operation [70].

Chapter 2

State of the art of measurement techniques

2.1 Introduction

For accurate characterization and performance assessment of SCs, it is essential to comprehend several measuring methods for SCs in the time and frequency domains. Practical metrics such as capacitance, *ESR*, and cycle life (order of million cycles) in real application are obtainable via time-domain approaches while dynamic behavior, energy dissipation, and impedance can be better comprehended using frequency-domain approaches. Combining these techniques can guarantee a full and accurate characterization of a SC.

The following standards exist, as a reference for repeatable measurements on EDLCs:

- EN IEC 62391-1:2022 - Fixed electric double-layer capacitors for use in electric and electronic equipment. Part 1: Generic specification [71] (described in Appendix A.1).
- IEC 62391-2: Fixed electric double-layer capacitors for use in electronic equipment - Part 2: Sectional specification - Electric double-layer capacitors for power application [72] (described in A.2).
- EN IEC 62576:2018 - Electric double-layer capacitors for use in hybrid electric vehicles - Test methods for electrical characteristics [73] (described in Appendix A.3).

Anyway, standards do not cope with accuracy very much, since they just suggest accuracy for current and voltage measurements, but do not care about the accuracy of the determination of the capacitance and the other parameters.

Moreover, currently no standard deals with frequency domain techniques like electrochemical impedance spectroscopy (EIS), which is briefly described in the following.

Standards in synthesis have the following main drawbacks, that in part are filled by this thesis work:

- Repeatability and preconditioning are not deepened in standards.
- Standards neglect equivalent circuits.
- Do not care about measurement accuracy and uncertainty estimation.
- Provides a method which is extremely time-consuming for leakage resistance determination
- Do not care about cyclic voltammetry
- Do not describe and completely ignore impedance spectroscopy.

2.2 Quantities of interest

The main quantities of interest are also the quantities that usually manufacturers declared in the SC specifications, and in particular:

Electrical series resistance (*ESR*) (Ω): As already introduced in Sect. 1.1, this is an equivalent parameter that takes into account the resistance effect due to electrode materials, electrolyte and contact between electrodes and connectors. This equivalent parameter, is very easily identifiable from the voltage drop appearing when the electrical current is injected or stopped in the circuit of the SC. This parameter is in the order of $m\Omega$ and is also an essential parameter to estimate the lifetime or cycle life of SC, because when it reaches its double value by cycling and aging, it verifies that the considered SC's lifetime is over. In this chapter, it is explained how to calculate this parameter with the acquired data from measurements.

Capacitance (F): Also described in Sect. 1.1. Calculating this parameter is very essential which can give us a lot of information about that SC other than the amount of capacity of the SC to store energy. This parameter is also useful for identifying the energy density, power density, *SoC*, *SoH*, the cycle life of SC (according to manufacturers this value is usually when SC's capacitance reaches 80% of its initial

value). Calculating this parameter with different measurement techniques are explained in this chapter

Leakage resistance (R_{lea}) (Ω): This parameter is a resistance and not a physical resistor, representing the self-discharge phenomena of SCs which is an internal chemical phenomenon (This phenomenon is already explained in Sect. 1.1). R_{lea} explained more in detail in Chapter. 4. R_{lea} is in the order of $k\Omega$. A new technique to calculate this parameter is presented in this thesis work and explaind in this chapter (Sect. 2.4.3).

2.3 Four terminals method

Since the *ESR* of SCs is in the order of tens of milliohms or less, the four-terminal measurements are necessary so as not to count the contact resistance in the determination of the series resistance, and the related voltage drop in the voltage measurement. Moreover, since the *ESR* influences more or less all the measurements, the four terminal method need to be always implemented.

Furthermore, contact resistance must be minimized anyway, to improve measurement accuracy. To reduce the contact resistance, we soldered fork contacts to the SCs terminals, and then used clamp terminals with banana plug contacts.

Fig. 2.1 shows the four terminal method and its application to our contacts. In this figure, R_{IC} is the contact current resistance, R_{CV} is the contact voltage resistance, *2QCG* is the two-quadrant current generator, *A* is the ammeter, *V* is the voltmeter.

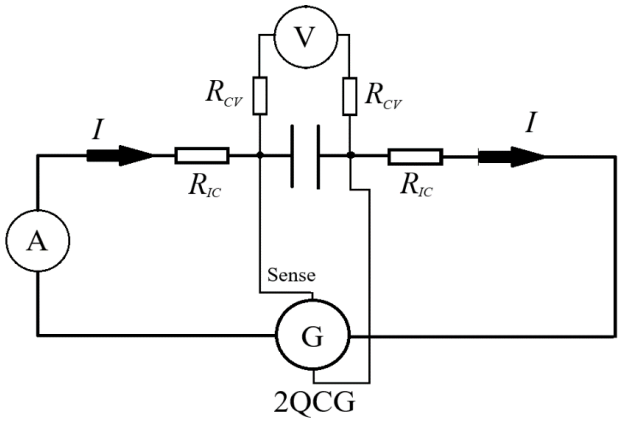

Figure 2.1. The scheme of the measurement circuit.

With the scheme shown in Fig. 2.1, the insertion of the voltage terminals meter is internal and towards the DUT and it avoids counting the voltage drop on the contact resistance R_{IC} and the two-quadrant generator sense is connected to the same points as the voltage meter. The voltage drop caused by R_{CV} is negligible. This is because the input impedance of the voltmeter is of the order of 1 $M\Omega$ and so the current in the voltage circuit is about a few microamperes. Consequently, the voltage drop on R_{CV} is of the order of microvolts, that is negligible compared to the measurement quantity of few volts.

2.4 Measurement techniques

Time-domain techniques concentrate on evaluating characteristics like capacitance, equivalent series resistance (*ESR*), leakage resistance, and charge-discharge efficiency. These techniques are needed for evaluating the performances of a SC, such as capacitance, cycle life, specific power, and specific stored energy.

The most common time-domain techniques are listed below:

- Galvanostatic charging discharging (GCD), briefly introduced in 2.4.1.
- Galvanostatic charging – self discharging (GCSD), briefly described in 2.4.2.
- Leakage resistance assessment, for which a new measurement technique is presented and reported in Sect. 2.4.3 and is one of the achievements of this thesis.
- Cyclic voltammetry (CV), briefly explained in 2.4.4.

The frequency response of a SC can be investigated using the frequency-domain technique EIS, which is briefly introduced in 2.4.5.

All measurement techniques, including those suggested by standards, require suitable training for preconditioning of the SCs. This is taken for granted in this chapter but is discussed in Chapter 3, Sect.4.

2.4.1 Galvanostatic charging-discharging technique (GCD)

GCD is measured by acquisition of current and voltage at the SC terminals. The different supply and load conditions are obtained by means of accurate two quadrants generators. GCD is normally obtained by a charging phase at constant current followed by a discharging phase with the same current. The switch between the two phases is immediate, with a dynamic which undergoes the limits of the rise

time of the two-quadrant generator. This method test is used for cycle life testing, which evaluates the SC's stability and durability over time through numerous charge-discharge cycles. The performance under various load conditions is further revealed by testing at various current densities. Fig. 2.2 shows the result of the galvanostatic charging and discharging of an Eaton 400 F SC, with constant charge-discharge currents of ± 15 amperes.

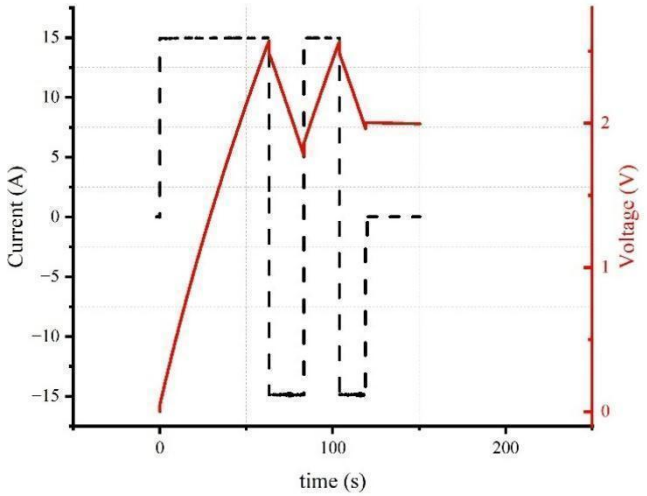

Figure 2.2. Imposed current behavior and the correspondent voltage behavior for performing GCD test on an Eaton XV series 400 F SC.

In a discharging phase at constant current, the specific capacitance of the capacitor can be computed as follows, as also suggested by IEC standards (see also appendix A.1 [71]):

$$C_{GCD} = \frac{I_d \Delta t}{m \Delta V} \tag{2.1}$$

in which C_{GCD} is the specific capacitance computed by GCD test (F/g), ΔV is the considered discharge voltage window (V) usually from $V_1 = 0.8 \times V_{rated}$ to $V_2 = 0.4 \times V_{rated}$, Δt is the discharging time (s) required for the considered ΔV, and I_d is the constant discharging current (A).

A voltage drop can be observed when the current reverses from charging to discharging, which is due to the resistance *ESR* and can be computed according to Eq. (2.2). Factor two in Eq. (2.2) is due to the fact that there is a positive voltage

drop due to charging current stop and a negative voltage drop due to the same discharging current which starts immediately. So, the ΔV is double if related to the current I (the same in charging and discharging). Another way to see the same phenomenon is to consider that the voltage drop ΔV is due to a current variation of 2 I.

$$ESR = \frac{\Delta V}{2I} \tag{2.2}$$

In (2.2), ESR is the equivalent series resistance (Ω), I is the current (A) that is kept constant during charging with positive sign and also kept constant with the same amplitude during discharging with negative sign, and ΔV is the voltage drop (V), which is obtained by extending the straight part of the terminal voltage curve of the capacitor by an auxiliary line. The auxiliary line is the extension of the linear discharge voltage behavior versus time, and it is intersected by the extension of the voltage drop segment in order to calculate the voltage drop ΔU_3 necessary to compute ESR: zoom is shown in Fig. 2.3. In Fig. 2.3, the voltage/time behavior of the SC in GCD test (with constant voltage charge) is shown, and the auxiliary line and its intersection with by the extension of the voltage drop segment is shown in the zoom.

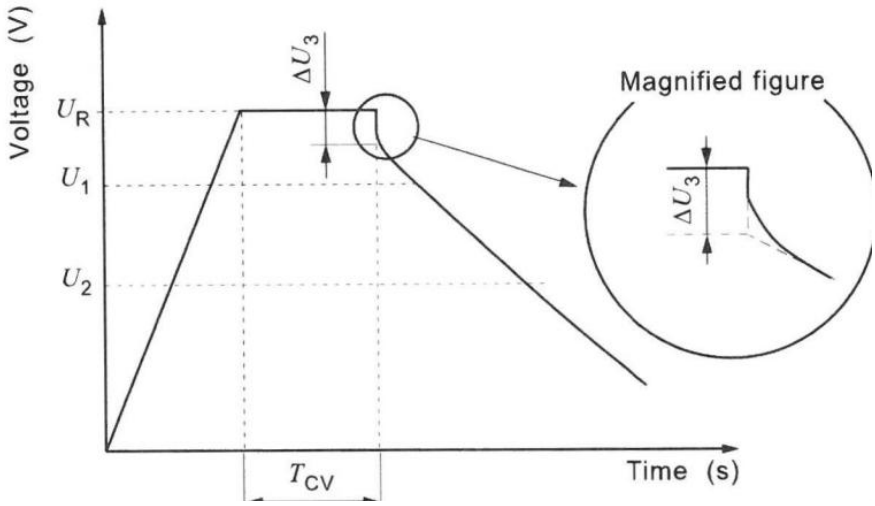

Figure 2.3. Voltage-time behavior of capacitor terminals in capacitance and internal resistance measurements [71].

2.4.2 Galvanostatic charging – self discharging (GCSD)

Charging and self-discharging technique is an important time-domain test for assessing the parameters of a SC, which can be identified as an equivalent circuit (see. Chapter 4). In this technique, the SC is fully charged with a constant current, then it is unplugged from the power source and goes through the open-circuit rest phase and the voltage natural drop over time is recorded. Actually, the voltage measured at the SC terminals il the sum of the SC voltage plus the voltage on the internal series resistance *ESR* of the SC: $V_d = ESR\ I_{charge}$. When the rated voltage V_{rated} is reached and the current stops, the voltage drop corresponding to V_d appears providing the typical peak in the diagram. Fig. 2.4 shows the voltage-time curve of a GCSD test performed on an Eaton 100 F SC [74]. for about 2400 seconds, where the peak after charging phase is evident.

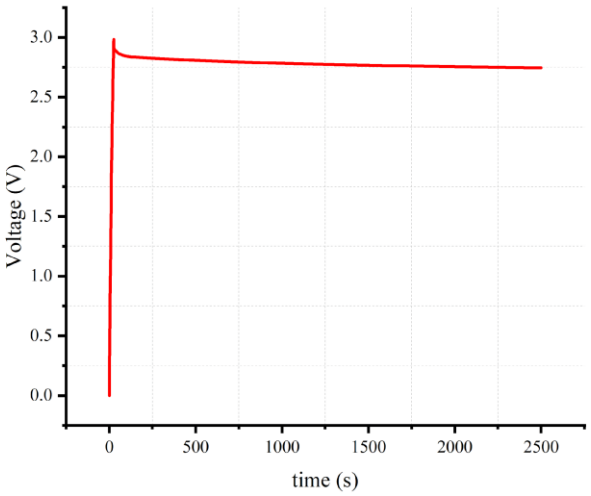

Figure 2.4. Sample of GCSD test performed on an Eaton 100 F SC.

2.4.3 Leakage resistance assessment

The leakage current is a crucial parameter influencing the energy retention and long-term performance of a SC. The SC charge loss is due to internal leakage currents, surface and interface effects in the dielectric, and in an equivalent circuit model (see. Chapter 4), it is represented by a voltage-dependent or time-dependent resistance R_{lea}.

The self-discharge voltage rate also offers information on the quality of a SC in terms of how well it retains the stored charge (and energy), and it could also be used as a diagnostic tool to assess the quality of the electrode materials and electrolytes, as they have a direct impact on the leakage behavior of SCs [75].

To assess the leakage resistance R_{lea} at least two methods are available, the first one being tuned during this thesis:

- R_{lea} obtained with a double self-discharge method with additional resistor.
- R_{lea} obtained with the use of a calibrator.

2.4.3.1 Double measurement self-discharge with additional resistor

This method is fully described in [12]. To determine R_{lea} for a SC, the method we have implemented at INRIM during my thesis, consists of charging the SC up to the rated voltage and then leaving it self-discharging for a few days (e.g. three days) by recording the terminal voltage $V_{t1}(t)$. Then, the charging and discharging procedure is repeated, and the terminal voltage $V_{t2}(t)$ is measured and recorded for a couple of days by connecting an auxiliary resistor, R_{aux}, in parallel with the SC (in parallel to R_{lea} in the equivalent circuit model shown in Chapter 4, Sect. 4.3, Fig. 4.2). R_{aux} can be chosen in order to significantly affect the voltage variation versus time, while avoiding a too quick discharge. Discharging is anyway quicker as the total resistance (the parallel of R_{lea} and R_{aux}) decreases.

The method explained in the following refers to a specific SC, which is a 400 F Eaton XV series SC. This allows the reader to fully understand the procedure looking at experimental results. In Fig. 2.5 a) the blue curve represents the discharge of the SC alone (R_{lea}), which is properly fitted by an exponential decay function with three-time constants:

$$V_{t1}(t) = V_{01} + a_{11}e^{-\left(\frac{t-t_{11}}{\tau_{11}}\right)} + a_{12}e^{-\left(\frac{t-t_{11}}{\tau_{12}}\right)} + a_{13}e^{-\left(\frac{t-t_{11}}{\tau_{13}}\right)} \quad (2.3)$$

where $\tau_{11}, \tau_{12}\ and\ \tau_{13}$ are three time constants and V_{01}, a_{11}, a_{12}, a_{13} and t_{11} are the other interpolation parameters.

The green curve represents the discharging of the SC with auxiliary resistor in parallel (R_{lea} // R_{aux}), which is properly fitted with an exponential decay function with two time constants $\tau_{21}\ and\ \tau_{22}$.

$$V_{t2}(t) = V_{02} + a_{21}\, e^{-\left(\frac{t-t_{22}}{\tau_{21}}\right)} + a_{22}\, e^{-\left(\frac{t-t_{22}}{\tau_{22}}\right)} \quad (2.4)$$

and where V_{02}, a_{21}, a_{22} and t_{22} are the other interpolation parameters.

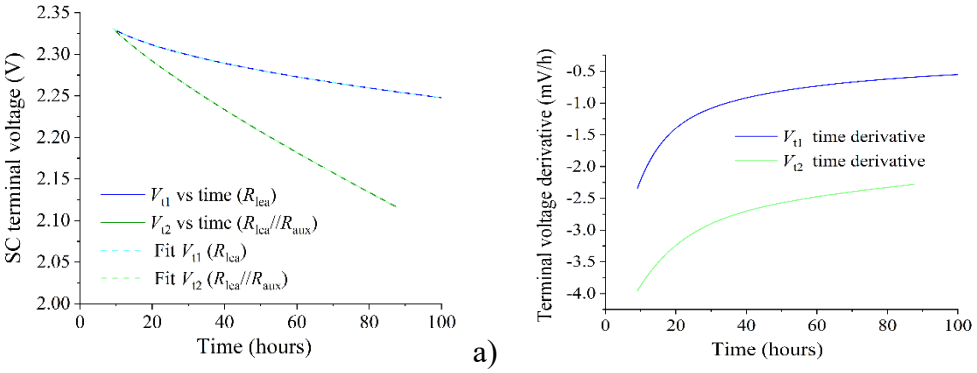

Figure 2.5. a) SC long term self-discharging behavior. Blue line: self-discharging. Green line: self-discharging with an auxiliary resistor in parallel. b) Time derivative of the curves in Fig. 2.5. a).

The equivalent circuit seen by the output resistance R_{lea} is a voltage-dependent capacitance with a small series resistance, which is negligible compared to the output resistance. Therefore, it is reasonable to hypothesize that the rate of variation of the voltage V_t at the terminals of the SC over time depends on the self-discharge current. Without an auxiliary resistor, the self-discharge current can be expressed as

$$\frac{V_{t1}}{R_{lea}(V_{t1})} = C(V_{t1})\ \frac{dV_{t1}(t)}{dt}\Big|_V \tag{2.5}$$

and in the presence of the auxiliary resistor, it can be obtained in accordance with

$$\frac{V_{t2}}{\frac{R_{lea}(V_{t2})\,R_{aux}}{R_{lea}(V_{t2})+R_{aux}}} = C(V_{t2})\ \ \frac{dV_{t2}(t)}{dt}\Big|_V \tag{2.6}$$

The time behavior of the voltage derivatives is shown in Fig. 2.5 b). To evaluate the output resistance, (2.5) and (2.6) must be considered at the same voltage (i.e., by horizontal lines in Fig. 2.5 a), because in this case, the capacitance seen by the output resistance is the same. The same voltage is obtained at different time instants, where we call t_{lea} the instant in which a specific voltage V_{t1} is obtained with only R_{lea}, and t_{aux} when the same voltage $V_{t2}(t_{aux}) = V_{t1}(t_{lea})$ is obtained in the case *of* R_{lea} // R_{aux}. At the evaluation points, the voltage is the same, and the ratio between (2.6) and (2.5) is simplified as

$$R_{lea}(V) = R_{aux}\left[\frac{dV_{t2}(t)}{dt}\Big|_{t=t_{aux}}\left(\frac{dV_{t1}(t)}{dt}\Big|_{t=t_{lea}}\right)^{-1} - 1\right] \quad (2.7)$$

The computed behavior of R_{lea} versus voltage [$R_{lea} = R_{lea}(V)$] provides a function that increases as the voltage decreases, as shown in Fig. 2.6 a) for the considered SC. The trend is well interpolated by the function with two time constants shown in (2.4). Because there is a one-to-one correspondence between the voltage during discharge (blue curve in Fig. 2.5 a) and time, the R_{lea} time behavior [$R_{lea} = R_{lea}(t)$] can be easily obtained, as shown in Fig. 2.6 b), which can also be useful in the simulations.

The interpolation of Fig. 2.5 b) can be obtained with a function similar to (2.4), and in particular,

$$R_{lea}(t) = A_0 + A_1\, e^{\left(\frac{t}{\tau_1}\right)} + A_2\, e^{\left(\frac{t}{\tau_2}\right)} \quad (2.8)$$

where $R_{lea} = R_{lea}(2 \cdot ST)$ is the initial value of R_{lea} that, for the considered SC, is equal to 6.06 kΩ. ST is the so-called "settling time", whose meaning is explained in Chapter 4. A_0, A_1 and A_2 are the interpolation coefficients.

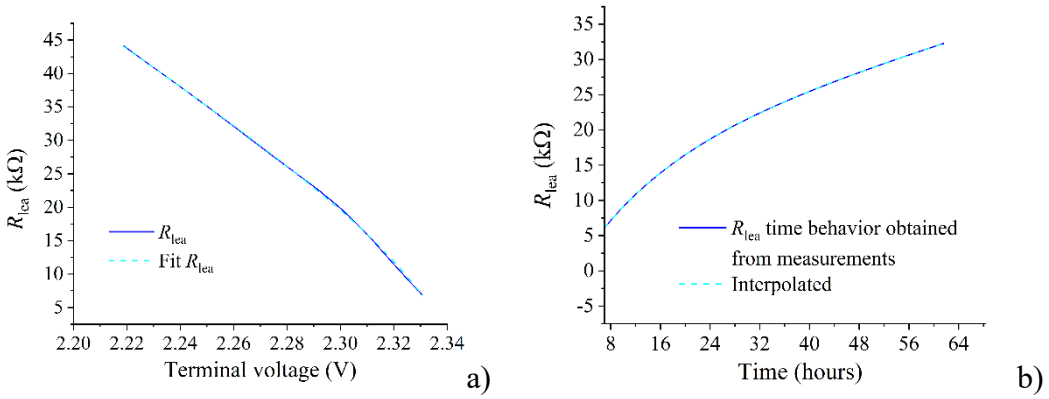

Figure 2.6. Leakage resistance behavior of a 400 F SC a) versus the SC terminal voltage and b) versus time.

In order to verify the pattern of R_{lea} in another SC and to verify the variation of the results changing the R_{aux} we tested a twin SC, same brand and same size, with 3 auxiliary resistors having values of 10 kΩ, 5 kΩ and 1 kΩ so having a one order of magnitude variation. The results are reported in Fig 2.6 a) and b). The behavior of the R_{lea} versus time is similar to the previous SC with a similar initial value, but with a lower resistance increase versus time. Fig. 2.7.a highlight that changing the

auxiliary resistor the R_{lea} trend versus time remains the same, but there is a non-constant bias in terms of resistance values at a specific time, which significantly reduces versus time. With respect to the determination with R_{aux} = 10 kΩ, such a bias determines a variation of the initial R_{lea} up to 37 % for R_{aux} = 1 kΩ and about 25 % with R_{aux} = 5 kΩ, and below 10 % after 36/42 hours (Fig. 2.6 b). Such a variation could seem quite high, however due to the low sensitivity of SC terminal voltages with respect to R_{lea} variations (see Chapter 4 Sect. 9), this does not compromise the effectiveness of R_{lea} behavior determination.

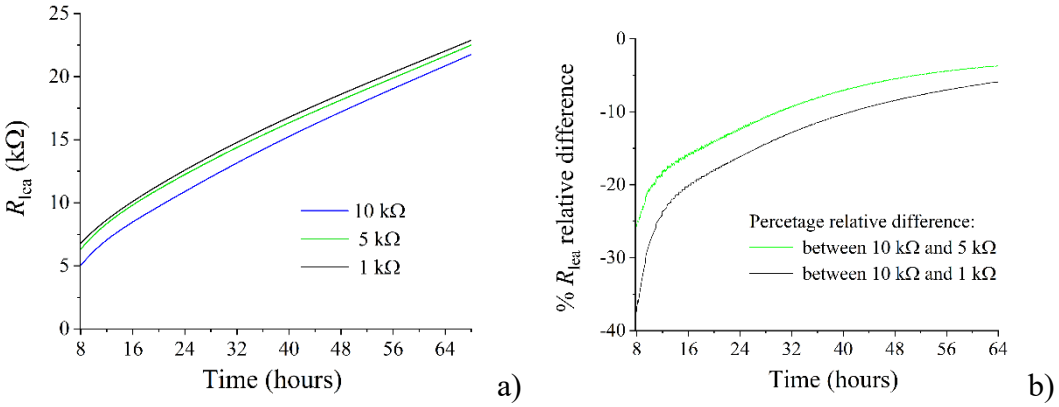

Figure 2.7. a) Leakage resistance vs time with three different R_{aux}, b) resistance percentage relative difference with respect to determination with R_{aux} = 10 kΩ.

2.4.3.2 Potentiostat self-discharge measurement technique

In [76], a quick self-discharge measurement (SDM) technique is introduced which is a potentiostatic technique that measures the self-discharge current directly and provides accurate self-discharge currents with a high resolution in the duration of some hours. This technique is based on the use of a calibrator and is suitable for measuring the low self-discharge currents of SCs in the range of a few µA or fractions of mA. The current limits are only due to the calibrator's current capabilities.

In Fig. 2.8, the equivalent circuit of test setup is shown. A voltage calibrator maintains the voltage at the SC terminals constant (V_t), and a micro-ammeter with suitable accuracy (about 0.25 µA) measures the resultant current (I_{Meas}). An output resistance (R_{out}), that may be adjusted and is mainly due to the microammeter,

connects this voltage source to the cell. With a time constant (τ), the voltage source current converges exponentially to an equilibrium value that matches the observed self-discharge current. The effective capacity (C) of the SC and the total series resistances, which are calculated as $\tau = (R_{out} + ESR) \bullet C$, where ESR is the equivalent series resistance of the SC under test, determine the time constant (τ).

With a lower output resistance (R_{out}) the self-discharge current to measure converges more quickly. However, because of the cell voltage swings, it also intensifies unwanted distortions and noise contributions.

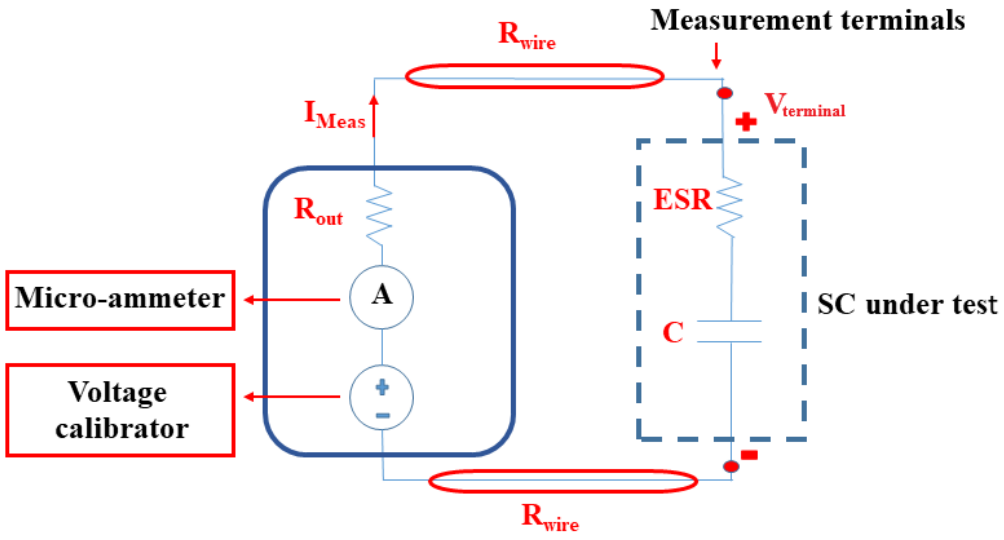

Figure 2.8. SDM measurement setup [76].

To fix the voltage drop in SDM that is ascribed to wire resistance (R_{wire}) in-situ calibration is carried out. This is accomplished by connecting the cells to the test fixture and measuring each SDM channel wire resistance using a low current (about 1 mA), followed by a 15-minute resting interval. Fig. 2.9 provides a sample of two chosen cells' raw and calibrated SDM data.

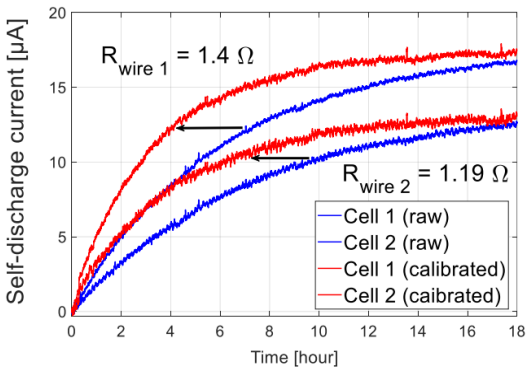

Figure 2.9. R_{wire} calibration and correction for two storage cells [76].

2.4.4 Cyclic Voltammetry technique (CV)

To evaluate the performance of SCs in electrochemistry is quite common to use cyclic voltammetry (CV). Performing CV tests is fast, easy and provides a graphic depiction of the behavior of charge and discharge. In this technique, the voltage steps and the scan rate (v), which is the constant rate of voltage variation with respect to time (V/s or mV/s) are the inputs and the recorded current response is the output, acquired as the voltage varies. The procedure is repeated over several cycles as the first one depends on the starting voltage and usually is not repeatable.

At INRIM, we have performed CV tests on some commercial SCs and also on some pouch cells produced in EMPHASIS project with different electrode materials. For each pouch cell the CV test is performed with five different scan rates (10, 20, 50, 100, 200 mV/s).

For an Eaton TV series 100 F SC, Figs. 2.10 and 2.11 show the cycles measured at INRIM. Fig. 2.10 shows the imposed voltage behavior and the correspondent current behavior compliant with the imposed voltage. Finally, Fig. 2.11 shows the cycle with three different scan rates.

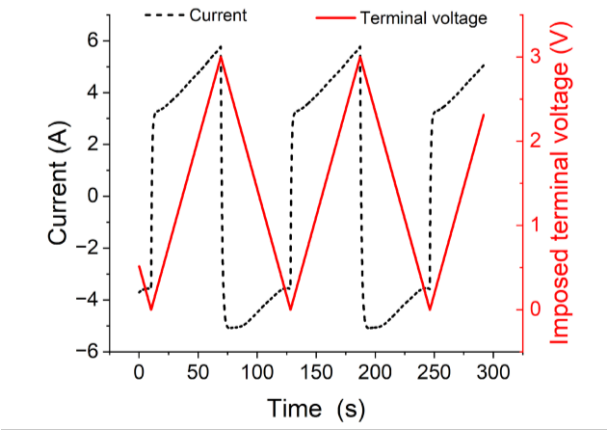

Figure 2.10. Imposed voltage behavior and the correspondent current behavior for performing CV test on an Eaton TV series 100 F SC, scan rate 50 mV/s.

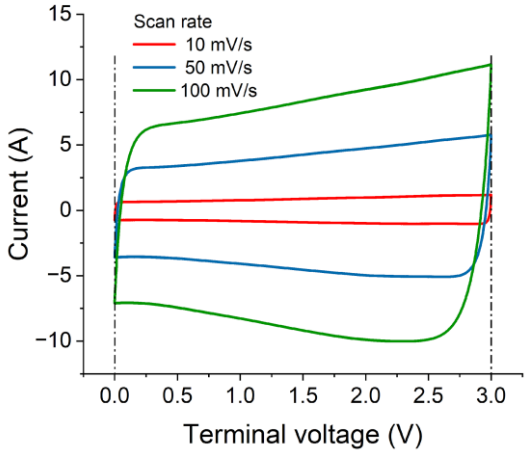

Figure 2.11. Cyclic voltammogram of an Eaton TV series 100 F SC with three different scan rates.

The area of the cycle increases by implementing a higher scan rate, since the current increases. It is possible to compute the specific capacitance from the stored charge according to Eq. (2.9), which is represented by the area that the I-V curve encloses. A typical pattern seen in CV plots is that the capacitance value drops as scan rate rises [77].

$$C_{cv} = 1/(2m\Delta V)[Q_A + Q_B] \quad (2.9)$$

In Eq. (2.9), C_{cv} is the specific capacitance of the SC computed by CV curve (F/g), m is the SC mass (g), ΔV is the range that the voltage cycles through ($\Delta V = V_{max} - V_{min}$) (V), Q_A and Q_B are the anodic and the cathodic charge (C), respectively, and $\frac{1}{2}$ is needed to average the two charges that in principle are equal but actually have very limited differences.

With considering the SC voltage sweeping over time by a constant scan rate ($v = \frac{dV}{dt}$) and thus having $dt = \frac{dV}{v}$, the charge equation can be written as below:

$$Q = \int_{t_{v\_min}}^{t_{v\_max}} I(t)dt = \int_{v_{min}}^{v_{max}} I(V)\frac{dV}{v} \quad (2.10)$$

in which $\int_{v_{min}}^{v_{max}} I(V)dV$ represents the area enclosed by the I-V curve. By combining the Eqs. (2.10) and (2.9), one can also use Eq. (2.11) to compute the specific capacitance of the SC by having the data from CV test.

$$C_{cv} = \frac{\int_{v_{min}}^{v_{max}} I(V)dV}{2mv\Delta V} \quad (2.11)$$

Also, in electrochemistry, the CV curve symmetry and shape reveal information about the SC electrochemical behavior, including the contributions of ion diffusion, faradaic reactions, and capacitive and pseudocapacitive processes. In this thesis we do not face these aspects as this work basically focuses on the measurement techniques. As an example, in Fig. 2.12 the results of the CV tests performed on two pouch cells with different electrode materials and produced in EMPHASIS project is shown which shows the effect of the electrode materials on the shape of the CV curve. For both pouch cells, the applied voltage range is the same (0 to 2 V) with five scan rates (10, 20, 50, 100, 200 mV/s).

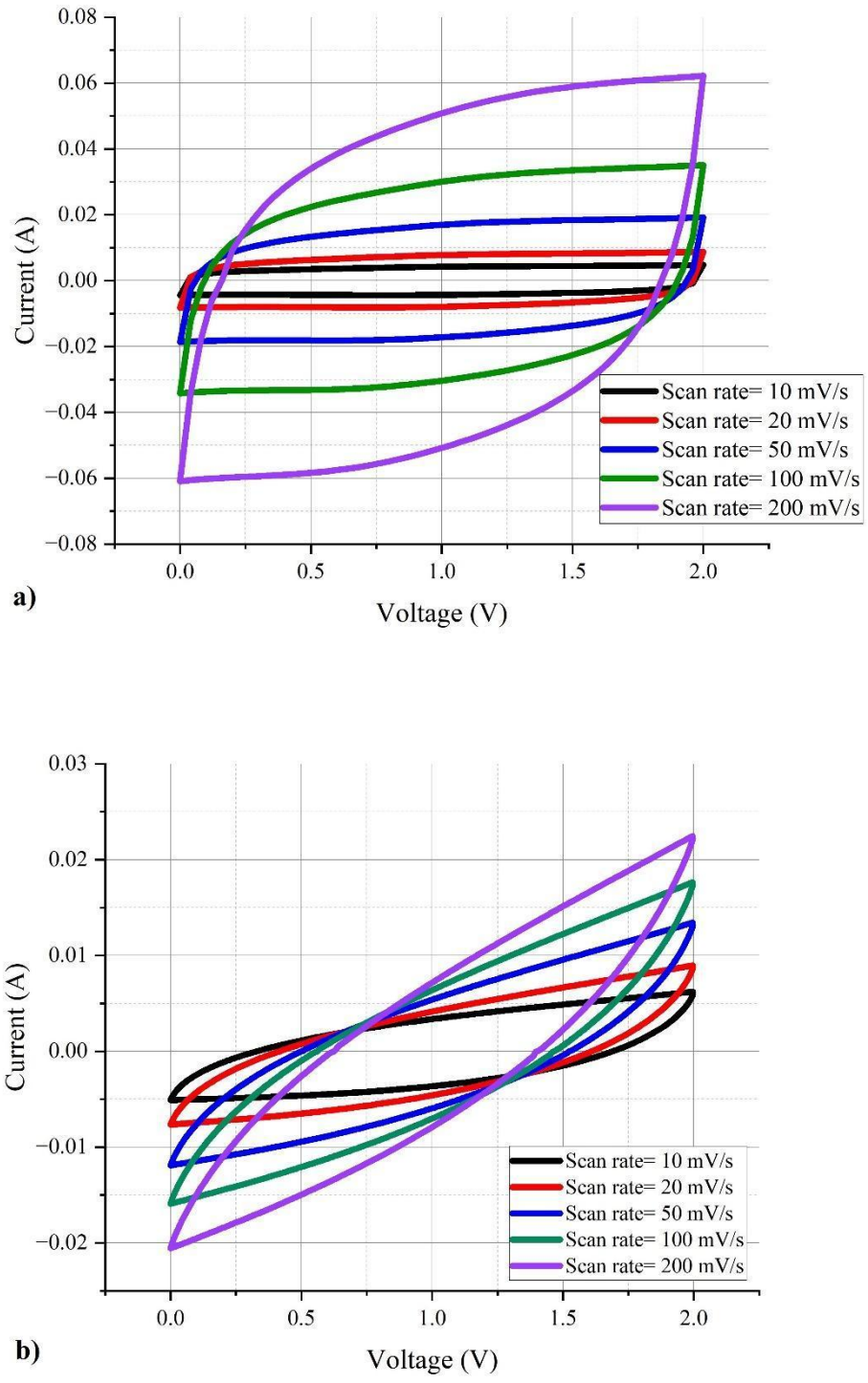

Figure 2.12. CV tests performed on two EMPHASIS project sample pouch cells at INRIM with specific capacitances of. a) 79.8 F/g, b) 65 F/g and also different electrode materials.

The result of calculation of the capacitance (F) for the same cell of Fig. 2.12. a), is presented in Table 2.1. The trend of decreasing capacitance with increasing the scan rate can be seen.

Table. 2.1. The calculated capacitance of a pouch cell (C_{sp}=79.8 F/g) for 5 different scan rates.

Scan rate (mV/s)	Capacitance (F)
10	0.38
20	0.35
50	0.30
100	0.26
200	0.21

2.4.5 Electrochemical impedance spectroscopy technique (EIS)

Electrochemical Impedance Spectroscopy is a measurement technique for SCs in frequency domain. SCs can be effectively characterized using the EIS approach. To produce an EIS response, a small (in order to avoid facing the nonlinearity) sinusoidal voltage perturbation is applied to the SC while the frequency is being changed. An important understanding of the processes of charge transfer, electrolyte behavior, and electrode-electrolyte interfaces can be gained by examining the impedance spectra [78]. For each specific frequency, the specific capacitance of SC can be calculated according to Eq. (2.12), with the data provided by EIS tests.

$$C_{EIS} = 1/(m\omega z'') \quad (2.12)$$

in which, C_{EIS} is the specific capacitance provided by EIS test data (F/g), ω=2πf is angular frequency (rad/s), m is the mass of the SC (g), and z'' is the absolute value of the imaginary part of the impedance. For calculating the equivalent capacitance for the whole frequency spectra, the EIS curve can be fitted with a suitable model.

In [79], for ideal symmetric SCs, the electrode specific capacitance is also defined as Eq. (2.13). This equation is derived from SC specific capacitance equation computed with the acquired data from any measurement techniques mentioned above and the multiplier 4 in this equation represents adjusting the mass of active material in a single electrode and the combined mass of the two electrodes.

$$c_{electrode=}4c_{SC} \quad (2.13)$$

Where $C_{electrode}$ is the electrode specific capacitance of the ideal symmetric SC (F/g), and C_{SC} is the specific capacitance of the whole SC (F/g).

EIS offers important insights into SCs behavior, by measuring the impedance across a range of frequencies using a small AC perturbation signal. Three frequency ranges can be distinguished in EIS spectra: low frequency (often below 10 mHz), medium frequency (10 mHz to 1 kHz), and high frequency (beyond 1 kHz). The low-frequency range provides information about ion diffusion in an intercalation electrode and mass transfer in solid-state materials. The medium frequency range is typically where processes like charge transfer reactions and electrical double-layer charging at the electrode-electrolyte interface are seen. Furthermore, the high-frequency region is where cell resistances such interfacial and electrolyte resistances take place [75].

A Nyquist plot, which plots the real part of the impedance (Z') against the negative imaginary part (-Z''), is a common way to view EIS data. The Bode plot (which consists of two types of plots: impedance magnitude versus frequency and impedance phase versus frequency), which has three primary regions described below, is the other kind of plot that can be used to show EIS test results."

The three main regions of Bode plot are as follows:

- High-frequency region (kHz- MH): in this region the impedance magnitude curve is flat or almost flat and the phase curve is around 0° representing the resistive behavior. In other words, the dominance of *ESR* is correlated with this region.
- Mid-frequency region (Hz- kHz): this is where the capacitance regulates the impedance. In this region the impedance magnitude is not flat and shows a negative slope with increasing frequency. The phase in this region goes up to around -45° degree, and the main phenomenon is diffusive.
- Low-frequency region (mHz- Hz): in this region the impedance magnitude increases significantly, and the phase tends to -90° degrees representing capacitive behavior.

2.4 Measurement techniques

The cell current and voltage serve as the basis for the first and second controlling modes, respectively. The hybrid controlling mode produces a fixed current-voltage response by combining galvanostatic optimizations with current changes. For cells with low impedance, where small errors in DC voltage result in high DC currents, the galvanostatic and hybrid controlling modes are primarily recommended [77]. So, in summary three principle controlling modes of EIS, include:

- Galvanostatic EIS: the voltage response is measured when the current is kept constant. This controlling mode is helpful when working with low-conductivity electrolytes or when researching systems with high resistance.
- Potentiostatic EIS: the current response is measured while the voltage is maintained constant. It is frequently employed in electrode characterization.
- Hybrid EIS: a mix of potentiostatic and galvanostatic control, with the two modes being switched according to system impedance to maximize stability and measurement accuracy.

Important parameters like electrolyte resistance, capacitance, interfacial resistance, charge transfer resistance, and ESR can be derived by analyzing EIS test results. In Fig. 2.13, a sample of Nyquist and Bode plots (both magnitude and phase), as a result of a test on an Eaton 1 F SC [80] at INRIM are shown. In Fig. 2.13. a) which is the Nyquist plot, the frequency at some points of the curve is also shown by black symbol. In Figs. 2.13. b), c) the three regions of the Bode plot described earlier in this section can be seen. In this figure, the high-frequency, mid-frequency and low-frequency regions are related to the frequency ranges of 1000-10000 Hz, 1-1000 Hz, and 0.1-1 Hz respectively. This test is performed by Bio-Logic cycler (BSC 810 module) [81], the tests are controlled, and the data are saved by BT-LAB software and analyzed in Origin software.

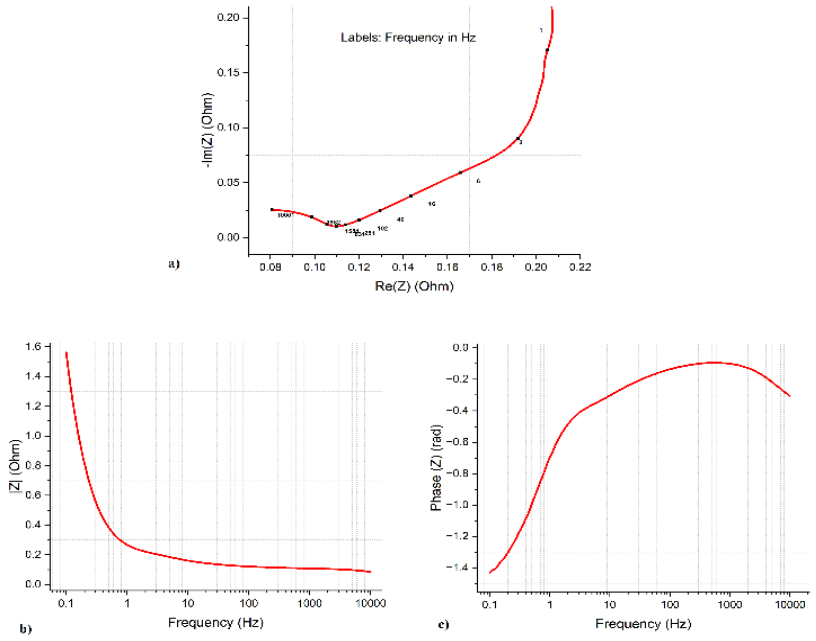

Figure 2.13. Sample of a) Nyquist plot, b) Bode (magnitude versus frequency) plot, and c) Bode (phase versus frequency) plot as a result of EIS test, performed at INRIM on an Eaton 1 F SC

Chapter 3

Measurements on SC

3.1 Introduction

In this chapter the measurement setup, and the devices under test (DUTs) are introduced. To achieve repeatability, suitable training for SCs is proposed and some preliminary repeatability tests and the results are reported and analyzed.

3.2 Measurement setup and the devices under test

The measurement setup and the devices under test for characterization and modeling of SCs in this thesis are described in the follow-up.

3.2.1 Measurement setup description

Electrical current measurements on different sizes of SCs have a wide range (from some hundreds of mA for the SCs with capacitance of 1 F or below, to tens of amperes for SCs with capacitances of hundreds of farads). On the other hand, voltage is generally limited from zero to 3 V for simple EDLCs.

The current and voltage measurements, and recording the measurements data in this thesis are performed with the following instruments:

1. A LEM IT_65-S Ultrastab transducer [82] (with an expanded uncertainty limited to 0.1‰ in DC), for currents above 6 A synchronized to voltage measurements performed both with a NI PXI-4461 board [Add 83]. The voltage is measured directly on one channel of the board with a voltage range of ±3.16 V.
2. For currents below 6 A, with direct measurements with two Keysight 34470 A multimeters [84], one for current and one for voltage.

Two channels of a National Instruments (NI) PXI-4461 board, fitted with a deltasigma analog-to-digital converter at 24 bits, were used as digitizers in experiments [83]. The NI boards have been calibrated at INRIM and described in Appendix B.

Measurements are recorded and managed using a program created in the LabVIEW environment

To provide constant charging and discharging currents, some bidirectional programmable DC power supplies are implemented in the experimental setup, and specifically ITECH IT-6015-C (maximum current 450 A) [85], and ITECH IT-M3415 (maximum current 3 A) [86], generators were utilized. Fig. 3.1 and Fig. 3.2 show the main components of the measurement setup.

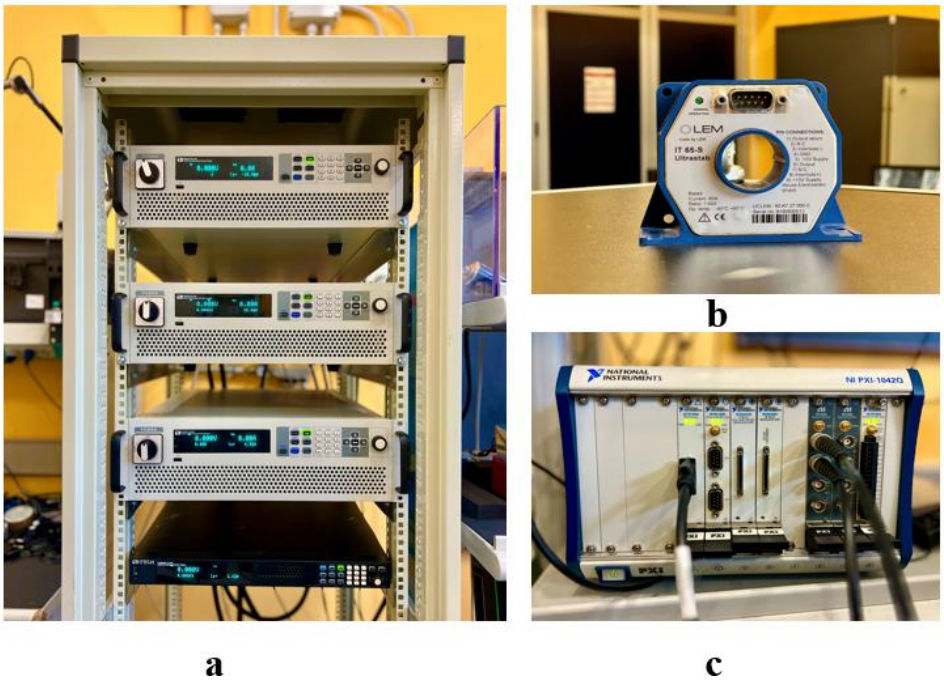

Figure 3.1. Some measurement setup components: a) Three ITECH IT-6015-C generators at the top and an ITECH IT-M3415 generator at the bottom, b) a LEM IT65S Ultrastab current transducer, c) NI PXI system including two 4461 boards.

For leakage resistance measurements standing-by for a few days or a week, voltage measurements were performed with a reference multimeter (Fluke 8588A) [87] with an input impedance greater than 10 GΩ and sampling interval of 10 s, with the help of a voltage calibrator Fluke 5730A [88] as the voltage reference during discharging.

3.2 Measurement setup and the devices under test

The instrumentation was calibrated at INRIM before the measurements. All the measurements and investigations were performed at a controlled room temperature of 23 ± 0.5°C.

Figure 3.2. Sample of the whole measurement setup at INRIM.

3.2.2 Devices under test

In this thesis a set of EDLCs were utilized for different analysis: Eaton HV series 1 F [80], two sizes from Eaton TV series [74] (60 F, 100 F), Eaton XV series 400 F [89], a big size from SPSCAP SCP-STA series (1500 F [90]). Some sample SCs are shown in Fig. 3.3 with nominal capacitances of 1500 F, 400 F, 100 F, 60 F, 35 F [74], 10 F [74] respectively from left to right. Some of these SCs have been used for preliminary tests and SCs of size 100 F, 400 F and 1500 F have been analyzed in more detail. Table 3.1 summarizes the main quantities of the considered SCs.

Figure 3.3. Samples of the SCs under test at INRIM. The fork terminals carry the current and are soldered to the SC terminals from which the sense terminals are derived by soldering, according to the 4-terminal method (see Sect. .3).

Table 3. 1. Main specifications of the DUTs given by manufacturer.

Capacitance (F)	**Part Number**	**Max. initial *ESR* (mΩ)**	**Max. voltage (V)**	**Continuous current (A)**	**Nominal leakage current (µA)**	**Peak power (W)**
1	HV0810-2R7105-R	0.2	2.7	0.8	10	1.9
60	TV1840-3R0606-R	0.013	3.0	6.7	135	173
100	TV1860-3R0107-R	0.011	3.0	11.7	225	205
400	XV3560-2R7407-R	3.2	2.7	26	850	570
1500	SCP1500C0-0002R7STA	4.7	2.7	83	Not mentioned	Not mentioned

3.3 *ESR*, capacitance and common conditioning of the SC

The two main parameters of interest for SCs are electrical series resistance (*ESR*) and capacitance. To measure these quantities many papers in literature suggest a preconditioning of the SC of about ten cycles of charging up to the rated voltage and then discharging (e.g. [91]), with both phases at constant current.

3.3.1 Definition and test

In this section, the results of computing *ESR* and capacitance of the SCs under test are reported. These preliminary results are then analyzed to evaluate the test conditions and the DUT conditions. In particular, the tests were also used to evaluate the repeatability of the results. As defined in International Vocabulary of Metrology (VIM) [92], analyzing the repeatability of a measurement means to see how close the measurements are when they are perfomed in the same conditions that is: same operators, the same measurement procedure, same operating conditions, same measurement system, same location, and repeating the measurements on the same DUT in a short period of time. Repeatability is important because it influences the accuracy of the measurements, together with the accuracy of the meters that perform the acquisition of the quantities of interest.

The measurement technique is GCD, and the SC is charged, then briefly remained at constant voltage and finally discharged with constant current provided by the bidirectional DC power supply ITECH IT-6015-C [84]. The acquisition time is 200 seconds with a rise and fall time of 0.01 seconds. The constant discharge current is 10 A. The DUT is the same 400 F SC described earlier. The measurements are repeated 10 times, on the same day.

ESR and capacitance reported in this section are computed according to Eqs. (3.1) and (3.2), and in order to speed up the computation, in this thesis work a MATLAB program is written for the calculation of this part.

$$ESR = \frac{\Delta V}{I_d} \tag{3.1}$$

$$C = \frac{I\Delta t}{\Delta v} = \frac{I_d \Delta t}{v_{max} - v_{min}} \tag{3.2}$$

where in Eq. (3.1), ΔV is the voltage drop (V) at the beginning of the discharging phase, which is obtained by extending the straight part of the terminal voltage curve of the capacitor by an auxiliary line (To correctly assess ΔV, see Appendix A.1.4.), and I_d is the discharge current (A). In Eq. (3.2), Δv is a selected voltage window in discharging phase to calculate the capacitance that is defined according to the IEC 62931 standard. Such a voltage window is defined as: $v_{max} = 0.8\, v_R = 0.8 \times 2.7 = 2.16\, V$ and $v_{min} = 0.4 v_R = 0.4 \times 2.7 = 1.08\, V$ and Δt is the time duration (s) of the voltage window.

Table 3. 2. calculated *ESR* and capacitance of the DUT in repeatability test.

Number	$ESR(m\Omega)$	**Capacitance (F)**
1	3.41	396.6
2	3.58	397.3
3	3.66	400.7
4	3.51	401.1
5	3.38	401.6
6	3.26	401.8
7	3.51	400.0
8	3.36	398.5
9	3.46	399.8
10	3.68	398.8

In Table 3.2 the computed *ESR* and capacitance are given and the variation of these two parameters in these 10 experiments are shown in Fig. 3.4. The distribution of the capacitance is shown in red dots, where the mean value is 399.62 F, close to the nominal value, and the standard deviation is 1.76 F (0.44 % of the mean value). Anyway, as reported in Table 3.3, the difference between the minimum and the maximum value of capacitance is about 6 F, which means 1.5 % of the rated value.

The resistance variation, shown by blue stars in Fig. 3.4, is from 3.26 to 3.68 $m\Omega$. Table 3.3 shows an average value of 3.48 $m\Omega$ (manufacturer specification provides 3.2 $m\Omega$). The standard deviation is 0.13 $m\Omega$ (3.8 % of the average) which shows the measurement dispersion is quite limited.

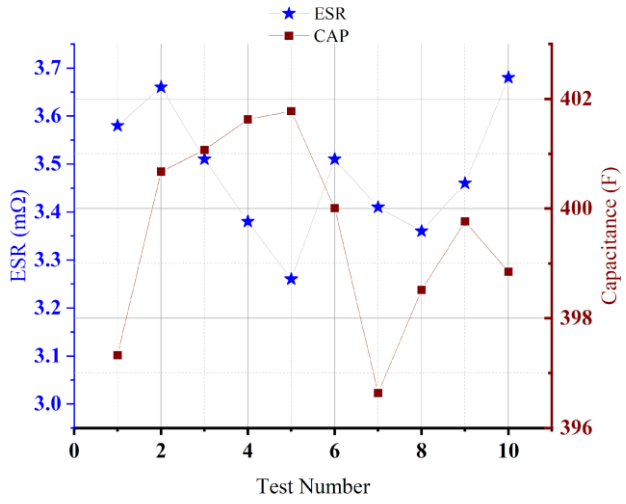

Figure 3.4. The capacitance and *ESR* variation in the repeatability test for an Eaton 400 F SC.

Table 3. 3. Statistical data on the calculated capacitance and *ESR* of Eaton400 F SC in repeatability test.

N	Mean (F)	Standard Deviation (F)	Minimum (F)	Median (F)	Maximum (F)
10	399.6	1.76	396.6	399.9	401.8

N	Mean ($m\Omega$)	Standard Deviation ($m\Omega$)	Minimum ($m\Omega$)	Median ($m\Omega$)	Maximum ($m\Omega$)
10	3.48	0.13	3.26	3.48	3.68

	ESR **($m\Omega$)**	**Capacitance (F)**
Uncertainty (U_A)	0.04	0.55

As defined in VIM [92], the uncertainty evaluated based on statistical analysis of the data acquired from some measurements which are performed under certain measurement conditions, is known as uncertainty type A. The standard deviation and uncertainty type A of n measurements are calculated according to the known Eqs. (3.3) and (3.4) as follows [93].

$$s = \sqrt{\frac{\sum_{i=1}^{n}(x_i - \underline{x})^2}{n-1}} \tag{3.3}$$

$$U_A = \frac{s}{\sqrt{n}} \tag{3.4}$$

In Eqs. (3.3) and (3.4), s is standard deviation, x_i is each data point, x is the average value, n is the number of measurements and U_A is the uncertainty type A.

3.3.2 Test repetition at different currents

The experiment of the previous section, performed at constant current equal to 10 A, is here repeated for currents from 13 A to 22 A with 1 A step, for each experiment. The computed capacitances and the *ESR*s from the measurement results are reported in Table 3.4 and shown in Fig. 3.5. The discharging voltage windows for this SC at different discharging currents is shown in Fig. 3.6 for the time interval of 0.6 s to 9 s of discharging phase. In Table 3.5, the statistical analysis of these 10 tests is given.

Table 3. 4. The current behavior of an Eaton 400 F SC.

Current (A)	***ESR*** $(m\Omega)$	**Capacitance (F)**
13	3.63	391.1
14	3.64	393.5
15	3.53	392.1
16	3.5	395.2
17	3.45	390.4
18	3.47	387.5
19	3.47	390.4
20	3.46	389.7
21	3.48	387.3
22	3.49	387.8

Table 3. 5. Statistical analysis on the calculated capacitance and *ESR* of an Eaton 400 F SC in current behavior test.

N	**Mean (F)**	**Standard Deviation (F)**	**Minimum (F)**	**Median (F)**	**Maximum (F)**
10	390.5	2.61	387.3	390.4	395.2

N	**Mean $(m\Omega)$**	**Standard Deviation $(m\Omega)$**	**Minimum $(m\Omega)$**	**Median $(m\Omega)$**	**Maximum $(m\Omega)$**
10	3.51	0.07	3.45	3.49	3.64

	ESR **$(m\Omega)$**	**Capacitance (F)**
Uncertainty (U_A)	0.02	0.82

3.3 ESR, capacitance and common conditioning of the SC

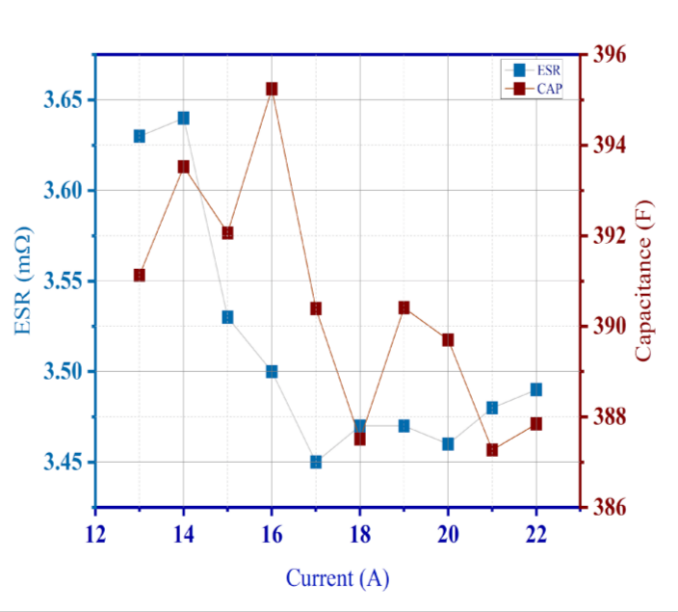

Figure 3.5. *ESR* and capacitance computed at different currents for an Eaton 400 F. SC.

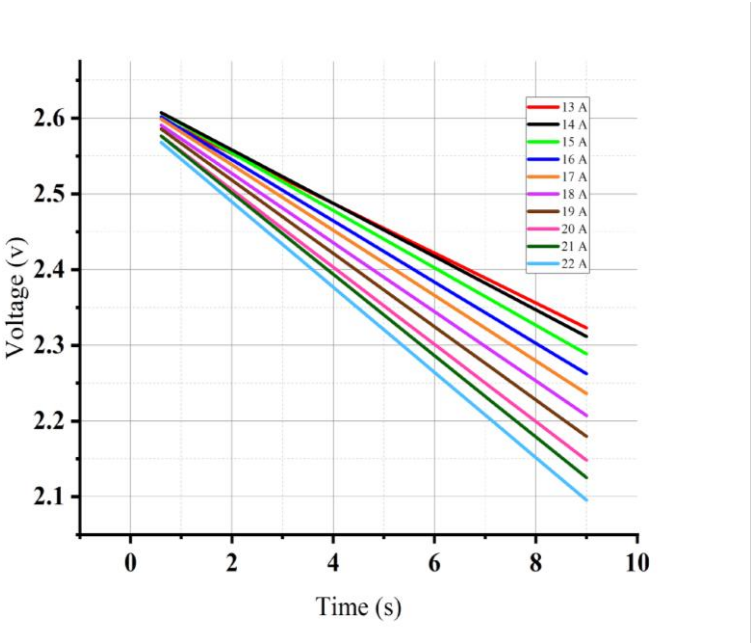

Figure 3.6. Discharging voltage window at different discharging currents for an Eaton 400 F SC.

The variability of the measurement with the capacitance does not follow a trend and it varies from 387 to 395 F with some ups and downs. This shows an issue from the measurement point of view. In fact, the repeatability of the capacitance seems to be very limited with a variation of about 3 % versus the current variation. This limit comes from two reasons: 1) the SC preparation (training) can be improved, as was done in this thesis and shown in the next section, 2) the capacitance is not voltage (and so also current) independent as will be underlined by the modeling investigation in the next chapter.

3.3.3 Test repetition at different voltages

On the same SC, ten additional experiments were performed considering the same time window and a constant discharging current of 15 A but different voltage windows from 1.8 V to 2.7 V with 0.1 V step for each experiment. Of course, these tests do not respect the indication of standards but provide a view on their variability versus voltage. Computed parameters with these measurements are reported in Table 3.6.

In this test it is even more evident that the capacitance is voltage dependent and that a model considering this variability is needed.

In Fig. 3.7, the red squares show the capacitance points for these 10 tests, which vary from 353.12 to 397.12 F. Statistical analysis on these data points is given in Table 3.7 and shows an average value of 371.68 F (92.9 % of the nominal capacitance in specification). The standard deviation is 13.74 F (3.7 % of the average). The resistance, shown by blue squares in Fig. 3.8, varies in the range of 3.50 to 4.15 $m\Omega$, with the average value of 3.76 $m\Omega$. As given in Table 3.7, the standard deviation is 0.28 $m\Omega$ (7.4 % of the average).

in Fig. 3.8 the discharging voltage window at different voltage levels for this SC is shown.

3.3 ESR, capacitance and common conditioning of the SC

Table 3. 6. The voltage behavior of an Eaton 400 F SC.

Voltage (V)	***ESR*** **($m\Omega$)**	**Capacitance (F)**
1.8	3.50	353.8
1.9	3.59	353.1
2	3.56	362.7
2.1	3.51	363.3
2.2	3.52	374.4
2.3	3.59	373.1
2.4	3.99	375.9
2.5	4.1	380.0
2.6	4.15	383.5
2.7	4.06	397.1

Table 3.7. Statistical analysis on the calculated capacitance and *ESR* of an Eaton 400 F SC in voltage behavior test.

N	**Mean (F)**	**Standard Deviation (F)**	**Minimum (F)**	**Median (F)**	**Maximum (F)**
10	371.7	13.7	353.1	373.7	397.1

N	**Mean ($m\Omega$)**	**Standard Deviation ($m\Omega$)**	**Minimum ($m\Omega$)**	**Median ($m\Omega$)**	**Maximum ($m\Omega$)**
10	3.76	0.28	3.50	3.59	4.15

	ESR **($m\Omega$)**	**Capacitance (F)**
Uncertainty (U_A)	0.088	4.35

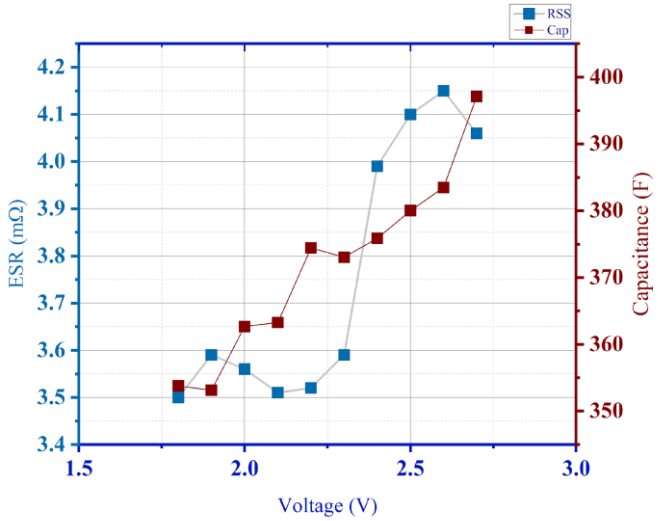

Figure 3.7. *ESR* and capacitance computed at different voltages for an Eaton 400 F SC.

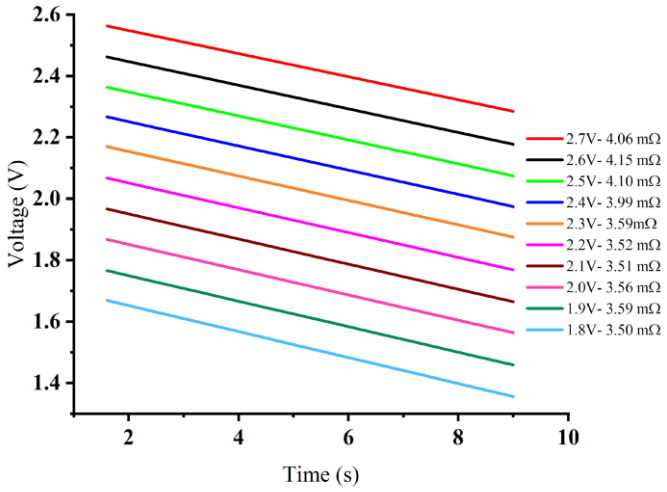

Figure 3.8. Discharging voltage window at different voltage levels for an Eaton 400 F SC.

3.4 Training of SCs

Complete discharge of the SCs can be very long, from hours up to days depending on the SC size and type. As a result, in the dynamic behavior of these components always an amount of charge remains in the device, and it affects the SC behavior in the following cycles. This remaining SC charge, which is also called “residual

charge", affects the charging time and discharging behavior of the SC [91]. For practical reasons in the experiments in this thesis, we considered a SCs discharged when the discharging current is below 1 mA and the residual voltage below 1 mV.

Also, the complete charge of a SC is a process that requires a repetition of charging and discharging phases. From a new SC, from a first set of charging one can recognize an improvement of the stored charge and a reduction of the self-discharge rate. The physical explanation of this behavior [80] is based on the fact that, during each charging phase, the amount of charge stored inside the SC macropores available at the electrode–electrolyte increases, and consequently, it participates actively in the subsequent charging phase. Once the availability of macropores is saturated (this happens generally after about ten cycles), the charge reaches its maximum value.

So, a new SC exhibits a different behavior than an 'operating' SC. Similarly, when a SC undergoes a very long stand-by phase or remains unused for a long time, its behavior resembles that of a non-trained SC. Training is important for measurements in order to reach stable conditions, and also to be able to make comparisons between different measurements, furthermore when we want to observe the accuracy of the parameter identification of SCs, it is important to compare the simulated voltage curves with the trained and stable SC behavior.

To observe the training effect, three new EDLC Eaton XV series SC with a nominal capacitance of 400 F are tested at INRIM and the results are shown in Fig. 3.9. The main specification of these SCs is given in Table 3.1 and [88]. For the first and second SC, the charging current is 20 A, and the third SC is charged with 10 A.

The five first charge-self-discharges of the first SC under test are shown in Fig 3.9.a. The charging time of these five cycles are shown in the zoomed part. As can be seen, in Fig. 3.9.a), in the first four cycles which were performed in the same day, the most difference between the terminal voltage value after 20 minutes of self-discharging is between the first and the second curves which is 130 mV and 4.8% of the rated voltage of this SC (2.7 V). The slope of the self-discharge curves is going to decrease by repeating the tests, and the third and fourth cycles are almost overlapped having a relative difference of almost 5 mV after 20 minutes of self-discharging which is about 0.2 % of the rated voltage of this SC (2.7 V). The fifth test is performed after two days and as can be seen, the voltage drop is less than the first charge and more than the rest. The relative difference between this curve and

the fourth after 20 minutes is less than 3 % of the rated voltage (about 70 mV). In the zoomed part, it can be seen that the charging time is going to be shorter as we repeat the cycles and the most difference is almost 1.5 seconds which is between the first and the second charging times, and the others are so close to each other and have the difference less than 100 milliseconds. This proves the importance of the training to reach repeatability. Likewise, if a SC remains inactive even for some days, it undergoes a relaxation and redistribution phase, resulting in a lower output voltage during self-discharge compared to a trained capacitor. This phenomenon is analogous to that previously described.

Fig. 3.9.b), shows the same tests on the second SC with the same size and manufacturer, this SC shows the same behavior as the first SC and after four cycles, the voltage discharge curves are so close to each other, for example the difference between the fifth and the sixth terminal voltage curve after 20 minutes of self-discharging is less than 1 mV which means 0.03% of the rated voltage of this SC, while this difference between the first and the second curve is 180 mV means 6.7% of the rated voltage. The difference between the first and second charging time is almost one second, and between the other successive curves it is less than 400 milliseconds.

As shown in Fig. 3.9.c), for the third SC, the same experiments are done but with 10 A constant current. The first six cycles of this SC show by repeating the cycles the self-discharge voltage curves are going to be closer to each other. The first and the second voltage curves have almost 150 mV difference after 20 minutes and the fifth and sixth curve are almost overlapped by having 5 mV difference after the same duration of self-discharge. These values are correspondence to 5.5% and 0.18% of the rated voltage, respectively. The difference between the charging times of the different cycles of this SC is also more than the other two SCs, which is about 7 seconds for the first and second cycles and less than 500 milliseconds between the other successive curves.

3.4 Training of SCs

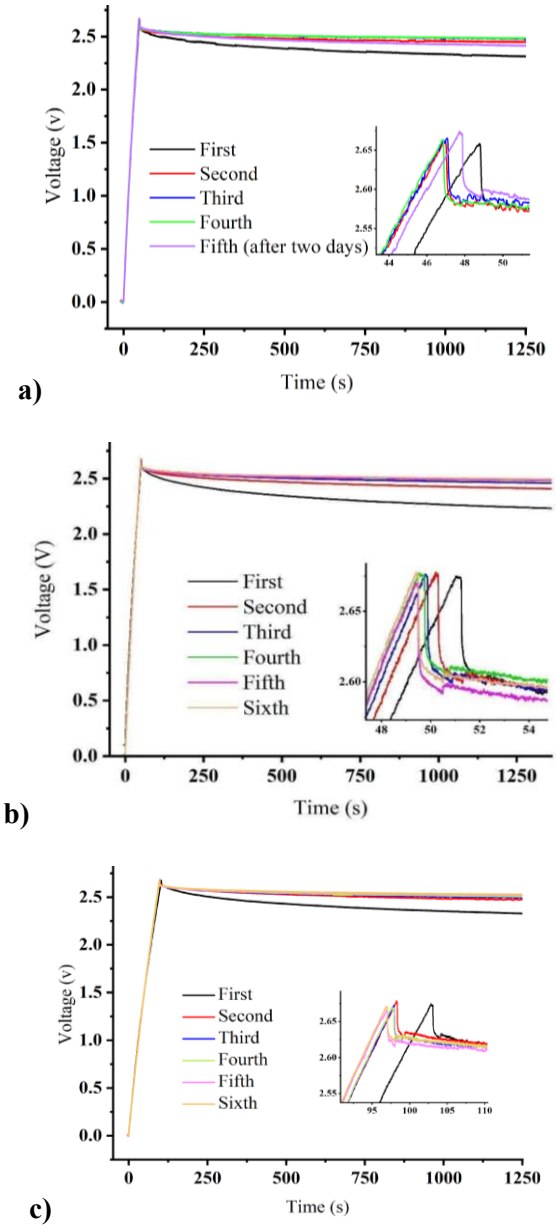

Figure 3.9. Training of three unused Eaton XV series 400 F SCs to reach a stable output voltage. First charge and self-discharges for a), b) first and second SCs with charging current of 20 A, c) the third SC with charging current of 10 A

By carrying out further training and adding 30 minutes of constant voltage charging phase between the charging and self-discharging cycles, it was found that this significantly increases the repeatability of the device.

This kind of tests were performed on another SC of 1500 F (its main specification is given in Table 3.1) on different days. After approximately ten complete cycles, the charge, constant voltage and self-discharge cycle repeatability become acceptable even for larger, new SCs or SCs subjected to long stand-by phases. Fig. 3.10 shows the training (only charge and self-discharge cycles) of the 1500 F SPS-CAP SC whose training was recorded from its state 'just purchased, new'. Its training performance is typical and similar to that of the other two SCs. Fig. 3.10.a) shows the first six cycles performed on a SC on the first day, whereas Fig. 3.10.b) shows the same number of cycles performed the following day. At this point, a reasonable repeatability is achieved, which is maintained even after several days. Fig. 3.10.c) and 3.10.d) show the cycles repeated five and six days after the previous cycles. Fig. 3.11.a) shows in full scale the set of all the cycles of all the days, while Fig. 3.11.b) shows in full scale all the cycles, except for the first ten cycles. The last figure represents the cycles suitable for the study of repeatability and that of the training should be discarded. As shown in [80], there is better repeatability in the charging phase than in the self-discharge phase. Because the cycles do not perfectly overlap, this implies a certain variability in the circuit parameters. To evaluate such variability, it is necessary to have a large group of charging and self-discharging curves, where the equivalent circuit parameters are identified for each. Because this process is time-consuming, once the training is performed, it is sufficient to record a number of curves greater than or equal to the circuit unknowns, which are seven in the three-branch model. Generally, 10 or 12 curves are sufficient for an overdetermined system to assess the parameter variability. As discussed in the next chapter; by applying the proposed method, it is possible to reconstruct the parameter variability starting from a single identification procedure.

3.4 Training of SCs

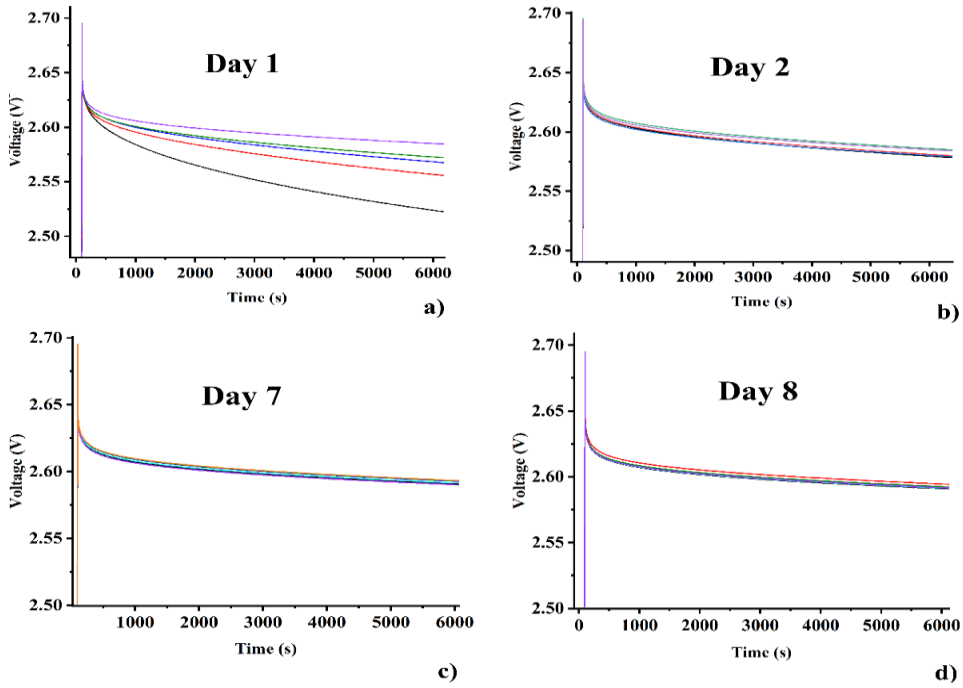

Figure 3.10. Charge and self-discharge diagrams for a 1500 F SC (SPSCAP SCP 1500C0-0002R7STA), a), b), c) and d) repeated and measured on different days.

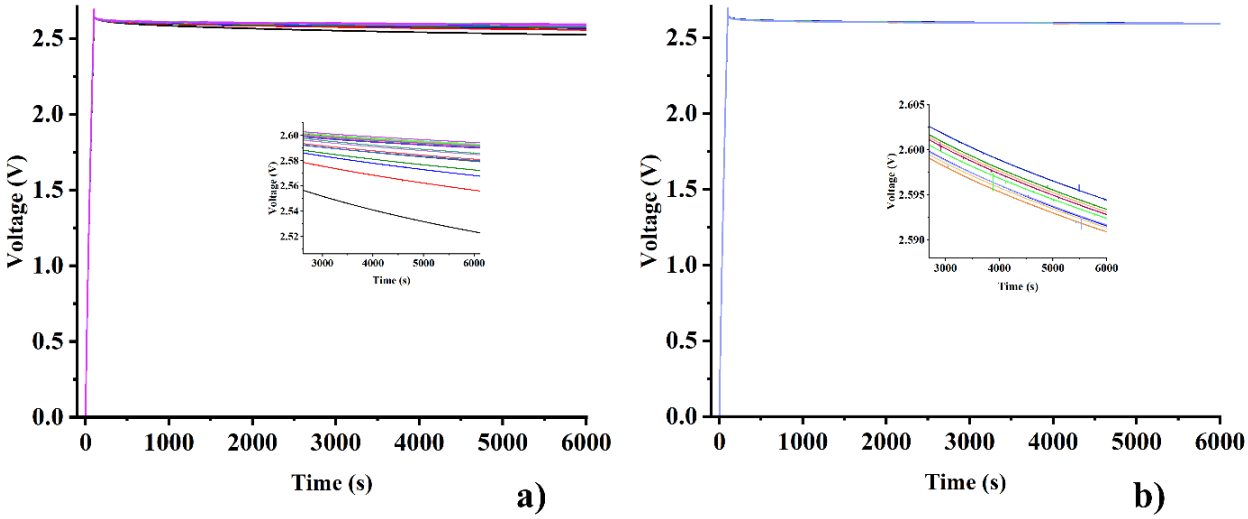

Figure 3.11. Charge and self-discharge diagrams for a 1500 F SC (SPSCAP SCP 1500C0-0002R7STA) a) the overall full-scale diagram of all cycles and b) the diagram of all cycles except the first 10.

Generally, the models proposed for SCs are designed to identify a 'trained' SC. Also, the analysis in this study refers to trained SCs. In this way, each experiment starts from a known and possibly repeatable condition.

Based on the experience developed during this thesis, effective training is therefore summarized as follows.

1) Complete discharge of the SC with a negative constant current and then reducing the current up to a residual voltage below 1 mV.
2) Charging the SC with constant current up to the rated voltage;
3) Charging the SC at constant voltage, at the rated voltage for 30 minutes;
4) Complete discharge of the SC with a negative constant current and then reducing the current up to a residual voltage below 1 mV.
5) Charging the SC with constant current up to the rated voltage;
6) Self-discharge of the SC for a time which is related to the slow time constant (see next chapter, for a 400 F SC is about 90 minutes).
7) Repeat the previous steps in order to achieve good repeatability, which means differences in the measured voltage behaviors of the self-discharge phase below a certain threshold. Such a threshold depends on the size of the SC and should be below 20 mV. Usually from 5 to 10 cycles are needed to reach repeatability.

The training performed on all our DUTs follow the same steps, but with different constant current and voltages suitable for each SC. The diagram of the training for a 400 F SC is shown in Fig. 3.12.

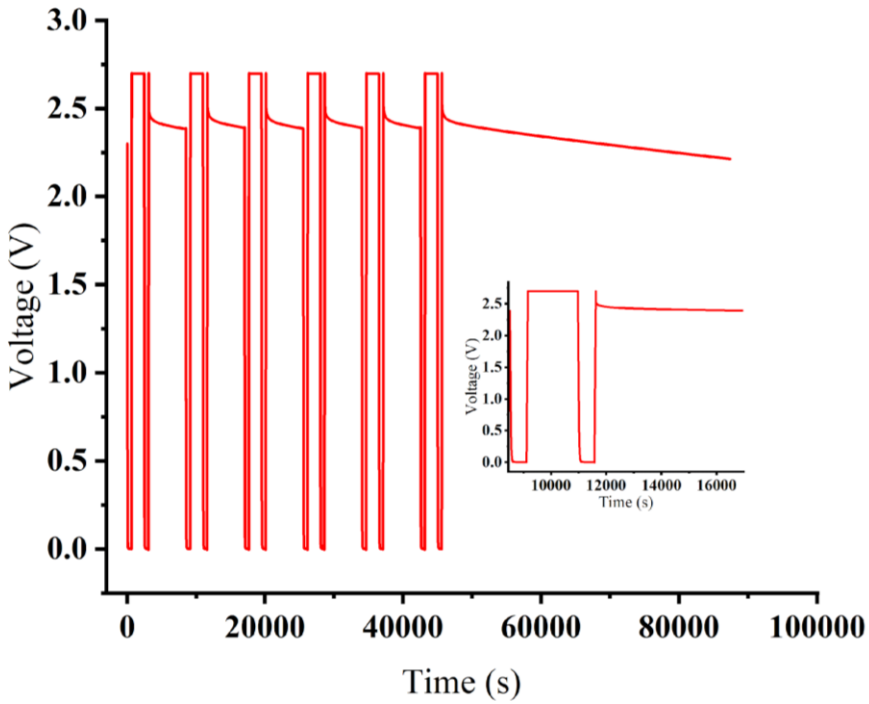

Figure 3.12. Sample of the training on an Eaton 400 F SC.

3.5 Repeatability of SCs with training

After performing the training described in the previous section, some tests are done under repeatable conditions on some SCs of different sizes and the results for a 60 F SC is reported in this section. These tests are performed to firstly observe the closeness of the voltage curves of the SCs which is known as repeatability of the measurements and already defined in Sect.3.3.1, secondly, to identify the parameters of the equivalent circuit of the considered SCs, and thirdly to compare these measured voltage curves with the simulated voltage curves resulting from the equivalent circuit (fully described in the next chapter). The sampling frequency for all these tests is 1 kS/s.

For the 60 F SC, the tests are done with the constant charging current of 5 A on four different days during the time interval of eleven days. On each day, 8 tests are performed, and the duration of the self-discharge phase is 5000 seconds, which is enough also for parameter identification of this SC. The resulting voltage-time behavior curves of these tests limited to charge and self-discharge cycles are shown in Fig. 3.13. Fig. 3.13.a), b), c), d) diagrams, show the voltage curves on each single day. As expected, on the first day the

repeatability is the worst (43 mV voltage difference between the curves after 5000 seconds), and as the tests are repeated more and more in successive days the curves are going to be closer to each other (about 10 mV voltage difference), which in other words means better repeatability (Fig. 3.13.b), c)). On the other hand, if the SC goes under a rest phase for some days (in this case six days (Fig. 3.13.d)), the repeatability decreases (about 30 mV difference), but it is still better than the first day.

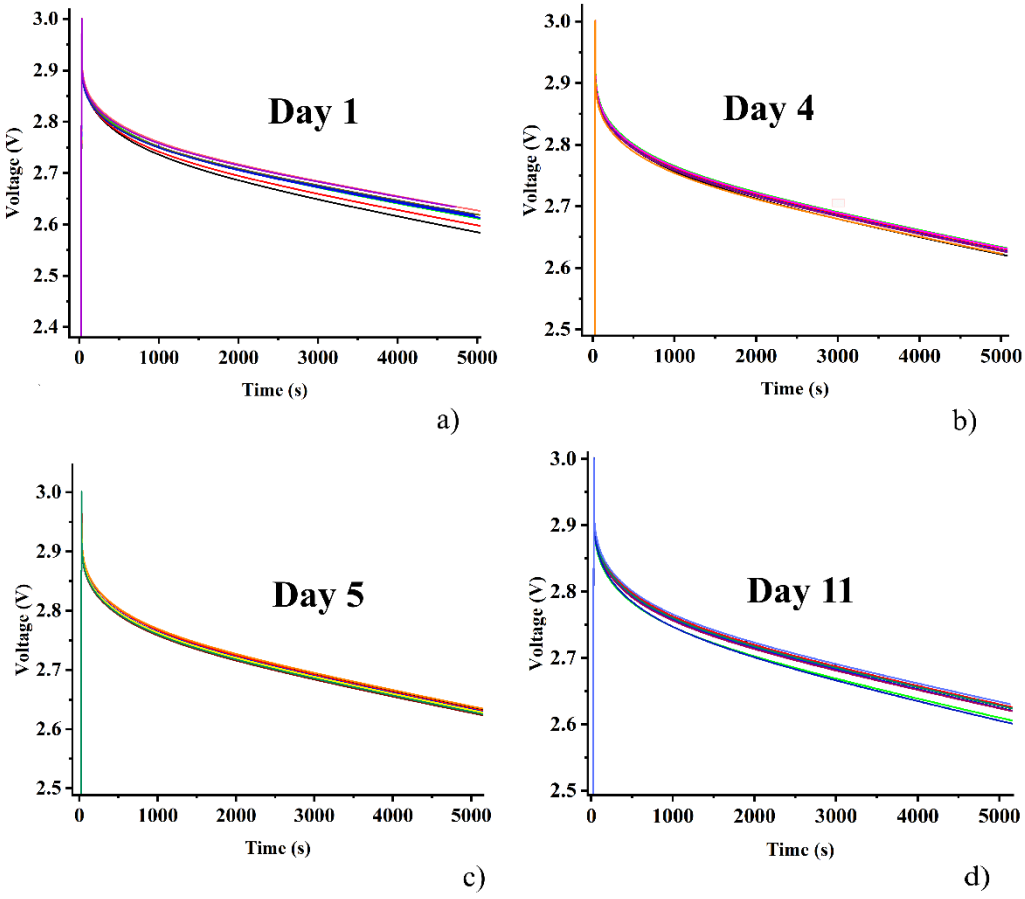

Figure 3.13. Charge and self-discharge diagrams for a 60 F SC a), b), c) and d) repeated and measured on different days.

In Fig 3.14.a) all the 32 curves and their zoomed version can be seen in one graph which shows the maximum voltage difference of 68 mV (2.26 % of the rated voltage) after 5000 seconds, and finally Fig 3.14.b) shows all the curves except the first seven curves with the zoomed version. It can be seen in this figure that by ignoring the first seven curves, the maximum voltage difference

after 5000 seconds reduces to 17 mV (0.5 % of the rated voltage) and the curves are repeatable enough.

In the next chapters, the measurements data are related to SCs that have undergone the training described in Sect. 3.4 and shown in Fig. 3.12.

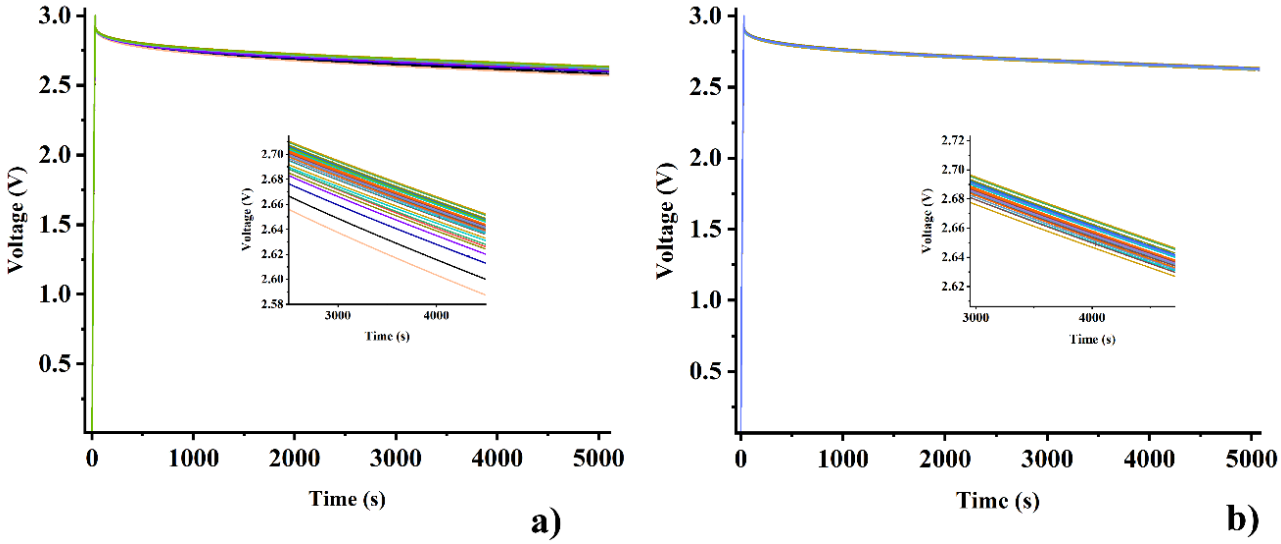

Figure 3.14. Charge and self-discharge diagrams for a 60 F SC a) the overall full-scale diagram of all cycles and b) the diagram of all cycles except the first 7.

Chapter 4

Modeling and parameter identification of SCs

4.1 Introduction

In recent years, modeling of SCs has become an important tool for predicting their performance and optimizing their design. A model can provide a mathematical representation of the physical and chemical processes that occur in a SC, allowing researchers to simulate its behavior and predict its performance under different operating conditions. Furthermore, electrochemical models can provide insight into the underlying mechanisms that determine the performance of SCs, which can help in the development of improved electrode materials, electrolytes, and device architectures.

This thesis focuses on behavioral/phenomenological models based on equivalent circuits. Several equivalent circuit models (ECMs) have been developed to describe the behavior of SCs. Such models are necessary to provide a full representation of SC parameters and the electrical behavior. They are also necessary to control the SCs in charge management systems (CMS) especially in parallel to batteries and battery management systems (BMS).

The choice of the correct ECM depends on the accuracy required and on the level of complexity that can be accepted, also considering the computational burden. In this thesis it was decided to focus our investigation on the three-branch model which is a good compromise between accuracy and complexity. A new identification method for the assessment of the improved three-branch model has been tuned during this thesis work, which is described and discussed in this chapter.

Furthermore, in this chapter, the variable leakage resistance (discussed earlier in Chapter 2), is introduced. The results reported here have been preliminarily published in the paper [12].

4.2 ECMs state-of-the-art

A lot of ECMs with different layouts are presented in the literature for SCs. However, some require time-consuming procedures that are difficult to implement by designers, others show a lack of accuracy, and in a few studies, it is not clear how to identify some parameters.

A comprehensive review of the metrics, mechanisms, and models of SCs can be found in [17], [94]- [100], and some electrochemical models, intelligent models, and thermal models are presented in [17], [95], [101]. Other alternative ECMs are the fractional-order models. With a different mathematical approach, they exhibit good capabilities of fitting experimental data with fewer model parameters. Examples are reported in literature following time domain [102]- [106] or frequency domain approaches [107], [108].

In the following, the most important equivalent circuit models presented for SCs are mentioned and can be seen in Fig. 4.1.

The one branch model is shown in Fig. 4.1 a), whereas Fig. 4.1 b) and Fig. 4.1 c) show a three-stage ladder model [109] and the so-called dynamic model [110], respectively. A comparison between these three models is discussed in [111]. The one-branch model is suitable for a rough design of storage systems but lacks the accuracy required to properly reproduce the behavior of SCs. Fig. 4.1 d) shows the two-branch model analyzed in [112] and [113]. In [114], the authors proposed an optimization of a two-branch equivalent circuit that matches the experimental data with a mean relative discrepancy ranging from 0.5 % to 4 %, depending on the current. The transmission line model is a generalization of the three-stage ladder model, as shown in Fig. 4.1 e). In [96], the authors compared three models: i) the RC model, ii) the two-branch model, and iii) a multi-branch model with respect to the experimental results shown in [115]. The comparison reveals that the multi-branch model better satisfies the experimental results. Fig. 4.1 f) shows a modified two-branch circuit [116], while Fig. 4.1 g) is the well-known three-branch Zubieta-Bonert model [117]. Fig. 4.1 h) represents a combination of configurations 4.1 f) and 4.1 g), which is particularly suitable for real-time modeling [118].It is worth mentioning that in the two-branch model and the three-branch model shown in Fig 4.1 d), g), the last branch containing the leakage resistance R_{lea} is not part of the

dynamic response of the supercapacitor in terms of seconds, minutes or hours, but R_{lea} is a parameter added to describe the self-discharge behavior of the SC in many hours, days or weeks. So, this parameter that mimic internal leakage phenomena, is not part of the dynamic circuit of the SC but is introduced in the equivalent circuit for completeness. In a simulation of the dynamic behavior of a SC can be safely disregarded. For this reason, R_{lea} is not considered as a branch of the equivalent circuit in numbering the branches of the model.

Generally, the models are designed to identify the trained SC. In fact, a new SC exhibits different behavior than an operating SC, as already discussed in Chapter 3, Sect. 4.

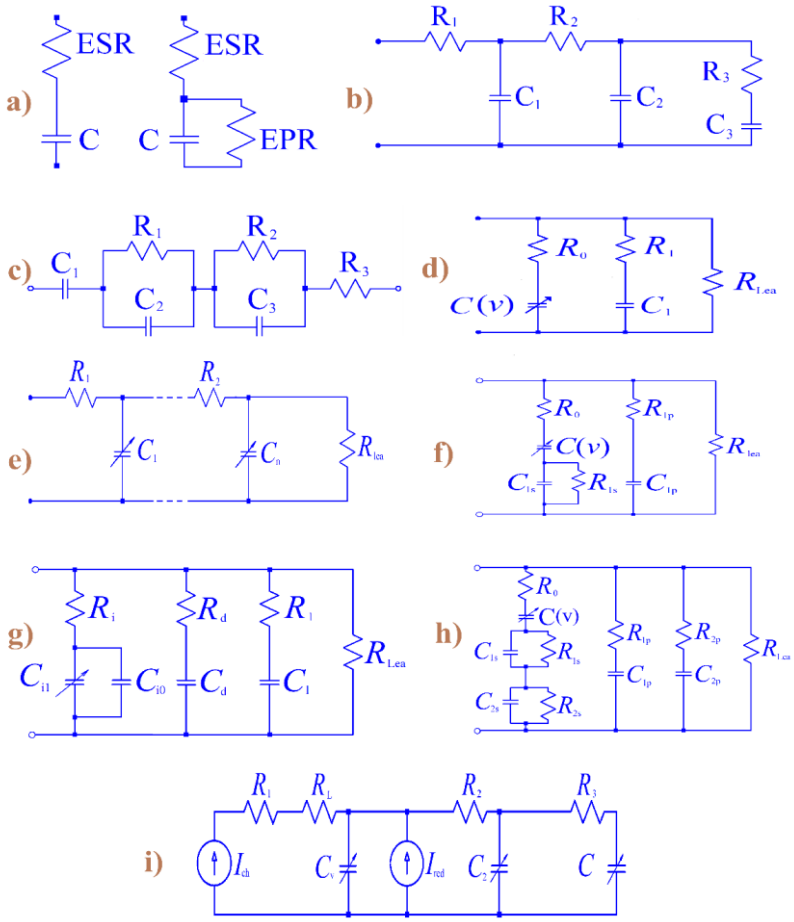

Figure 4.1. Equivalent circuit models of SCs: a) one branch model, b) three-stage ladder model, c) dynamic model, d) two-branch model, e) transmission line model, f) modified two-branch circuit, g) three-branch Zubieta-Bonert model, h) De Carne and colleagues' model, i) Torregrossa and colleagues' model.

The model is built for a SC that starts from a known and possibly repeatable condition and is then controlled over time. Once training has been carried out on the SC, possibly repeated after a long period of relaxation, so that the charge-self-discharge cycle is repeatable, a reference condition is defined. The parameters of the proposed ECM are defined under this condition.

4.3 The three-branch equivalent circuit

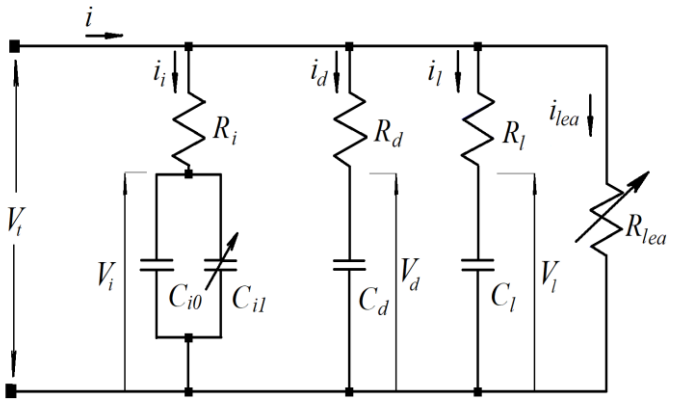

Figure 4.2. Three-branch equivalent circuit of a SC.

Compared to the classical three-branch model in literature, in this study a variable leakage resistance is introduced, whose original computation has already been discussed in Chapter 2. This variable leakage resistance is extremely important for the simulation of the behavior of the SC during long lasting time self- discharges.

The three-branch equivalent circuit can provide an excellent simulation of the behavior of SCs with limited complexity. Unlike the two-branch approach, the three-branch circuit allows the simulation of real-time behavior over a long timespan. The SC is charged with a constant current i up to the rated voltage (voltage peak); subsequently, the charging current drops to zero, and the SC undergoes a self-discharging phase, mainly owing to the relaxation and charge redistribution phenomena. The three-branch model proposed in [117] is illustrated in Fig. 4.2 improved with the variable leakage resistance. Each branch has its own time constant, and it makes measuring the parameters of the model easier. The first, second, and third branches are called immediate, delayed, and long-term branches respectively based on their time constants. The first or immediate branch with parameters R_i , C_{i0} , and the voltage-dependent capacitor C_{i1}represents the charging phase of the SC and has the time range of seconds. The second or delayed branch with parameters R_d, C_d , represents the terminal behavior in the durations of

minutes, and finally the third or long-term branch with parameters R_l , C_l represents the SC behavior for times more than 10 minutes up to one or two hours. To simulate the further self-discharge of SCs, the non-linear leakage resistor R_{lea} is added. This qualitative explanation does not properly describe the interdependence between the three branches. For what concern R_{lea}, there are limited references in the literature describing a method to assess this parameter [12], but here we refer to the method described in Chapter 2.

The behavior of a SC capacitance shows a voltage-dependent characteristic, but in [103], for simplicity in calculation, it is common approach to consider the capacitance non-linearity only in the first branch. To do so, a voltage dependent capacitor called C_{i1} is introduced in the model.

To calculate the voltage-dependent capacitance of this model, we can't use the linear definition of the capacitance ($C = \frac{Q}{V}$) as its capacitance does not follow this linear trend. The differential capacitance is used to show the change of charge at a given voltage as in Eq. (4.1). In this equation, Q is the stored charge in the SC and dQ and dV are, i) the charge variation and ii) the voltage variation, due to charging or discharging, respectively. The differential capacitance is represented by a constant capacitor (C_{i0}) in parallel to a voltage-dependent capacitor C_{i1} in ECM.

$$C_{diff} = \frac{dQ}{dV} \tag{4.1}$$

$$C_{diff} = C_{i0} + C_{i1}V \tag{4.2}$$

However, by neglecting R_{lea} as a first approximation, an easy estimation of the other seven circuit parameters in Fig. 4.2 can be obtained according to [117].

4.4 First branch optimization

As also verified by other authors (e.g., [91], [120], [121]), the approach proposed in Zubieta-Bonert [117] tends to underestimate the final voltage of the SC in the charging phase; therefore, at least an optimization of the first branch parameters is required to improve the accuracy.

A simple and effective optimization of the Zubieta-Bonert model can be achieved as follows. The voltage on the first branch capacitors can be expressed as where $Q_i(t)$ is the charge stored in the SC versus time and t is the time and C_i is as defined in Eq. (4.2). The current i_i during charging is equal to the total charging

current, as the current of the other branches are negligible. So, this is the imposed charging current, which is an input and is usually coming from measurement.

$$V_i(t) = \frac{Q_i(t)}{C_i} = \frac{\int_0^t i_i dt}{C_{i0}+C_{i1}V_i} = \frac{i_i t}{C_{i0}+C_{i1}V_i} \tag{4.3}$$

so

$$C_{i1}\, V_i^2(t) + C_{i0}\, V_i(t) - i_i\, t = 0 \tag{4.4}$$

$V_i(t)$ can be obtained by solving Eq. (4.4), where only the positive solution has a physical meaning as follows.

$$V_i(t) = \frac{\left(-C_{io}+\sqrt{C_{io}^2+4C_{i1}i_i t}\right)}{2C_{i1}} \tag{4.5}$$

The terminal voltage in the ECM shown in Fig. (4.2) can be obtained as Eq. (4.6) and in Eq. (4.7), the objective function to be minimized is defined as the difference between the measured terminal voltage $V_{tmeas}(t)$ and the terminal voltage V_t obtained by the model.

$$V_t = V_i + R_i\, i_i \tag{4.6}$$

$$f_{obj}(t) = V_{t_{meas}}(t) - V_i(t) - R_i i_i \tag{4.7}$$

Therefore, by substituting $V_i(t)$ from Eq. (4.5) in Eq. (4.7), the objective function $f_{obj}(t)$ is defined as

$$f_{obj}(t) = V_{t_{meas}}(t) - \frac{\left(-C_{io}+\sqrt{C_{io}^2+4C_{i1}i_i t}\right)}{2C_{i1}} - R_i i_i \tag{4.8}$$

Starting from the initial parameters $z_0 = (C_{io}, C_{i1})_0$ identified according to [103], the function $f_{obj}(t)$ is nonlinear. Therefore, a nonlinear minimization approach is required to optimize the vector parameter $z = (C_{io}, C_{i1})$. This can be achieved by solving a nonlinear least-squares problem, where $f_{obj}(t)(z)$ is a vector, with *n* elements being the function values at each measured time sample $V_{tmeas}(t)$. So that

$$f_{obj}(z) = \left[f_{obj1}(z)\, f_{obj2}(z) \,\vdots\, f_{objn}(z)\right] \tag{4.9}$$

The nonlinear least-squares problem can be solved efficiently in the Matlab™ environment using the 'lsqnonlin' function, according to the command:

z = lsqnonlin ($f_{obj}(z), z_0$). As the output, the function returns the optimized parameters $z_{opt} = (C_{io\_opt}, C_{i1\_opt})$ with a CPU time lower than one second, on a common personal computer.

In order to make a comparison between the optimized model above described and the real behavior of a SCwe have made a comparison for our first Eaton 400 farads SC. The comparison is made between Zubieta model, Zubieta optimized model just described, RC model with physical capacitance, RC model with nominal capacitance and the real acquisition. For identification of the ECM parameters of the DUTs in this thesis, a LabVIEW program performs the acquisitions and a MATLAB program elaboratedthe acquired charging and self-discharging data identifying and optimizing the circuit parameters that are utilized for the simulation of the ECM. The measured and simulated voltage curves are compared in the diagram as shown in Fig. 4.3, using as input the profile data of the charging current.

A comparison between the measured values and those obtained using the optimized model is shown in Fig. 4.3 a). In the same figure, the results of the one-branch model and of the model [117] are also shown for completeness. As can be seen, the closest modeling approach to real behavior is Zubieta optimized model.

The Zubieta optimized model is the best among others in this comparison. The Zubieta model clearly has a voltage bias that must be corrected by the optimization. The simple RC model has a higher voltage drop than measurements and in the self-discharge phase does not show a voltage decrease since neither long time-constant branch are present nor leakage resistance.

Fig. 4.3 b), shows the absolute voltage difference between the measured and computed values using the optimized model. The maximum discrepancy of 0.11 V, corresponding to a relative difference of 4 % with respect to the rated voltage, occurs when the voltage peak drop is reached, and is mainly due to a time-shift introduced by the model. Except for this peak error, in most of the considered timespan, the error does not exceed 1.5 % (± 0.04 V). After a few hundred seconds, the error shows an increasing trend with time. Indeed, the model does not seem to be suitable for long stand-by phases of the SC. To overcome this problem, a new high-accuracy modeling approach is proposed.

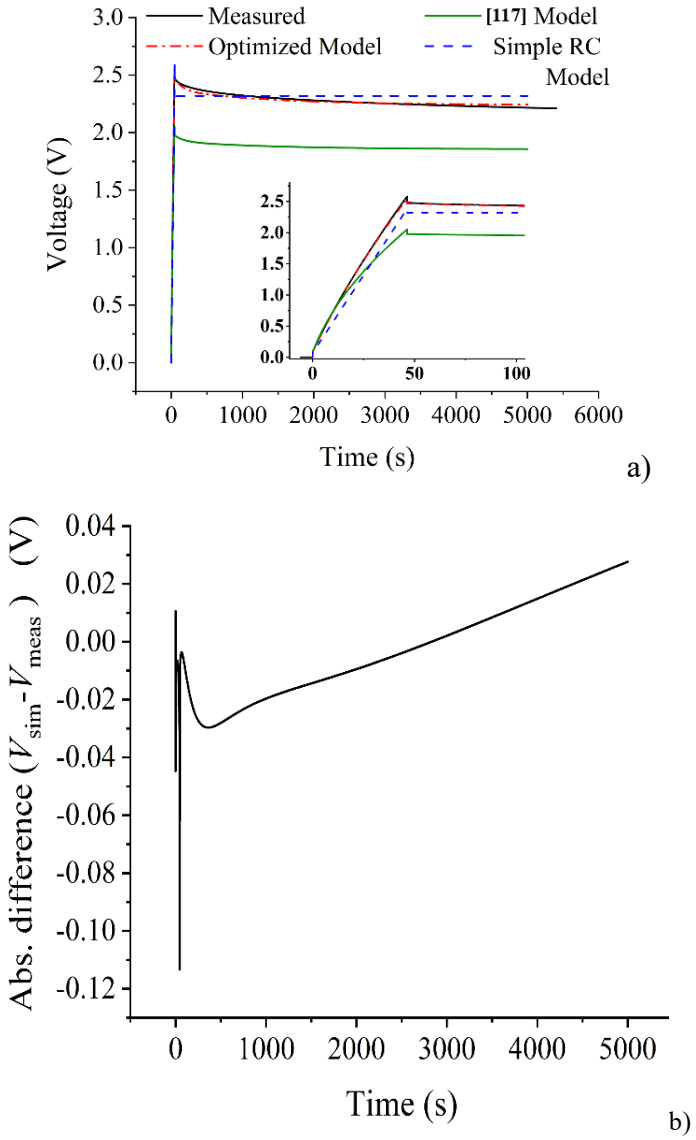

Figure 4.3. a) Comparison between the measured galvanostatic charging and self-discharging for the: i) one-branch model (simple RC), ii) Zubieta model, and iii) optimized model. b) Absolute difference between the measured voltage and the one computed through the optimized [103] model.

4.5 Settling time and R_{lea} introduction

Following the charging of the SC, once the rated voltage is reached and the charging current ceases, a self-discharge process occurs, which can be divided into three parts. In the first part, there is a sudden voltage decrease near the peak, lasting a

few milliseconds to tens of milliseconds, corresponding to the voltage drop in the internal resistance when the current ceases. Then, in the second part, the voltage decreases owing to the charge redistribution between the three branches of the equivalent circuit, which lasts for approximately a few hours (Fig. 4.4). Finally, in the long-lasting third part (which can extend for many hours or even days), the voltage decreases owing to the internal electrochemical phenomena. The last part is considered in the model by the leakage resistance R_{lea} which is simply a representation of the phenomenon, even if its physical/chemical nature is likely not only resistive.

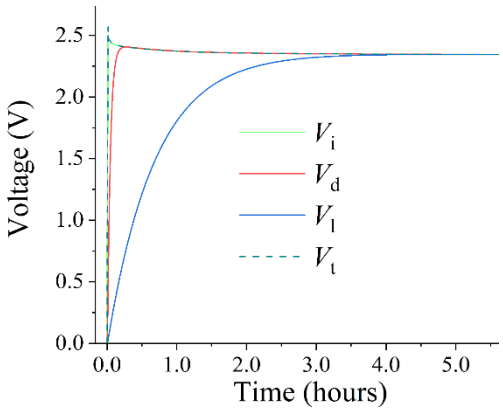

Figure 4.4. Computed behavior of the SC terminal voltage V_t during charging and self-discharging lasting 6 hours. The figure shows also the behavior of the voltages of the capacitors C_{i0} and C_{i1} (V_i), C_d (V_d), and C_l (V_l) of the equivalent circuit (Fig. 3). A 400 F SC was considered.

During self-discharging the voltage decreases owing to the charge redistribution between the three branches of the equivalent circuit. Finally, in the long-lasting self-discharge lasting from a few hours to many hours or even days, the voltage decreases owing to the internal electrochemical phenomena. This last part is considered in the model by the leakage resistance R_{lea}. In the model without R_{lea}, the voltage remains constant indefinitely when the three branches reach an equilibrium, which is not physically reasonable.

Starting from a discharged SC, we can define the time from the beginning of the SC charging, up to the time where the equilibrium between the internal capacitances is reached, as 'settling time' (ST). This time is approximately 4 hours for the considered DUT (Fig. 4.4). For a specific SC, the ST can be verified using the SC model described in Sect. 4.6. R_{lea} is introduced in the simulation after the ST.

4.6 State equation-based model

An alternative to the classical identification of the Zubieta-Bonert model presented in [117] has been developed in the framework of this thesis work and was published in [12].

The idea is again to make reference to a charge-long self-discharge cycle and to obtain the parameters of the equivalent circuit by minimization between the equivalent circuit response and the measurements. What is different is the model description in terms of equations.

The approach is based on the circuit state equations, and the resistance R_{lea} is considered constant to the initial value determined at the ST as specified in the previous section.

The vector state equation can be obtained with reference to the circuit shown in Fig. 4.2, as follows

$$\dot{v} = Av + b \tag{4.10}$$

Where $\boldsymbol{v}$ is the vector representing the state variables, which are the capacitor voltages (4.11) and $\dot{v}$ is the time-derivative of the state variables vector (4.12).

$$v = \begin{bmatrix} V_i \\ V_d \\ V_l \end{bmatrix} \tag{4.11}$$

$$\dot{v} = \begin{bmatrix} \frac{dV_i}{dt} \\ \frac{dV_d}{dt} \\ \frac{dV_l}{dt} \end{bmatrix} \tag{4.12}$$

Eq. (4.10) is nonlinear because the matrix of coefficients $\boldsymbol{A}$ depends on V_i, and $\boldsymbol{b}$ is the control vector.

It is possible to start from Kirchhoff equations at circuit nodes like

$$i_l = \ i - i_i - i_d \tag{4.13}$$

and loop equations

$$\begin{cases} V_i - V_d = R_d \cdot i_d - R_i \cdot i_i \\ V_d - V_l = R_l \cdot i_l - R_d \cdot i_d \\ V_l - V_i = R_i \cdot i_i - R_l \cdot i_l \end{cases} \tag{4.14}$$

by considering that currents are the time derivatives of capacitors charge as:

$$\begin{cases} i_i = \frac{dQ_i}{dt} = C_i(V_i) \cdot \frac{dV_i}{dt} \\ i_d = \frac{dQ_d}{dt} = C_d \cdot \frac{dV_d}{dt} \\ i_l = \frac{dQ_l}{dt} = C_l \cdot \frac{dV_l}{dt} \end{cases} \tag{4.15}$$

Concerning the first equation in (4.15) we can better specify that:

$$i_i = \frac{d}{dt}[(C_{i0} + C_{i1}\, V_i(t))V_i(t)] = C_{io}\, \frac{dV_i}{dt} + 2\, C_{i1}\, V_i\, \frac{dV_i}{dt}$$

so that $C_i(V_i)$ is:

$$C_1(V_i) = C_{i0} + 2C_{i1}V_i \tag{4.16}$$

Combining (4.13) and (4.13), one can obtain the currents as a function of the state variables, of the resistances, and of the total input current *i*. By substituting the right side of (4. 15) to currents, matrix ***A*** and vector ***b*** can be easily computed as follows

$$A = \begin{bmatrix} \frac{-(R_d+R_l)}{den \cdot C_1(V_i)} & \frac{R_l}{den \cdot C_1(V_i)} & \frac{R_d}{den \cdot C_1(V_i)} \\ \frac{R_l}{den \cdot C_d} & \frac{-(R_l+R_i)}{den \cdot C_d} & \frac{R_i}{den \cdot C_d} \\ \frac{R_d}{den \cdot C_l} & \frac{R_i}{den \cdot C_l} & \frac{-(R_i+R_d)}{den \cdot C_l} \end{bmatrix} \tag{4.17}$$

$$b = \begin{bmatrix} \frac{R_d\, R_l\, (i-i_{lea})}{den \cdot C_1(V_i)} \\ \frac{R_l\, R_i\, (i-i_{lea})}{den \cdot C_d} \\ \frac{R_i\, R_d\, (i-i_{lea})}{den \cdot C_l} \end{bmatrix} \tag{4.18}$$

where:

$$den = R_iR_l + R_iR_d + R_dR_l \tag{4.19}$$

When (4.10) is solved, the SC terminal voltage can be obtained as (4.20).

$$V_t = \frac{R_d\, R_l\, V_i + R_i\, R_l\, V_d + R_i\, R_d\, V_l + R_i\, R_d\, R_l\, (i-i_{lea})}{den} \tag{4.20}$$

4.7 Optimization based on state equations

Model identification is performed by comparing the model results and experimental measurements within a timespan that is limited but sufficient to allow each of the three branches to affect the terminal voltage of the SC. In our experiments, we verified that one-third of the ST is sufficient for a good model identification.
The optimization is obtained using the objective function, which is the difference between two voltages, the one at the terminals of the SC simulated by the model $V_t(t)$ and that measured in the laboratory at the SC terminals $V_{tmeas}(t)$. In addition to the objective function, the optimizer requires some other input data: i) the model equations (matrix $\boldsymbol{A}$ and vector $\boldsymbol{b}$), ii) an initial value of the parameters to be identified (R_d, R_l, C_{i0}, C_{i1}, C_d, C_l,)$_0$, iii) the initial value of R_{lea} and of the state variables $(V_i, V_d, V_l)_0$, and iv) the value of R_i.

The nonlinear optimizer that we found effective is based on the family of Conventional Trust Region Reflection (CTRR) algorithms [122], [123]. If the optimization algorithm reaches the convergence threshold set by the user, optimized parameters are provided.

An efficient tool that implements the CTRR optimization is provided by Matlab™ called "nonlinear grey-box model" parameters estimation, which responds to the command 'nlgreyest' and that can solve the optimization problem of the circuit, which is summarized in Fig. 4.5.

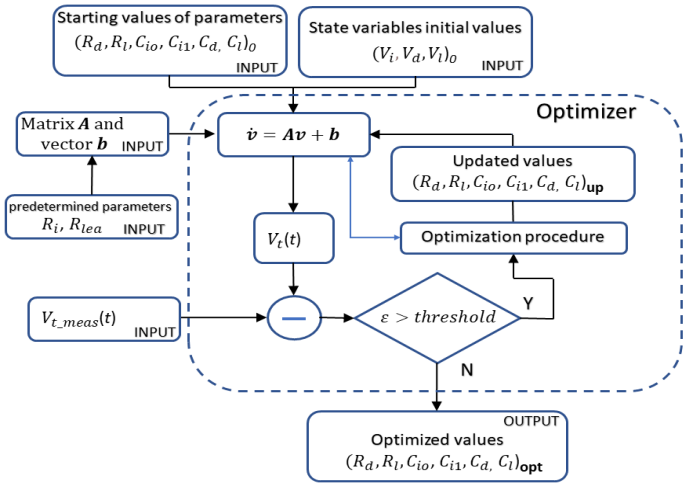

Figure 4.5. Basic scheme of optimization based on state equations. Optimal parameters search is based on CTRR optimization.

Two clarifications regarding the initial parameters. It should be noted that the resistance R_i is missing. R_i is defined as in [117] by the voltage drop at the starting of the charging. If I_{ch} is the charging current a voltage drop on the *ESR* R_i is observed both at the beginning of the charging (the voltage immediately passes from 0 to ΔV) and at the end of the charging phase, as shown in Fig. 4.6 (when the rated voltage is reached and the current suddenly drops to zero).
The resistance can be computed in both cases as

$$R_i = \frac{\Delta V}{I_{ch}} \tag{4.21}$$

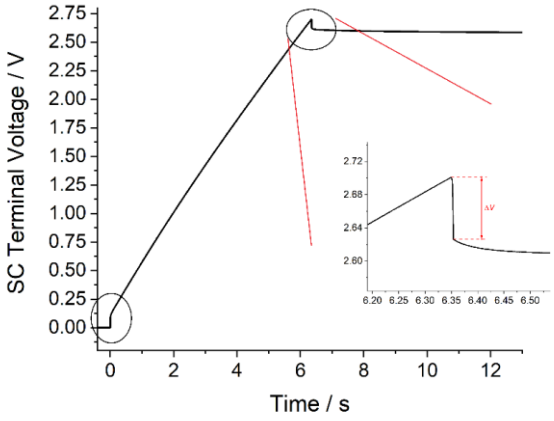

Figure 4. 6. Charging and self-discharging of a 1 F SC tested at INRIM.

Regarding the other parameters, it is not necessary to have particularly accurate initial parameters; however, coarse parameters are sufficient for the convergence of the algorithm. Prior identification of the parameters, as in [103], is not necessary but is welcomed, making the convergence of the method quicker. Finally, the initial values of the state variables are equal to zero, and the initial value of R_{lea} must be identified according to Sect. 4.5.

A point worth of attention is the presence of a bias in the measured current, which is the input for the model, together with the measured voltage at the SC terminals, V_t. Even a very small bias of a few milliamperes, when the current approaches zero, can provide significant variations in the model results.

4.8 Sensitivity analysis

Starting from the state equation-based model, a sensitivity analysis was performed by varying one circuit component value (resistance or capacitance) at a time of ± 5 % and ± 10 % with respect to the identified nominal value in the considered DUT. The variations in the SC terminal voltage owing to the variations in the resistance and capacitance values are shown in Fig. 4.7 for the parameters R_i, R_{lea}, C_{i0}, C_{i1}, and Fig. 4.8 for the parameters R_d, C_d, R_l, C_l. From this analysis, some interesting clues can be deduced regarding the sensitivity of the model output to the circuit parameters and the choice of an appropriate timespan for parameter optimization. Fig. 4.7a) shows the variation in the SC terminal voltage V_t owing to the relative variation in the input resistance R_i and clearly shows that the variation in the voltage is associated with the variation in the input current. Fig. 4.7.b) shows the effect of R_{lea} variations on the terminal voltage. As shown, the variations in R_{lea} affect the output voltage less significantly than other parameters, but its influence increases with time. However, if R_{lea} is not properly chosen or measured and its order of magnitude is incorrect, it can have a significant effect on the identification of the other parameters. Fig. 4.7.c) and Fig. 4.7.d) show the variation in the SC terminal voltage owing to the relative variations in C_{i0} and C_{i1}, respectively. The sensitivity is very high compared with that of the other parameters. This variation is prevalent during the charging phase of the capacitor. The concavity of the variations for these two parameters is opposed, which is appropriate for optimization. Therefore, from the sensitivity analysis, a suitable timespan for the optimization of these two parameters can be approximately equal to the SC charging time of the equivalent circuit first branch. Fig. 4.8.a) shows the variation in the SC terminal voltage owing to the relative variations in resistance R_d. In this case, the sensitivity is more than one order of magnitude lower than that of the previous branch, and the effect is maximum after the voltage peak and becomes negligible in approximately half of the settling time. Fig. 4.8.b) show the variation in the SC terminal voltage owing to the relative variations in the capacitance C_d. Also in this case, the sensitivity is about one order of magnitude lower than that of the first branch parameters and the effect is maximum in about one third of the settling time and then remains almost constant, with a slow decrease. Fig. 4.8.c) and Fig. 4.8.d) show instead the variation of the SC terminal voltage due to the relative variation of the resistance R_l and the capacitance C_l, respectively. Here the initial shape of the graph is similar to those of R_d and C_d, but the time is expanded to about one order of magnitude. The sensitivity is comparable to the other one and, as in the previous case, the sensitivity for the resistance has an opposite sign compared

to that of the capacitance. The different behaviors in time and shape of these graphs, and their similar sensitivities, allow us to consider the optimization of R_d, C_d, R_l and C_l, with a proper choice of the timespan, approximately from the end of the charging of the first branch to the end of the ST of capacitances C_d and C_l (e.g., from 2 minutes to 4 hours in Fig. 4.4).

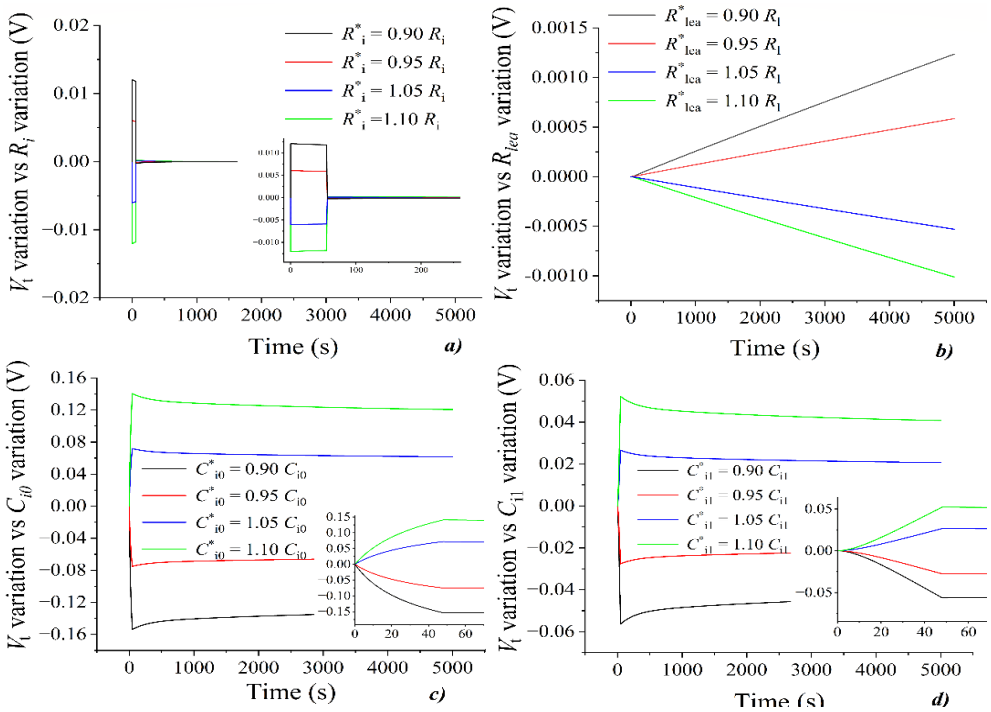

Figure 4.7. Absolute variation (V_t - V^* t) of the SC terminal voltage V_t induced by a variation ± 5 % and ± 10 % of the following parameters: a) Ri, b) R_{lea}, c) C_{i0}, d) C_{i1}, respectively.

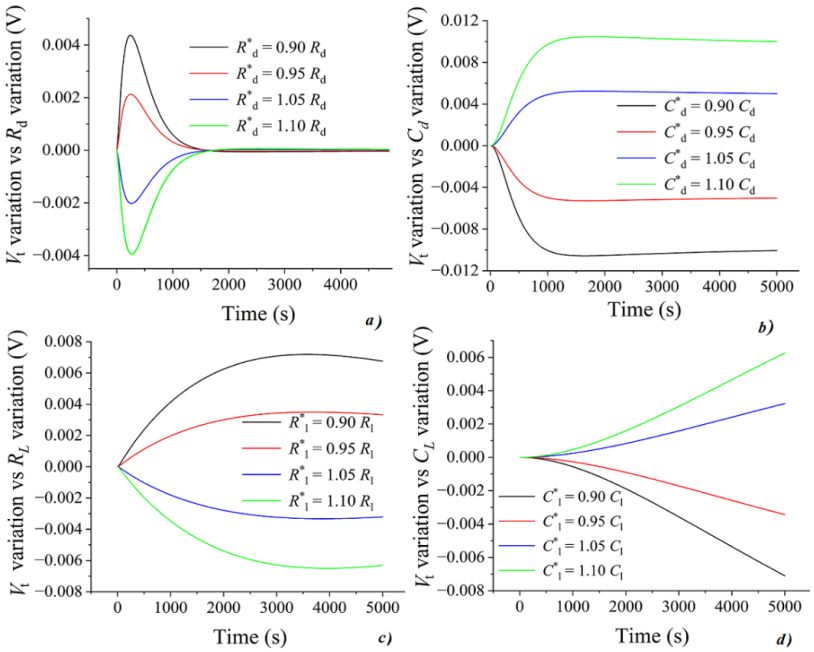

Figure 4.8. Absolute variation (V_t - V^* t) of the SC terminal voltage V_t induced by a variation ± 5 % and ± 10 % of the following parameters: a) R_d, b) C_d, c) R_l, and d) C_l, respectively.

4.9 Model validation

The state equation-based model was used to identify the model of the DUT already considered in Sect. 4.3 and Sect. 4.5, and its parameters are listed in Table 4.1.

Table 4. 1. 400 F SC equivalent circuit parameters.

R_i (mΩ)	C_{i0} (F)	C_{i1} (F)	R_d (Ω)	C_d (F)	R_l (Ω)	C_l (F)
5.69	261.6	33.05	12.74	11.77	189.1	13.4

Fig. 4.9.a) shows the identification results, where the absolute error, calculated as the difference between the terminal voltage computed by the model and that measured, does not exceed 50 mV around the voltage peak, and then settles to values ten times lower. It should be noted that unlike the identification performed in Sect. 4.3 (Fig. 4.3.b), the error does not increase significantly over time. For longer stand-by periods, the previously computed behavior of R_{lea} versus time, as shown in Fig. 4.4), is included in the model. As highlighted in Fig. 4.9.b), the trend of V_t computed with the nonlinear R_{lea} behavior is very close to the measured one,

with discrepancies not exceeding 50 mV. It was pointed out in Sect. 4.5 that the determination of R_{lea} nonlinear behavior is affected by a significant uncertainty and measurements in Sect. 4.5 highlighted variations up to about 40 % in the initial R_{lea} values which are dependent on the choice of the R_{aux}. Due to the small sensitivity of the terminal voltage with respect to R_{lea} variations, as highlighted in Fig. 4.8.b), a variation of ± 40 % in the R_{lea} nonlinear behavior leads to a discrepancy lower than 50 mV with respect to the measured values (< 2 %). Even if the determination of R_{lea} has poor sensitivity with respect to the terminal voltage, this fact does not mean that R_{lea} can be determined only approximately and the procedure for its determination must be better tuned and refined in the future.

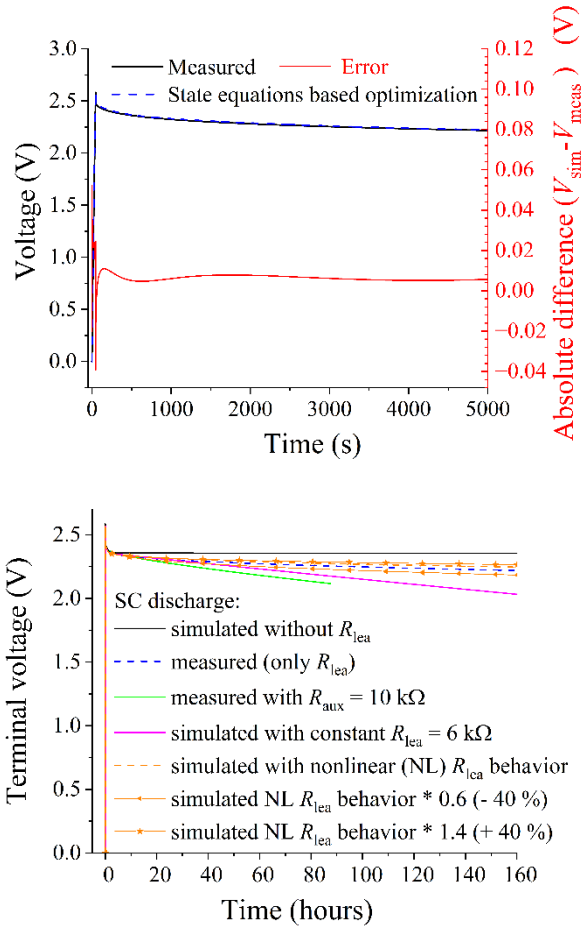

Figure 4.9. Comparison between the voltage measured at the SC terminals and the one computed with the three-branch model identified through the state equations based optimization. The discrepancy ('error') is also shown in red. a) Static model with constant R_{lea}, b) long-term model with variable R_{lea}.

On the contrary, the same diagram highlights that the results obtained with constant R_{lea} clearly show larger discrepancies and are less reliable.

Figs. 4.10.a) and 4.10.b) show how, even under dynamic conditions, without (Fig. 4.10.a) or with (Fig. 4.10.b) a significant stand-by phase, the absolute error with respect to the measurements remains limited to 50 mV.

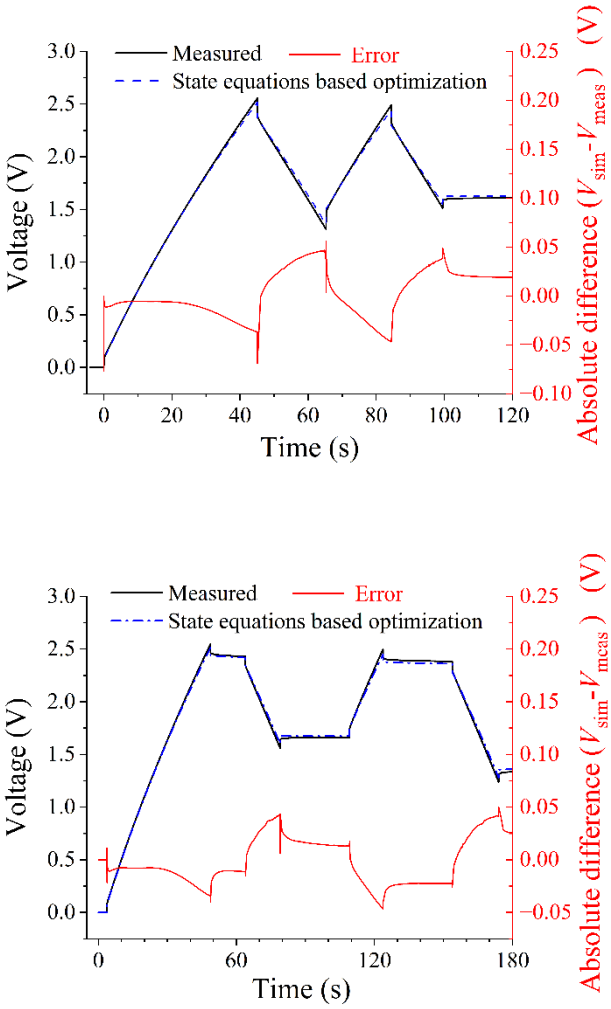

Figure 4.10. Comparison between the SC voltage computed and measured for a) a first sequence and b) a second sequence with stand-by phases. The absolute discrepancies between measured and computed results ('error') are also shown in red.

4.10 Discussion

In this chapter a method to accurately identify the three-branch equivalent circuit of SCs is proposed. Specifically, the novel technique for the determination of the variable leakage resistance presented in Sect. 2.2.3 is merged here with a SC ECM based on a three-branch circuit. A new method for the identification of the circuit based on the state equations has been presented and discussed. The parameters of the SC ECM are identified through an optimization approach which is based on the CTRR algorithm which minimized the difference between the measurements and the model giving as output the circuit parameters, except R_{lea} and the *ESR* that are identified offline.

Also, the sensitivity of the circuit parameters to the terminal voltage is discussed. It is interesting to notice how resistive and capacitive parameters have a sensitivity of different signs. The optimization of the circuit parameters is achieved by minimizing the differences between measured and simulated voltage terminals., The difference in sign of the sensitivities allows shaping the circuit response and therefore tuning the voltage at the terminals in order to obtain an excellent minimization of the difference between measurements and model..

The most important advantage of this approach is an improved accuracy of the model and its validity for a wide time span, even for days. Models presented in literature usually show an error that increases versus time even after one hour of self-discharge. Even for long stand-by phases continuing for a few days, high accuracy is guaranteed.

Chapter 5

Uncertainty assessment of SCs equivalent circuit parameters

5.1 Introduction

The identification of an equivalent circuit through measurements is not a trivial process. Although many studies have discussed the ability of a model to reproduce a SC voltage terminal, there are not many references describing the evaluation of uncertainty in the determination of the parameters, including repeatability.

The novelty of the study presented in this chapter is the proposal of an effective and general method for evaluating the uncertainty in the determination of circuit parameters, which has been validated for two- or three-branch models [12]. The results reported here have been preliminarily published in the papers [124], [125].

This chapter is organized as follows. Sect. 5.2 highlights how same relative variations of each circuit parameter have a different effect on the voltage at the SC terminals. Sect. 5.3 discusses the uncertainty term due to the repeatability of the measurements. Finally, Sect. 5.4 discusses the uncertainty terms obtained from the measurements which are necessary for identification, and an overall assessment of the uncertainty in the estimation of the circuit parameters is carried out.

5.2 Quantities of interest

The considered ECM in this study is the three-branch model described in Sect. 4.3. This analysis is done for discharges shorter than two hours; hence, the leakage resistance is assumed as constant here.

The variation of each of the parameters of this ECM has a different effect on the terminal voltage in terms of the amplitude and time span. An estimation of the parameter variation effect can be obtained by sensitivity analysis, which is not limited to the three-branch model analyzed here.

In a *n*-branch SC model, the voltage at the terminals can be expressed as:

$$u(t) = f(P_1, P_2, \dots, P_k, i(t)) \tag{5.1}$$

where $u(t)$ is the time behavior of the terminal voltage, $i(t)$ is the time behavior of the current, P_1, P_2…, P_k are the generic parameters which here are the circuital parameters in Fig. 4.2.

If a specific function of the measured current $i_m(t)$ is considered, the sensitivity of the output $u(t)$ can be analytically or numerically evaluated as a function of every parameter. The sensitivity parameters can be computed by the equivalent circuit described in Sect. 4.3. choosing a charge-self-discarge reference curve, by imposing a parameter variation ∂P_j (ΔP in a discrete approach) and checking the voltage terminal variation $\partial u(t)$ (Δu(t) in a discrete approach).

The sensitivity is defined as

$$S_{P_j}(i_m(t), t) = \frac{\partial u(t)}{\partial P_j} = \frac{\partial f(P_1, P_2, \dots, P_k, i_m(t))}{\partial P_j} \tag{5.2}$$

In a discrete approach, by imposing a parameter variation $\Delta P_j = \alpha_j P_j$, where $-0.1 \leq \alpha_j \leq 0.1$, the sensitivity can be expressed as

$$S_{P_j}(i_m(t), t) = \frac{\Delta u(t)}{\Delta P_j} = \frac{\Delta u(t)|_{\alpha_j P_j}}{\alpha_j P_j} \tag{5.3}$$

where $S_{P_j}(i_m(t), t)$ is the absolute sensitivity owing to the absolute parameter variation. The sensitivity to the relative change of parameter P_j can be written as

$$S_{R,P_j}(i_m(t), t) = \frac{\Delta u(t)|_{\alpha_j P_j}}{\frac{\alpha_j P_j}{P_j}} \tag{5.4}$$

With respect to the previous chapter, where absolute sensitivity was considered, the main advantage of the sensitivity to the relative change of parameter P_j is the immediate comparability among the different parameters (5.4).

5.2 Quantities of interest

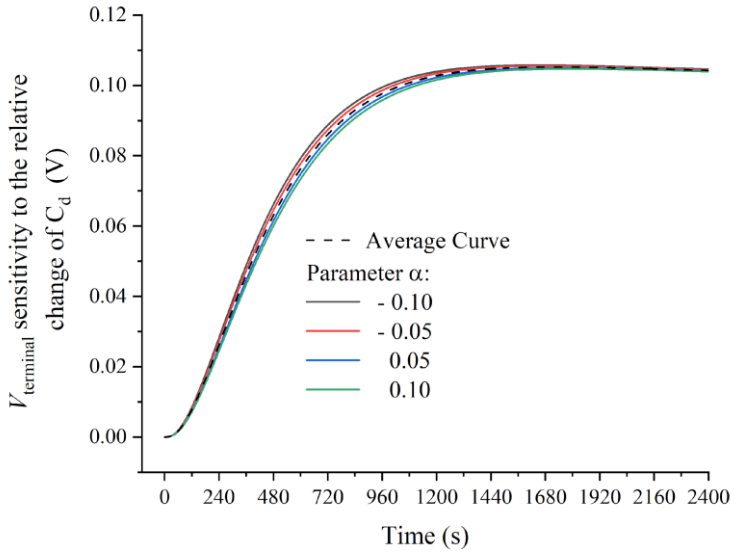

Figure 5.1. Computed time behavior of the sensitivity of relative change of the parameter C_d for 400 F SC.

Because the behavior of a SC is nonlinear, the sensitivity analysis also shows nonlinearity, although to a limited extent. Fig. 5.1 shows the sensitivity related to the parameter C_d for imposed variations of the parameter equal to ± 5 % and ± 10 %. As can be seen, the curve has a slight drift when changing the parameter variation from -10 % to +10 %. In the following, the average sensitivity curve, which is highlighted in the same diagram for C_d, is referenced without losing analysis generality.

Fig. 5.2 and Fig. 5.3 compare the relative sensitivities of all the parameters. As the S_R of C_{i0} and C_{i1} is approximately one order of magnitude higher than that of the others, it has been reported in a separate diagram (Fig. 5.2).

The S_R of the leakage resistance is nearly negligible, less than 0.012 V, and has not been reported because this parameter is determined offline using a separate method [12].

As already mentioned in Chapter 4, it can be noted that the S_R of the resistance parameters have the opposite sign to that of the capacitances, which allows the equivalent circuit to obtain excellent measurement fitting.

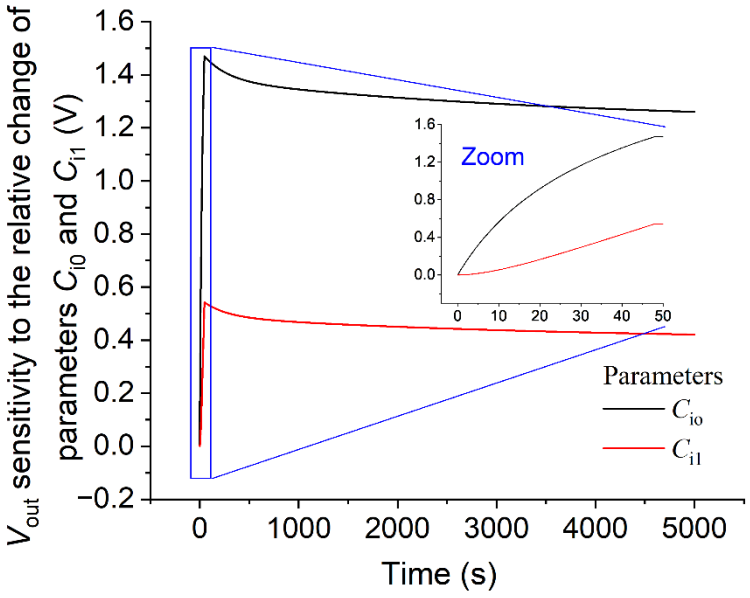

Figure 5.2. Computed time behavior of the sensitivity to the relative change of parameters C_{i0} and C_{i1} (400 F SC).

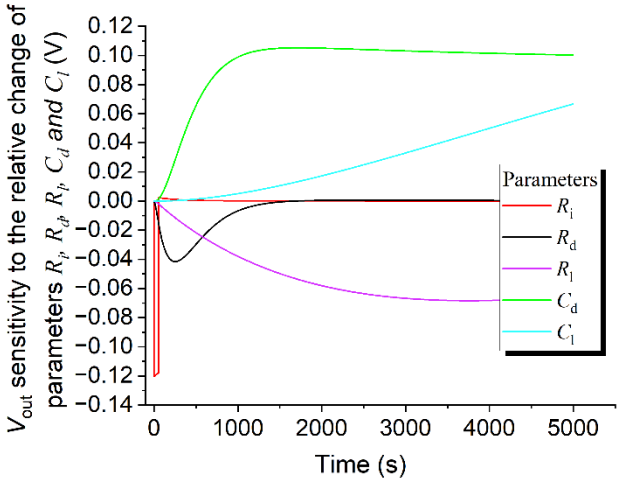

Figure 5.3. Computed time behavior of the sensitivity to the relative change of parameters R_i, R_d, R_l, C_d and C_l, (400 F SC).”

Table 5.1 lists the maximum sensitivity values and normalized percentage values to the relative change of various parameters. These values will be useful in the discussion on Sect. 5.3.

Table 5. 1. Sensitivity to the relative change of the 7 circuital parameters for 400 F SC. This table provides the absloute deviation of the terminal voltage over time caused by the relative variation of the parameters (± 10%).

	C_{i0}	C_{i1}	C_d	C_l	R_i	R_d	R_l
$\lvert S_{R\_max}\rvert$ **(V)**	1.470	0.543	0.105	0.067	0.120	0.041	0.068
Norm. $\lvert S_{R\_max}\rvert$ **%**	100	36.9	7.1	4.6	8.1	2.8	4.6

5.3 A method to speed-up the repeatability assessment

Starting from a set of charge and self-discharge cycles, with at least $(m+1)$ measured behaviors of the current and voltage $i_m(t)$ and $u_m(t)$ at the SC terminals, where m > k and k is the number of electrical parameters, one can choose a specific measurement as a reference $u_{ref}(t)$, for example, the one closest to the mean behavior. For every measurement set, we define the voltage difference function as follows:

$$u_j(t) = u_j(t) - u_{ref}(t).$$

Considering n time samples t_1, t_2, …, t_n for every measurement set, expressing the set of variations in matrix form, we obtain

$$\begin{bmatrix} \Delta u_1(t_1) & \dots & \Delta u_m(t_1) \\ \dots & \dots & \dots \\ \Delta u_1(t_n) & \dots & \Delta u_m(t_n) \end{bmatrix} =$$

$$\begin{bmatrix} S_{P_1}(i_m(t_1), t_1) & \dots & S_{P_k}(i_m(t_1), t_1) \\ \dots & \dots & \dots \\ S_{P_1}(i_m(t_n), t_n) & \dots & S_{P_k}(i_m(t_n), t_n) \end{bmatrix} \times \begin{bmatrix} \Delta P_{11} & \dots & \Delta P_{1m} \\ \dots & \dots & \dots \\ \Delta P_{k1} & \dots & \Delta P_{km} \end{bmatrix} \quad (5.5)$$

that is:

$$\Delta \boldsymbol{u} = \boldsymbol{S}_P \cdot \Delta \boldsymbol{P} \quad (5.6)$$

where Δu is the matrix containing the voltage-difference functions in the columns, S_P is the sensitivity matrix, and ΔP is the parameter variation for every measurement set, which is unknown in this investigation.

The optimal circuit parameters P_0 can be estimated only for the reference curve (single measurement) according to the method described in the previous chapter.

Table 5. 2. Parameters and variations for 100, 400, 1500 F SCs.

Param	**Param. Value** P_0	**Averaged variation** ΔP_{avg}	**Standard deviation** σ_{P_rea}	**Param.Percent.variation** ***PPV*** **/ %**
100 F				
R_i **(mΩ)**	7.46	-0.38	0.25	7.06
C_{i0} **(F)**	48.5	0.38	0.24	0.98
C_{i1} **(F)**	12.18	0.02	0.12	1.97
R_d **(Ω)**	6.52	0.67	0.84	23.37
C_d **(F)**	4.71	-0.33	0.22	10.05
R_l **(Ω)**	262.8	3.30	18.7	14.05
C_l **(F)**	3.09	0.25	0.19	11.38
400 F				
R_i **(mΩ)**	8.28	-0.069	0.062	1.51
C_{i0} **(F)**	260.0	-0.51	0.72	0.55
C_{i1} **(F)**	36.83	0.29	0.34	1.83

R_d (Ω)	11.13	0.028	0.42	7.53
C_d (F)	13.60	0.062	0.61	8.92
R_l (Ω)	249.3	-0.51	15.49	12.4
C_l (F)	12.08	0.38	1.22	19.58
1500 F				
R_i (mΩ)	1.00	-0.004	0.002	0.40
C_{i0} (F)	1352.6	-0.17	0.43	0.06
C_{i1} (F)	224.84	0.32	0.25	0.22
R_d (Ω)	42.53	0.17	0.41	1.92
C_d (F)	27.10	0.01	0.16	1.18

The distribution of the parameters around the optimal ones can be computed by repeating the voltage measurements, as follows.

$$\Delta \boldsymbol{u}(t) = \boldsymbol{S}_{P_1}(i_m(t), t) \cdot \Delta \boldsymbol{P}_1 + \cdots + \boldsymbol{S}_{P_k}(i_m(t), t) \cdot \Delta \boldsymbol{P}_k \qquad (5.7)$$

By applying the least-squares principle [126] we can derive the parameter variations for the set of measurements as follows.

$$\Delta \boldsymbol{P} = (\boldsymbol{S}_P^T \cdot \boldsymbol{S}_P)^{-1} \cdot \boldsymbol{S}_P^T \cdot \Delta \boldsymbol{u} \qquad (5.8)$$

where, for a specific test current, the sensitivity and matrix $(\boldsymbol{S}_P^T \cdot \boldsymbol{S}_P)^{-1} \cdot \boldsymbol{S}_P^T$ are computed only once.

Table 5.2 presents the analysis of the parameter variability for the three considered SCs. Eq. (5.8) provides a variability vector for each parameter whose distribution, as shown in Fig. 5.4 for the parameters R_d and C_d, tends toward a

Gaussian distribution. According to "Evaluation of measurement data — Guide to the expression of uncertainty in measurement" [93] for analyzing the frequency distribution of the observations or measurements, at least 10 observations or measurements are needed and the given frequency distribution in Fig. 5.4, is based on the data acquired from 20 charge and self/discharge cycles.

The average parameter variability, P_{avg} is presented in Table 5.2. The percentage parameter variation (PPV) defined as

$$PPV = \frac{2\sigma_{P\_rea}}{P_0 + P_{avg}} \cdot 100 \tag{5.9}$$

Where σ_{P_rea} is the standard deviation owing to repeatability; PPV and σ_{rea} are included in Table 5.3.

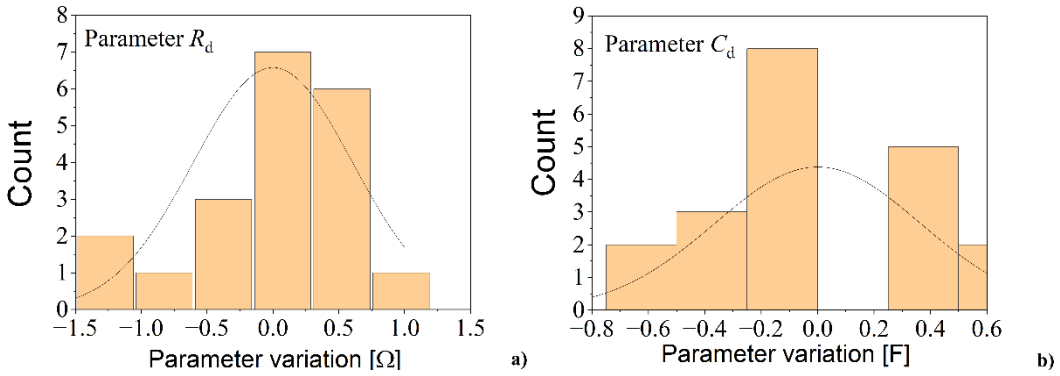

Figure 5.4. Frequency distribution obtained for the 400 F SC circuital parameters a) R_d and b) C_d, with 20 charge and self-discharge cycles.

Table 5. 3. Product $|S_{R_max}|\cdot$PPV.

SC	R_i	C_{i0}	C_{i1}	R_d	C_d	R_l	C_l
400 F	0.18	0.81	0.99	0.31	0.94	1.49	1.31

5.3.1 Discussion on repeatability

It is interesting to compare the results in Table 5.2 with Table 5.1 and Fig. 5.2 and Fig. 5.3. The parameter C_{i0}, which shows the highest S_{Rmax} at the terminal voltage, has the lowest PPV variation. The parameter C_{i1}, which has an S_{Rmax} about one third of C_{i0}, has a PPV of about three times. The other parameters, which have an S_{Rmax} less than one tenth of that of C_{i0}, have a PPV that is about an order of magnitude

higher. In general, it can therefore be stated that the parameters that show a higher PPV have a lower sensitivity, and vice versa. Table 5.3 shows how the product $|S_{R\_max}|$·PPV produces results of the same order of magnitude, which means that parameters with different percentage variations owing to repeatability produce comparable maximum variations in the SC terminal voltage. This means that all the components of the equivalent circuit contribute to the definition of the terminal voltage during the charge and self-discharge process. It is also interesting to note that the variability of the parameters decreased as the SC size increased, as shown in Fig. 5.5.

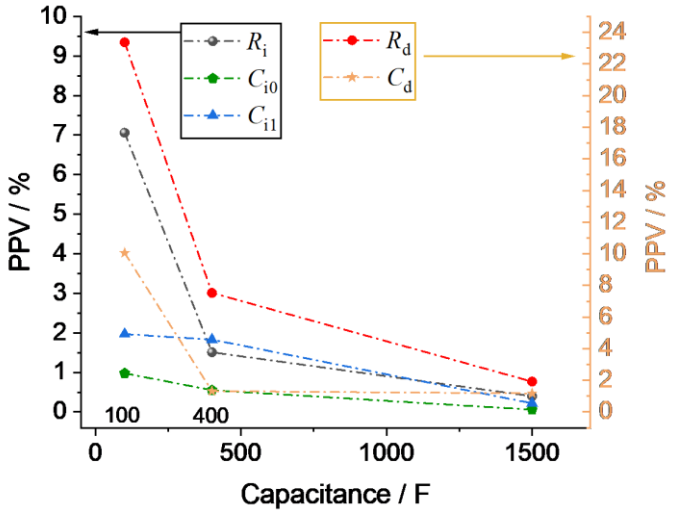

Figure 5.5. Parameter percentage variation versus the SC size.

5.4 Uncertainty evaluation

To obtain the value of the overall uncertainty, it is important to emphasize that the data acquisition system and current sensor used for this application have been calibrated before being used. The calibration of PXIe 4461 was obtained for both the voltage and current channels with a Fluke 5730A calibrator with a maximum expanded uncertainty of 45 μV under static conditions, considering a rectangular distribution.

First, several amplitudes ranging from 0 to 3.6 V were generated by the calibrator and acquired by the acquisition board. Starting from the experimental data, a first-order curve fit was identified with an associated Root Mean Square Error (RMSE) lower than 200 μV. The curve obtained was adopted for systematic error compensation when performing the measurements. For each measurement

point, the associated uncertainty u_{vms} was determined by considering the uncertainty of the calibration and the RMSE.

5.4.1 Uncertainty contribution of the measuring system

5.4.1.1 Current Measurement.

The inaccuracies of the instrumentation used for the voltage and current measurements contributed to the uncertainty in the determination of the equivalent circuit parameters. The uncertainty related to the measurement of the current generated by the current generator can be evaluated for both the two currents $i_{ch}(t)$ and $i_{s\_dis}(t)$ (charge and self-discharge currents, respectively), the uncertainties of which can be considered as a first approximation, constant in both periods, and uncorrelated. Because the discharge part is self-discharge, the current is generated by SC internal phenomena, the generator circuit is open in this phase, and the generated current is equal to zero. This self-discharge current is two or three orders of magnitude lower than the charging current. The current measurement uncertainty u_{i_ch} was estimated during sensor calibration to be lower than 100 µA/A, which includes the uncertainty of the PXI acquisition card. From the variations of the charging current ΔI_{ch} set equal to the absolute variation corresponding to the measurement uncertainty versus time, it is possible to evaluate the variations of the resulting voltage at the terminal of the SC as u_{cur}, which is the vector of the variation of the terminal voltage at each time instant obtained from the two or three-branch circuit model, by applying an excitation current variation equal to ΔI_{ch}. The variation of the parameters P_{cur} is obtained from the maximum current variation ΔI_{ch} as

$$\boldsymbol{P}_{cur} = \left|\left(\left(\boldsymbol{S}_P^T \cdot S_p\right)^{-1} \cdot \boldsymbol{S}_P^T\right)^T \cdot \Delta \boldsymbol{u}_{cur}\right| \tag{5.10}$$

The results in the parameter variation estimation are shown in Table 5.4.

5.4.1.2 Voltage Measurement

For the uncertainty of the voltage measuring system during the charging and self-discharging cycles, we do not know the exact behavior of the error as a function of time, which would be necessary to determine the variation in the circuit parameters. However, we only know its uncertainty as a function of the voltage. Different approaches can be used to evaluate the uncertainty correctly.

- A calculation with a statistical evaluation that would require some assumptions regarding the correlation of the error at different time instants.
- Hypothesizing a series of values related to the instrumentation error function, reported as time functions, and then evaluating the distribution of the circuit parameter variations, as for the repeatability (Sect. 5.3).
- A third possibility, that certainly maximizes the effect of the error, is the one considered below, which uses the maximum absolute variation of the voltage error function, after the correction of the systematic effects of the instrumentation, as a function of time (point by point).

From the maximum error at any time instant, the maximum variation of each parameter can be evaluated using the absolute values of the matrix elements:

$$\boldsymbol{P}_{vms} = \left|((\boldsymbol{S}_P^T \cdot \boldsymbol{S}_P)^{-1} \cdot \boldsymbol{S}_P^T)\right| \cdot |(\boldsymbol{u}_{vms})| \quad (5.11)$$

Where P_{vms} is the module of the maximum value of the parameter variations due to the voltage measurement system (subscript *vms*), and $|(u_{vms})|$is the maximum absolute value of the voltage error due to the measurement system as a function of time.

5.4.2 Overall uncertainty

In Table 5.4, we report the average parameter values for each SC as the parameter values identified with the model corrected by the average value obtained from the repeatability analysis (Table 5.2). The overall uncertainty is also added for each SC, which includes the following contributions: i) the repeatability standard deviation $\sigma_{P_{rea}}$, ii) the parameter variation due to a maximum current variation corresponding to the current uncertainty, computed according to Eq. (5.10), and iii) the maximum parameter variation due to voltage uncertainty related to the measurement system ΔP_{vms} computed according to Eq. (5.11).

Table 5. 4. Overall uncertainty.

Param.	Average param. Value	Standard deviation due to repeatab.(Table 5.2)	Param. max. variation due to current uncert. Eqn. (5.10)	Max. param. variation due to voltage uncert. Eqn. (5.11)	Overall expanded uncert. (k=2)
100 F	$P_0+\Delta P_{avg}$	σ_{P_rea}	**ΔPcur**	**ΔPvms**	**U_P**
R_i (mΩ)	7.08	0.25	0.01	0.04	0.50
C_{i0} (F)	48.9	0.24	0.01	0.06	0.49
C_{i1} (F)	12.2	0.12	0.02	0.03	0.24
R_d (Ω)	7.19	0.84	0.19	0.20	1.71
C_d (F)	4.38	0.22	0.02	0.05	0.44
R_l (Ω)	266.1	18.7	3.12	2.97	37.73
C_l (F)	3.34	0.19	0.02	0.12	0.41
400 F	$P_0+\Delta P_{avg}$	σ_{P_rea}	***ΔPcur***	***ΔPvms***	***U_P***
R_i (mΩ)	8.21	0.062	0.01	0.02	0.13
C_{i0} (F)	259.5	0.72	0.08	0.24	1.47
C_{i1} (F)	37.12	0.34	0.01	0.11	0.69
R_d (Ω)	11.16	0.42	0.88	0.17	1.33
C_d (F)	13.66	0.61	0.30	0.11	1.27
R_l (Ω)	248.8	15.49	8.11	16.15	37.35

C_l (F)	12.46	1.22	3.05	3.90	6.22
1500 F	$P_0+\Delta P_{avg}$	σ_{P_rea}	$\Delta Pcur$	$\Delta Pvms$	U_P
R_i (mΩ)	0.996	0.002	0.001	0.01	0.01
C_{i0} (F)	1352.43	0.43	0.19	0.97	1.43
C_{i1} (F)	225.16	0.25	0.03	0.36	0.65
R_d (Ω)	42.7	0.41	0.06	0.84	1.27
C_d (F)	27.11	0.16	0.04	0.35	0.52

The overall expanded uncertainty comes from the composition of the three terms as follows.

$$U_P = k \cdot \sqrt{(\sigma_{P\_rea})^2 + \left(\frac{\Delta P_{cur}}{\sqrt{3}}\right)^2 + \left(\frac{\Delta P_{vms}}{\sqrt{3}}\right)^2} \quad (5.12)$$

The results are summarized in Table 5.4.

5.5 Discussion

The method for the uncertainty evaluation presented in this chapter is general but is here applied to a three-branch and a two-branch circuit identified by a charge and self-discharge cycles. The analysis highlights several aspects.

- The uncertainty arising from the limited repeatability of the measurements influences parameters C_{i0} and C_{i1}, which largely describe the charging phase. In this case, the expanded uncertainty is ≤ 2 %, < 1.9 %, and < 0.3 % for the 100 F, 400 F, and 1500 F SCs, respectively. The uncertainty of the measurement system has little weight in the charging phase: < 0.2 %, < 0.2 %, and < 0.1 % for the 100 F, 400 F, and 1500 F SCs, respectively.

- The charging behavior is mainly influenced by parameters C_{i0} and $C_{i1\ but}$ changes due to the initial and the peak voltage drops on the *ESR*. The overall expanded uncertainties for parameter R_i are: ≤ 7 %, ≤ 1.5 %, and ≤ 1.2 %, for the 100 F, 400 F, and 1500 F SCs, respectively. The uncertainty of the measurement system is, also in this case, lower than the ones due to repeatability. Even though R_i overall uncertainty is higher than that of the other charging parameters, its terminal voltage sensitivity is significantly lower (see Figs. 5.2 and 5.3).
- The self-discharge in the initial phase is largely governed by the parameters R_d and C_d, which extend their influence for minutes in smaller capacitors or tens of minutes in larger capacitors. In this case, the uncertainty in the determination of the parameters is ≤ 24 %, < 12 %, and ≤ 3 % for the 100 F, 400 F, and 1500 F SCs, respectively, whereas the instrumental uncertainty is ≤ 2.2 %, ≤ 6 %, and ≤ 1.4 % for the three SCs, respectively. For these parameters, even a small bias (order of 1 mV) related to instrument uncertainty has a significant influence on the identification results. The positive outcome is that for these parameters the sensitivity with respect to the voltage at the terminals is reduced (see Fig. 5.3).
- The effect of the bias is even more important in the identification of the parameters R_l and C_l. The uncertainty, term coming from the instrumentation, is of the same order of magnitude than the repeatability term, and even bigger for the 400 F SC. The overall uncertainty of the two parameters R_l and C_l is < 15 % and ≤ 12 %, respectively, for the 100 F SC and, ≤ 15 % and < 50 % respectively, for the 400 F SC. In this last case (400 F), the overall uncertainty mainly depends on the bias arising from the instrumental uncertainty and is possibly due to the incomplete charge of the capacitance C_l during the considered charging time.

5.6 Conclusion

The SC capacitance is treated by manufacturers as a constant quantity, while it is a parameter depending on voltage. Moreover, the datasheet delivered by the manufacturers provides only a few data. As an example, at room temperature, for the 400 F SC Eaton declared a capacitance tolerance of – 5 % to + 10 %, while SPS CAP for the 1500 F declared a capacitance tolerance of – 10 % to + 20 %. Apart from the series resistance, manufacturers do not provide the circuit parameters of the SC and provides just the capacitance, the energy/energy density of the SC, the nominal and maximum current values, the rated voltage, the useful life cycles and little else.

5.6 Conclusion

In other words, the data provided by manufacturers are fine for a rough sizing of storage systems but are not sufficient to implement SCs in complex applications.

As mentioned before, the availability of SC equivalent circuits is useful for the modeling of SCs in complex electronic circuits often with batteries. SCs have to cope with fast charging and discharging phases (e.g. in electric vehicles during break and accelerations, in PV panel, in UPS) and they must be controlled by systems which drive the source or the load on the SC instead of the battery. These CMSs (Charge Management Systems) are an extension of the battery management systems (BMS) and, to work properly, they need to control the SC using an equivalent circuit model. The parameters of the ECM must be identified accurately, and the uncertainty of such parameters must be estimated.

This chapter provided clear knowledge about parameters assessment and uncertainty estimation and provides guidance on how to go beyond the raw datasheet values to implement SCs in complex devices for applications, particularly in synergy with batteries.

Chapter 6

Conclusion and future work

This thesis contributed to better defining repeatable and accurate measurements on EDLCs and provided a new identification procedure of a three-branch ECM. Moreover, this work proposes a method for the calculation of the uncertainty of the circuit parameters and defines a new measurement method for the assessment of the nonlinear leakage resistance.

This work introduced the following accomplishments:

- An efficient training to increase the repeatability of the DUTs;
- A new parameter identification method is introduced based on the state equations with reference to the three-branch model. After optimizing the acquired parameters with CTRR algorithm, which is suitable to optimize the nonlinear equations, the maximum error between the measured and simulated voltage-time behavior of our DUTs remained below 50 mV in voltage peak and below 5 mV in the rest of the self-discharge phase. It is worth to mention the identified ECM shows constant difference between the measured and the simulated voltage with time, while in the existing ECMs in the literature the error increases with self-discharge time;
- A nonlinear voltage-dependent leakage resistance measured by a two-step experiment. With this parameter the ECM is able to mimic the real behavior of the SC in long self-discharges even after many days. For example, for a 400 F SC the discrepancy in terms of terminal voltage between the measurements and the simulated identified ECM after more than 6 days of self-discharge was found below 50 mV.

- a general method in order to assess the ECM parameter uncertainty starting from a single model identification and a limited number of repeated measurements. Such a method provides a reliable estimation of the parameter's uncertainty taking into account both, instrumental uncertainty and repeatability.

Such achievements contributed to the publications:

- Zucca, M., Hassanzadeh, M., Conti, O., & Pogliano, U. (2023). Accurate Parameters Identification of a Supercapacitor Three-Branch Model. *IEEE Access*, vol. 11, pp. 122387-122398, 2023, DOI: 10.1109/ACCESS.2023.3328803
- M. Zucca et al., (2024) "MetSuperCap: Metrology for static and dynamic characterisation of supercapacitors", *Measurement: Sensors*, 101434, https://doi.org/10.1016/j.measen.2024.101434
- M. Zucca, M. Hassanzadeh, D. Signorino and U. Pogliano (2024), "Measurement Repeatability of a Supercapacitor Equivalent Circuit Parameters," *2024 Conference on Precision Electromagnetic Measurements (CPEM)*, Denver, CO, USA, 2024, pp. 1-2, DOI: 10.1109/CPEM61406.2024.10645978.
- M. Zucca *et al.*, "The project 'Metrology for Static and Dynamic Characterization of Supercapacitors' – MetSuperCap," *2024 Conference on Precision Electromagnetic Measurements (CPEM)*, Denver, CO, USA, 2024, pp. 1-2, DOI: 10.1109/CPEM61406.2024.10646148.
- M. Zucca, M. Hassanzadeh, D. Signorino and U. Pogliano (2025) "Uncertainty Evaluation of a Supercapacitor Equivalent Circuit Parameters," in *IEEE Transactions on Instrumentation and Measurement*, DOI: 10.1109/TIM.2025.3544362

6.1 Perspectives and future work

There is still a lot of room for further studies on the characterization of SCs. To contribute to a deeper understanding of this device, our research is going on and in the next steps, our focus will be on the objectives as follows.

- To extend the model versus temperature as the temperature strongly affects the behavior, lifetime, efficiency and other parameters of SCs and it seems crucial to consider the temperature effect in the model.

- Performing analysis with Electrochemical Impedance Spectroscopy.
- The extension of the model to fit the EIS analysis is also another important goal.
- To correlate the ECM parameter variation to *SoC* and *SoH* in order to improve predictive maintenance and control of SCs.
- To extend the models for other types of SCs like SC banks and hybrid SCs.

Appendix A

Review of International Standards

A.1 International standard IEC 62391-1:2022

International standard IEC 62391-1 named as “Fixed electric double-layer capacitors for use in electric and electronic equipment” covers fixed electric double-layer capacitors, also known as capacitors, which are primarily utilized in DC circuits of electrical and electronic devices [71].

For use in sectional and detailed specifications of electronic components for quality assessment or any other purpose, this section of IEC 62391 specifies standard terminology, inspection protocols, and test methodologies. The main parts of this standard are mentioned in this section.

A.1.1 Measuring equipment:

According to this standard the accuracy of the measuring equipment should be equal to or less than $\pm 1\%$ to measure the current and voltage. The power supply should be able to charge the capacitor with constant current and 95 % efficiency. For the DC voltage recorder, the sampling rate of 100 ms or less and 5 mV resolution is required.

A.1.2 Measurement of capacitance and internal resistance by constant current discharge

To calculate the capacitance and the internal resistance by this method, the capacitor should be charged and discharged with constant current.

A.1.2.1 Classification of the capacitors according to capacitance and internal resistance

To choose the suitable measuring conditions for the capacitor, they are classified into five groups according to their capacitance and internal resistance which defines their application class. It is worth mentioning that the same discharge current condition can be appropriate for all five classes, but this classification is made in order to obtain the best accuracy in measurement.

Table A.1: Classification of the capacitors according to their capacitance and internal resistance.

Class Number	Application	Capacitance	Internal resistance
Class 1	Memory backup	Low	High
Class 2	Energy storage	High	No consideration
Class 3	Power	High	Low
Class 4	Instantaneous power	Low	Low
Class 5	High power	High	Low

For both of the classes 3 and 5, high capacitance and low internal resistance are needed. But class 5, which is suitable for high power applications like automotive and railway, requires higher capacitance and lower internal resistance than the capacitors in class 3 which are mostly suitable for driving motors. In Fig. A.1, the data given in table A.1 can be seen.

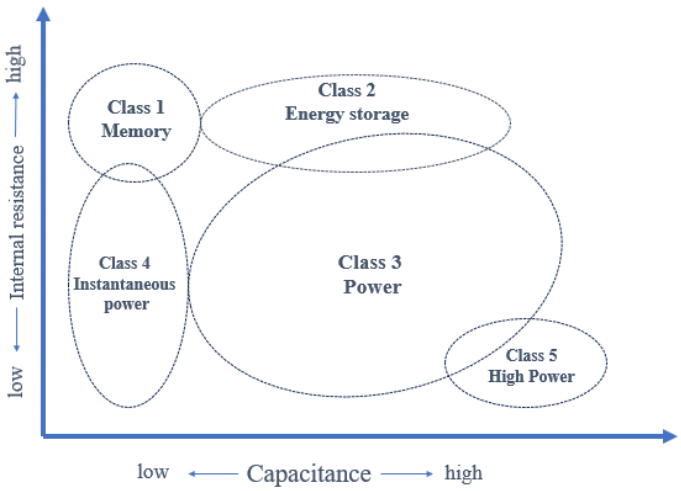

Figure A.1: Capacitors classification in terms of their *ESR* and capacitance [71]

A.1.2.2 Measuring procedure

The measurement shall be done to capture and analyze the voltage-time behavior of the capacitor, and the voltage means the voltage between the two terminals of the capacitor. Two measuring methods with sets of measuring conditions are defined in this section of the standard as methods 1-A and 1-B, and the suitable method for each capacitor should be chosen according to its application classification which is summarized in Table A.1.

The measuring procedure is the same for both methods, but the measuring conditions are different. The measuring procedure is specified as follows for these two methods:

a) The constant current should be used to charge the capacitor.
b) The charging of the capacitor should be continued with constant voltage when the power supply reaches its specified voltage value.
c) The capacitor should be discharged with a constant current.
d) The time from the beginning of the discharge to the point that the capacitor terminal voltage reaches U_1 and U_2 should be measured. (U_1 and U_2 are defined in the following sections).

According to the standard, in both measuring methods, for the discharge current values of less than 10 A, the calculated values should be presented in one digit, and the second digit should be rounded down. And for discharging currents more than 10 A, two digits are needed for the calculated values and the third digit should be rounded down.

A.1.2.3 Measuring methods

Measuring method 1A

The constant charging current can be calculated by $I_{CC} = \frac{U_R}{38R_N}$ in which U_R is the rated voltage and R_N is the nominal internal resistance and should be able to charge the capacitor with the charging efficiency of 95 %. The constant discharge current corresponds to the nominal capacitance.

In this method, which includes classes 1 to 4, the measurement conditions should be as given in Table A.2.

Table A.2: Measuring conditions for measuring method 1-A.

Measuring conditions	Class 1	Class 2	Class 3	Class 4
Constant current charging (mA)	95 % charging efficiency	95 % charging efficiency	95 % charging efficiency	95 % charging efficiency
Constant voltage charging time (min)	30	30	30	30
Constant discharging current for capacitance measurement (mA)	C_N	$0.4C_N$	$4C_N$	$40C_N$
Constant discharging current for *ESR* measurement (mA)	$10C_N$	$4C_N$	$40C_N$	$400C_N$
U_1	$0.8U_R$	$0.8U_R$	$0.8U_R$	$0.8U_R$
U_2	$0.4U_R$	$0.4U_R$	$0.4U_R$	$0.4U_R$

Measuring method 1B

In this method the constant charging current is calculated the same as method 1A ($I_{CC} = \frac{U_R}{38R_N}$), but the constant discharge current is different and is calculated by ($I_d = \frac{U_R}{40R_N}$) and it should be able to discharge the capacitor by 95 % discharging efficiency.

This method includes classes 3 to 5, and the measuring conditions for this method shall be as given in Table A.3.

Table A.3: Measuring conditions for measuring method 1-B.

Measuring conditions	Class 1	Class 2	Class 3	Class 4
Constant current charging (mA)	95 % charging efficiency	95 % charging efficiency	95 % charging efficiency	95 % charging efficiency
Constant voltage charging time (min)	5	5	5	5
Constant current discharging	95 % charging efficiency	95 % charging efficiency	95 % charging efficiency	95 % charging efficiency
U_1	$0.8U_R$	$0.8U_R$	$0.8U_R$	$0.8U_R$
U_2	$0.4U_R$	$0.4U_R$	$0.4U_R$	$0.4U_R$

As can be seen, classes 3 and 4 exist in both methods 1A and 1B.

A.1.3 Methods for calculating capacitance

According to the standard, two methods for calculating capacitance are defined. The first is based on the straight-line approximation method and the second is the energy conversion method and the equations are as follow:

A.1.3.1 Calculating the capacitance with straight line approximation method

$$C = \frac{I_d(t_2 - t_1)}{U_1 - U_2} \quad \text{(A.1)}$$

In which:

C is the capacitance of the capacitor (F)

I_d is the discharge current (A)

U_1 is the starting voltage of the voltage window (V)

U_2 is the final voltage of the voltage window (V).

t_1 is the time at which the terminal voltage of the capacitor reaches the U_1after the discharge starts (s).

$\boldsymbol{t_2}$ is the time at which the terminal voltage of the capacitor reaches the $\boldsymbol{U_2}$ after the discharge starts (s)

A.1.3.2- Calculating the capacitance with energy conversion method

$$C = \frac{2w}{U_1^2 - U_2^2} \quad \text{(A.2)}$$

in which:

w is the measured energy in joule, from the starting voltage (U_1) to the final voltage (U_2) of the voltage window.

A.1.4 Methods for calculating internal resistance

For calculating the internal resistance of the capacitor, also two methods are defined in this standard which are as follows.

A.1.4.1 Calculating the internal resistance of the capacitor with intersection line method

With this method the internal resistance of the capacitor can be calculated with the following equation:

$$R = \frac{\Delta U_3}{I_d} \quad \text{(A.3)}$$

in which:

R is the *ESR* of the capacitor (Ω).

I_d is the discharge current of the capacitor (A).

ΔU_3 is the voltage drop (V), which is obtained by extending the straight part of the terminal voltage curve of the capacitor, by an auxiliary line, shown in Fig. A.2.

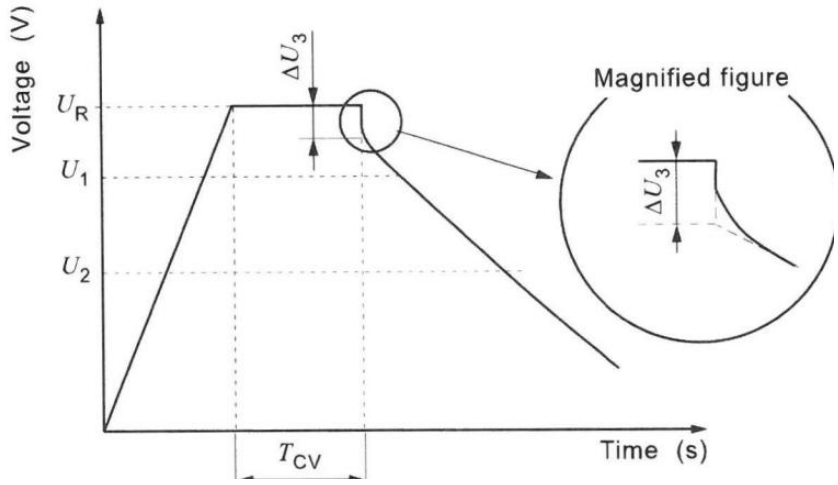

Figure A.2: Voltage-time behavior of capacitor terminals in capacitance and internal resistance measurements [71].

A.1.4.2 Calculating the internal resistance of the capacitor with the least square method

The equation for calculating the internal resistance of the capacitor with this method is the same as Eq. (A.3), and the difference is in the definition of ΔU_3 .In this equation, ΔU_3 is obtained by the straight-line approximation from U_1 to U_2 (which are calculation start and final voltages) by least squares method. The ΔU_3 is the difference of the intercept voltage value of this straight line at the beginning of the discharge time and the voltage that was set for the constant voltage charging in volt.

A.1.5 Method 2 for calculating capacitance and internal resistance.

A.1.5.1 Constant resistance charging for capacitance calculation.

The measuring circuit for this method is as shown in Fig. A.3.

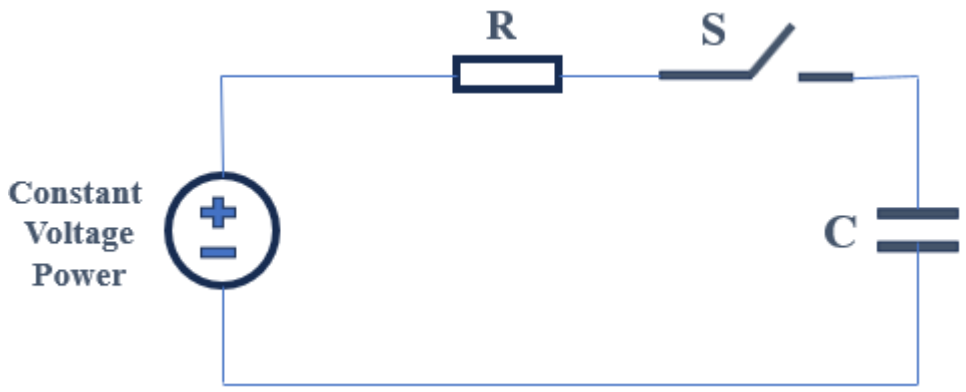

Figure A.3: Circuit for constant resistance charging method.

Before starting the measurement, capacitors should be discharged completely, and the value of the resistance should be selected in a range that as a result of that the time constant τ be in the range of 60 to 120 seconds. When the voltage U_R is applied, the time constant τ should be measured and the capacitance can be calculated according to Eq. (A.4):

$$C = \frac{\tau}{R} \qquad \text{(A.4)}$$

in which C is the capacitance (F), τ is the time constant (s), and R is the ESR (Ω).

A.1.5.2 AC method for measuring internal resistance

The measuring circuit for this method is as shown in Fig. A.4.

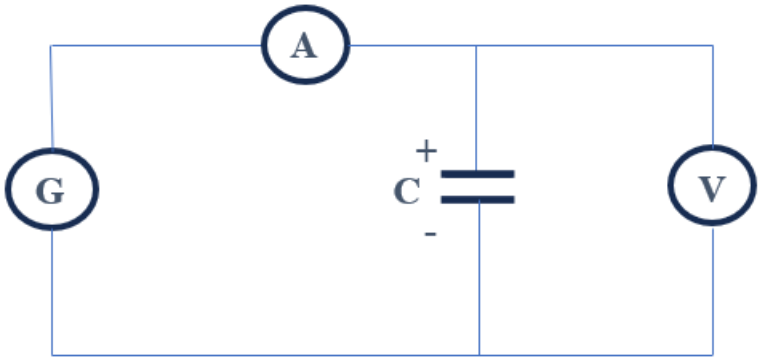

Figure A.4: Circuit for AC resistance method.

The measurement should be done with the frequency of 1KHz, and the current range from 1 mA to 10mA. The internal resistance can be calculated according to Eq. (A.5):

$$R_a = \frac{U}{I} \tag{A.5}$$

in which R_a is the internal resistance of the capacitor (Ω), and $U(V)$, $I(A)$ are the rms values of the ac voltage and current respectively.

A.1.6 Test conditions

It is mentioned in this standard that the atmospheric condition for all tests should be according to IEC 60068-1:2013, 4-3. Which can be summarized as follows:

- Temperature range: 15 to 35 C
- Relative humidity: 25 % to 75 %
- Air pressure 86 kPa to 106 kP

A.2 International Standard IEC 62391-2

IEC 62391-2 is called “Fixed electric double-layer capacitors for use in electronic equipment part 2: Sectional specification- Electric double layer capacitors for power applications”. This standard specifically covers the third Class of the measurement classification given in IEC 62391-1, which requires discharge currents between mA and A and includes high capacitance and low internal resistance [72] (see Table A.1).

A.3 International Standard IEC 62576

The purpose of this standard is to establish preferred ratings and characteristics, select the appropriate quality assessment procedures, tests, and measuring methods from IEC 62391-1, and provide specifications for the performance of this kind of capacitor.

A.2.1 Measuring the capacitance and *ESR*

The measurement method for calculating the capacitance and the *ESR* are the same as mentioned in IEC 62391-1 (see A.1.3 and A1.4. respectively) the only difference is that in this standard it is mentioned that the ambient temperature for these measurements should be $20℃ \pm 2℃$.

A.2.2 Calculation of power density

As a calculation method of power density, some steps are defined in this standard as follows.

- Step1: Calculating the *ESR* in accordance with IEC 62391-1 (see A.1.4.1).
- Step2: Calculating the discharge current value (equation $I = \frac{\Delta U_3}{R_d}$)(see Fig. A.2).
- Step3: Calculating the power density per mass by Eq. (A.6).

$$P_d = \frac{1}{2}(U - \Delta U_3 + U_e) \times \frac{I}{m} = \frac{(0.12\frac{U^2}{R_d})}{m} \quad \text{(A.6)}$$

in which power density per mass is shown with P_d (W/kg), Rd is the internal resistance in ohm, U is the rated voltage (V), ΔU_3 is the voltage drop (V), U_e is the 40 % of the rated voltage (V), I is the discharge current (A), and the capacitor weight (kg)is shown with m. By substituting the capacitor's volume for its mass, the same equation can be used to determine the power density per volume.

A.3 International Standard IEC 62576

According to the international standard IEC 62576 called “Electric double-layer capacitors for use in hybrid electric vehicles — Test methods for electrical characteristics”, both automakers and capacitor suppliers will benefit from standard evaluation and testing techniques to expedite the development and reduce the cost of such capacitors. Considering this, this standard establishes a framework that

facilitates the growing market for large capacity capacitors and electric cars while also offering fundamental and minimal requirements for electrical characteristic testing procedures [73].

According to this standard the accuracy of the measuring equipment should be equal to or less than $\pm 0.1\%$ to measure the current and voltage. The power supply should be able to charge the capacitor with constant current and 95 % efficiency. For the DC voltage recorder, the sampling rate of 10 ms or less and 5mV resolution is required.

According to IEC 62576, the capacitor can be used for tests, only if the number of completed cycles falls within the range that the customer and the manufacturer agreed upon, the capacitance is still more than 80 percent of the initial value, the internal resistance is less than 150 percent of its initial value and there is no obvious damage or electrolyte leakage.

A.3.1 Preconditioning and test procedure

Preconditioning is defined in this standard for the test which is as follows:

The capacitors must be fully charged and discharged prior to measurement, and they must then be incubated for two to six hours at room temperature or as directed by the relevant standards. If required, charging and discharge can be repeated until internal resistance and capacity are stable. This repetition can be done for example up to ten times like this:

- Step 1) discharge completely
- Step 2) charge to rated voltage
- Step 3) discharge to (0.5 rated voltage)
- Step 4) repeat steps 2 and 3 ten times.

After preconditioning and setting up the test equipment, the test procedure is introduced as follows:

- Constant current charging up to the rated voltage (with a constant charging current of $I_{CC} = \frac{U_R}{38R_N}$ in which R_N is capacitor's nominal internal resistance).
- Constant voltage charging at rated voltage for 300 s (this duration is 30 minutes in IEC 62391).

A.3 International Standard IEC 62576

- Constant current discharging down to 0.4 rated voltage (constant discharging current of $I_{dC} = \frac{U_R}{40R_N}$).

A.3.2 calculating the capacitance

The method for calculating the capacitance in this standard is in accordance with Eq. (A.2) which is based on the "energy conversion capacitance method" and introduced in IEC 62391. The only difference in defining this method for these two standards is the value of U_1 and U_2. In this standard U_1 is defined as $(0.9U_R)$ and U_2 is defined as $(0.7U_R)$.

A.3.4 calculating internal resistance

The method introduced in this standard to calculate the internal resistance of the capacitor is "Least square internal resistance calculation method" which is described in section A.1.4.2.

A.3.5 calculating the maximum power density

The name of this computation method is "matched impedance power density method" and the equation for calculating the maximum power density of the capacitor is defined as follows

$$P_{dm} = \frac{0.25U_R^2}{Rm} \quad \text{(A.7)}$$

Where P_{dm} is the maximum power density of the capacitor (W/kg or W/l), U_R is the rated voltage (V), R is the calculated internal resistance (Ω), and m is the capacitor's mass or volume (kg or l).

A.3.6 Calculating energy efficiency

The constant current charging and discharging method will be used to perform the energy efficiency test. The test preconditioning is like the one mentioned in section A.3.1, and after the preconditioning and the test equipment setup, the test procedure to calculate energy efficiency is as follows:

- Constant current charging ($I_{CC} = \frac{U_R}{38R_N}$), up to the half of the rated voltage $(0.5U_R)$.
- Constant voltage charging at $(0.5U_R)$ for 5 minutes.

- Constant current charging ($I_{CC} = \frac{U_R}{38R_N}$) from ($0.5U_R$) to U_R.
- Constant voltage charging at U_R for 10 seconds.
- Constant current discharging ($I_d = \frac{U_R}{38R_N}$) down to ($0.4U_R$).

As can be seen as a result of performing this test the voltage-time behavior and the current-time behavior of the capacitor will be as depicted in Fig. A.5.

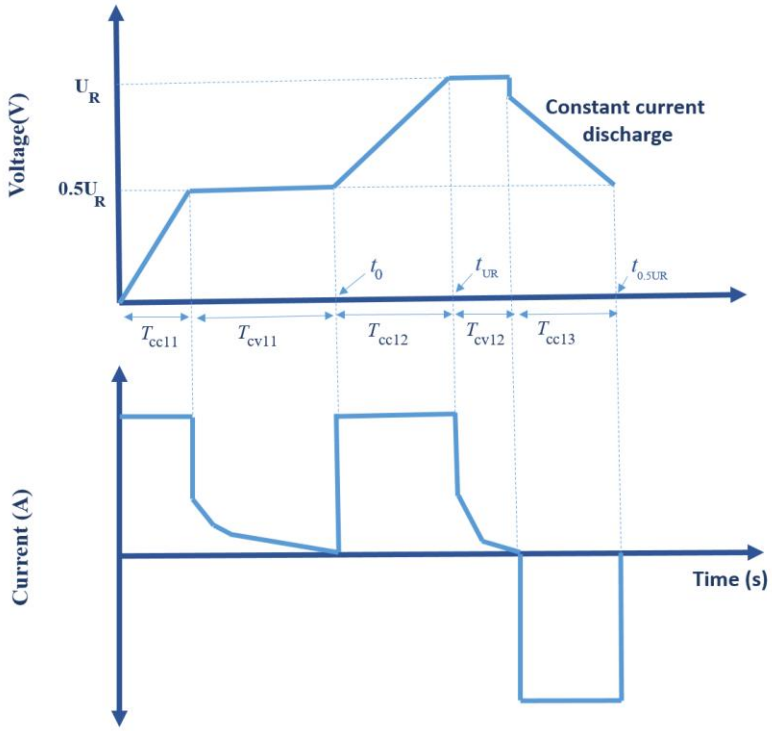

Figure A.5: Current-time and voltage-time behavior between the terminals of the capacitor in efficiency test [73].

In Fig. A.5, T_{CC11} is the duration of the constant current charging from 0 up to $0.5U_R$, T_{CC12} is the duration of the constant current charging from $0.5U_R$ to U_R, T_{CV11} is the duration of constant voltage charging at $0.5U_R$. The duration of constant voltage discharging at the rated voltage is T_{CV12}, and TCC_{13} is the constant current discharging duration (s) from U_R to 0.5 U_R.

Eq. (A.8), which is based on the voltage-time and current-time characteristics between 0.5 U_R and U_R, can be used to determine the energy efficiency E_f.

A.3 International Standard IEC 62576

$$E_f = \frac{W_d}{W_c} \times 100 \quad \text{(A.8)}$$

in which E_f is the energy efficiency in percentage, W_d electrical energy (J) that is discharged during the T_{CC13} time, and $W_c$is the electrical energy that is charged (J) during the $T_{CC12} + T_{CV12}$ interval.

W_d and W_c can be obtained by Eqs. (A.9) and (A.10) respectively.

$$W_d = \int_{t_{U_R}}^{t_{0.5U_R}} I_d U_t dt \quad \text{(A.9)}$$

$$W_c = \int_{t_0}^{t_{U_R}} I_C U_t dt \quad \text{(A.10)}$$

Appendix B

DC Calibration of the National Instruments PXI-4461 board

B.1 Description of the calibration procedure

To calibrate the acquisition system, it is needed to compare the measured values with a known reference system. The calibrator used here is Fluke 5730 A multi-product calibrator. For each voltage range, we define around 15 steps to be generated and then be compared with the data acquired by the measurement system. Each voltage step is generated with 50000 samples in one second, and is repeated 20 times to calculate the uncertainty type A. We consider a delay time of around 5 seconds, to pass the transient part and just consider the steady state. We define the expected value of the voltage and in this way the best working range for the calibration system will be chosen.

The frequency is put at zero because we are doing the DC calibration. To avoid mistakes in entering the input values and damaging the system, a limit is defined as the maximum voltage that can be generated (if the entered value is more than the limit, the generator stops automatically). The transducer parameter is the gain we want to be multiplied by the measured value to have the expected value as the output and we set it as 1.

For each voltage step, we have 20 iterations and for each iteration, the program calculates the average value of the 50000 samples; so, we have 20 values for each step. With this data, uncertainty type A can be calculated by Eq. (B.1) for each step.

$$u_A = \frac{Std\ (data)}{\sqrt{N}} \tag{B.1}$$

B.1 Description of the calibration procedure

In (B.1), *N* is the number of iterations which is 20 in our calibration process, data' is the set of average values of the 20 iterations for each voltage step.

A scale factor in the context of calibration is a numerical value as a multiplying factor used to correct or make up for measurement errors or disparities in a system, and to make sure that the calibrated output lines up with the desired reference standard or goal values [127]. Here, the scale factor is the ratio of the voltage acquired by the device under test and the voltage generated by the calibrator and can be calculated by Eq. (B.2):

$$SF = \frac{V_{in}}{V_{out}} \tag{B.2}$$

In (B.2), V_{in} is the reference voltage generated by the calibrator and V_{out} is the voltage measured by the device under test.

The uncertainty type B is related to the uncertainty of our reference system and can be acquired in the datasheet of the calibrator (Fluke 5730 A multi-product calibrator). In Table B.1, the absolute uncertainty column is divided into two timeframes which are related to the last calibration of the calibrator. So, if the calibrator is not calibrated for more than a year, we should use the data in the related column for calculating the uncertainty type B.

As given in the datasheet, the uncertainty type B for each step can be calculated by Eq. (B.3):

$$u_B = \pm(\%\ of\ output + \mu V) \tag{B.3}$$

In 1-year timeframe, the first column is related to the percentage value that should be multiplied by the output in the Eq. (B.3) and the second column is the voltage value that should be added in the Eq. (B.3) in μV.

The total uncertainty is calculated by Eq. (B.4):

$$u_C = \sqrt{u_A^2 + u_B^2} \tag{B.4}$$

Table B.1: DC voltage specification of the Fluke 5730 A multi-product calibrator.

Range	Absolute Uncertainty, tcal ± 5 °C ± (% of output + µV)				Stability 24 hours, ± 1 °C	Resolution µV	Maximum Burden [1]
	90 days		1 year		± (ppm output + µV)		
0 to 329.9999 mV	0.005	3	0.006	3	5 + 1	0.1	50 Ω
0 to 3.299999 V	0.004	5	0.005	5	4 + 3	1	10 mA
0 to 32.99999 V	0.004	50	0.005	50	4 + 30	10	10 mA
30 to 329.9999 V	0.0045	500	0.0055	500	4.5 + 300	100	5 mA
100 to 1020.000 V	0.0045	1500	0.0055	1500	4.5 + 900	1000	5 mA
Auxiliary Output (dual output mode only) [2]							
0 to 329.999 mV	0.03	350	0.04	350	30 + 100	1	5 mA
0.33 to 3.3 V	0.03	350	0.04	350	30 + 100	10	5 mA

[1] Remote sensing is not provided. Output resistance is < 5 mΩ for outputs ≥ 0.33 V. The AUX output has an output resistance of < 1 Ω.

[2] Two channels of dc voltage output are provided.

Range	Noise	
	Bandwidth 0.1 to 10 Hz p-p ± (ppm output + µV)	Bandwidth 10 to 10 kHz rms
0 to 329.9999 mV	1 µV	4 µV
0 to 3.299999 V	10 µV	50 µV
0 to 32.99999 V	100 µV	600 µV
30 to 329.9999 V	10 ppm + 1 mV	20 mV
100 to 1020.000 V	10 ppm + 5 mV	20 mV
Auxiliary Output (dual output mode only) [1]		
0 to 329.999 mV	5 µV	20 µV
0.33 to 3.3 V	20 µV	200 µV

[1] Two channels of dc voltage output are provided.

Any statistically valid data set with a normal distribution, also known as a Gaussian distribution, will produce a bell curve. The confidence in the data points within a specific standard deviation number from the mean value, is determined by the coverage factor, or "k" value.

According to the data set's mean and standard deviation, 68 % of the data points will be within one standard deviation of the mean (k=1), 95 % of them will be within two standard deviations of the mean (k=2), and 99.7 % of them will be within three standard deviations (k=3). The coverage for k=1,2,3 is shown in Fig. B.1.

Since k=1 allows a lot of room for passing false readings, it is not a threshold for reporting uncertainty that is acceptable. On the other extremity of the spectrum, k=3 truly requires an incredibly small window for passing false readings. The coverage factor for the statement of uncertainty is recorded as k=2, which represents approximately 95 % confidence (it is actually 95.4 %) [128].

B.1 Description of the calibration procedure

The total standard uncertainty (u_C) is calculated with coverage factor k=1. A number that is multiplied by the total standard uncertainty to get the expanded uncertainty is k=2 for calibration process. So, the expanded uncertainty can be calculated by Eq. (B.5).

$$U_c = ku_C \qquad (B.5)$$

In this equation, U_C is the expanded uncertainty, k is 2, and u_C is the total standard uncertainty.

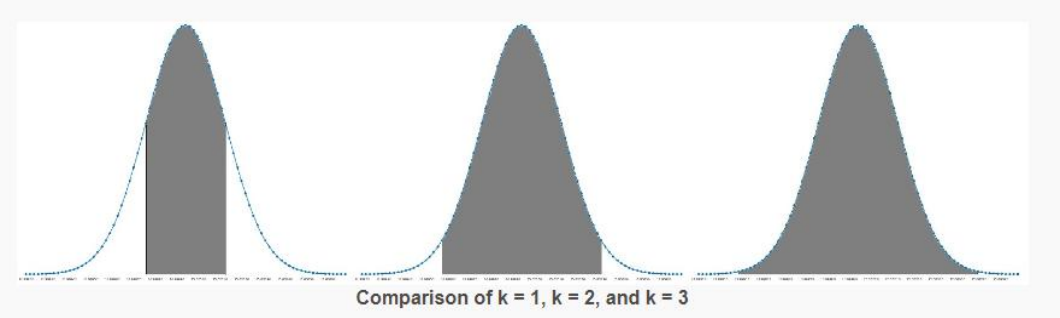

Figure B.1: Comparison of the coverage factors k=1,2,3 [128].

As a result of this calibration process for the National Instruments PXI-4461 board in the laboratory, the uncertainty below 120 ppm is obtained.

References

[1] Zucca, Mauro, et al. "MetSuperCap: Metrology for static and dynamic characterisation of supercapacitors." *Measurement: Sensors* (2024): 101434., https://doi.org/10.1016/j.measen.2024.101434

[2] Zucca, Mauro., et al. "The project 'Metrology for Static and Dynamic Characterization of Supercapacitors'–MetSuperCap." *2024 Conference on Precision Electromagnetic Measurements (CPEM)*. IEEE, 2024., Denver, CO, USA, 2024, pp. 1-2, DOI: 10.1109/CPEM61406.2024.10646148.

[3] Becker, Howard I. "Low voltage electrolytic capacitor." U.S. Patent No. 2,800,616. (1957).

[4] Miller, J. R. "The Evolution of Electrochemical Capacitor Technology: Future Performance Predictions." *Proc. 2003 International Conference on Advanced Capacitors (ICAC2003)*

[5] Miller, J. R. "A brief history of supercapacitors." *Battery+ Energy storage technology* 61 (2007)

[6] Burke, A. F., J. E. Hardin, and E. J. Dowgiallo. "Application of ultracapacitors in electric vehicle propulsion systems." *Proceedings of the 34th international power sources symposium*. IEEE, 1990.

[7] Afif, Ahmed, et al. "Advanced materials and technologies for hybrid supercapacitors for energy storage–A review." *Journal of Energy Storage* 25 (2019): 100852.

[8] Gualous, H., et al. "Experimental study of supercapacitor serial resistance and capacitance variations with temperature." *Journal of power sources* 123.1 (2003): 86-93.

[9] Torres, Jorge, et al. "Fast energy storage systems comparison in terms of energy efficiency for a specific application." *IEEE Access* 6 (2018): 40656-40672.

[10] Fletcher, S. I., et al. "The effects of temperature on the performance of electrochemical double layer capacitors." *Journal of Power Sources* 195.21 (2010): 7484-7488.

[11] Ricketts, B. W., and C. Ton-That. "Self-discharge of carbon-based supercapacitors with organic electrolytes." *Journal of power sources* 89.1 (2000): 64-69.

[12] Zucca, M., Hassanzadeh, M., Conti, O., & Pogliano, U. "Accurate parameters identification of a supercapacitor three-branch model." *IEEE Access* 11 (2023): 122387-122398., DOI: 10.1109/ACCESS.2023.3328803

[13] Khan, Humaira Rashid, and Abdul Latif Ahmad. "Supercapacitors: Overcoming current limitations and charting the course for next-generation energy storage." *Journal of Industrial and Engineering Chemistry* (2024).

[14] Chen, George Z. "Supercapacitor and supercapattery as emerging electrochemical energy stores." *International Materials Reviews* 62.4 (2017): 173-202.

[15] Moradian, Mehdi, and Kosala Gunawardane. "A Review: Supercapacitors' Suitability as an Alternative to Li-Ion Batteries in Ultra-Low Power Devices." *2022 IEEE Industrial Electronics and Applications Conference (IEACon)*. IEEE, (2022).

[16] Liu, Chunli, Qiang Li, and Kai Wang. "State-of-charge estimation and remaining useful life prediction of supercapacitors." *Renewable and Sustainable Energy Reviews* 150 (2021): 111408.

[17] Naseri, Farshid, et al. "Supercapacitor management system: A comprehensive review of modeling, estimation, balancing, and protection techniques." *Renewable and Sustainable Energy Reviews* 155 (2022): 111913.

[18] Li, Nan, et al. "SOH balancing control method for the MMC battery energy storage system." *IEEE Transactions on Industrial Electronics* 65.8 (2017): 6581-6591.

[19] Ouyang, Minggao, et al. "A dynamic capacity degradation model and its applications considering varying load for a large format Li-ion battery." *Applied energy* 165 (2016): 48-59.

[20] Feng, Xuning, et al. "Using probability density function to evaluate the state of health of lithium-ion batteries." *Journal of Power Sources* 232 (2013): 209-218.

[21] Bohlen, Oliver, Julia Kowal, and Dirk Uwe Sauer. "Ageing behavior of electrochemical double layer capacitors: Part I. Experimental study and ageing model." *Journal of power sources* 172.1 (2007): 468-475.

[22] Alcicek, G., et al. "Experimental study of temperature effect on ultracapacitor ageing." *2007 European conference on power electronics and applications*. IEEE, (2007).

[23] Chaari, Ramzi, et al. "How supercapacitors reach end of life criteria during calendar life and power cycling tests." *Microelectronics Reliability* 51.9-11 (2011): 1976-1979.

[24] Smith, A. J., et al. "Precision measurements of the coulombic efficiency of lithium-ion batteries and of electrode materials for lithium-ion batteries." *Journal of The Electrochemical Society* 157.2 (2009): A196.

[25] Miller, J. R. "Battery-capacitor power source for digital communication applications: Simulations using advanced electrochemical capacitors." *Proc. Electrochem. Soc. Conf*. Vol. 95. (1995).

[26] I. N. Varakin, A. D. Klementov, S. V. Litvienko, S. V. Starodubtsev, and A. B. Stepanov "Application of Ultracapacitors as Traction Energy Sources," Proc. *7th International Seminar on Double Layer Capacitors and Similar Energy Storage Devices*, Deerfield Beach, FL (December 8-10, 1997).

[27] Kurra, Narendra, and Qiu Jiang. "Supercapacitors." *Storing Energy*. Elsevier, 2022. 383-417.

[28] Joshi, Mahendra Chandra, and Susovon Samanta. "Improved energy management algorithm with time-share-based ultracapacitor charging/discharging for hybrid energy storage system." *IEEE Transactions on Industrial Electronics* 66.8 (2018): 6032-6043. DOI: 10.1109/TIE.2018.2871799

[29] V Bolborici, Valentin, Francis P. Dawson, and Keryn K. Lian. "Hybrid energy storage systems: Connecting batteries in parallel with ultracapacitors for higher power density." *IEEE Industry Applications Magazine* 20.4 (2014): 31-40. DOI: 10.1109/MIAS.2013.2288374.

[30] C Zhao, Chen, He Yin, and Chengbin Ma. "Equivalent series resistance-based real-time control of battery-ultracapacitor hybrid energy storage systems." *IEEE Transactions on Industrial Electronics* 67.3 (2019): 1999-2008., DOI 10.1109/TIE.2019.2901640.

[31] Mamun, Abdullah-Al, et al. "An integrated design and control optimization framework for hybrid military vehicles using lithium-ion battery and supercapacitor as energy storage devices." *IEEE Transactions on Transportation Electrification* 5.1 (2018): 239-251, DOI: 10.1109/TTE.2018.2869038.

[32] Vitan, Liviu–Danut, et al. "Supercapacitor city minibus bonded–NdFeB IPMSM propulsion system: design and system modeling methodology via a case study and laboratory experiments." *IEEE Transactions on Industry Applications* 59.2 (2022): 1405-1417., DOI: 10.1109/TIA.2022.3220500.

[33] Xun, Qian, et al. "Drive cycle energy efficiency of fuel cell/supercapacitor passive hybrid vehicle system." *IEEE Transactions on Industry Applications* 57.1 (2020), vol. 57, no. 1, pp.894-903, Jan.2021, DOI: 10.1109/TIA.2020.3035551.

[34] T. Mesbahi, P. Bartholomeüs, N. Rizoug, R. Sadoun, F. Khenfri, and P. L. Moigne, "Advanced Model of Hybrid Energy Storage System Integrating Lithium-Ion Battery and Supercapacitor for Electric Vehicle Applications," *IEEE Transactions on Industrial Electronics*, vol. 68, no. 5, pp. 3962-3972, May 2021, DOI: 10.1109/TIE.2020.2984426.

[35] A. Tani, M. B. Camara, and B. Dakyo, "Energy Management in the Decentralized Generation Systems Based on Renewable Energy—Ultracapacitors and Battery to Compensate the Wind/Load Power Fluctuations," *IEEE Transactions on Industry Applications*, vol. 51, no. 2, pp. 1817-1827, March-April 2015, DOI: 10.1109/TIA.2014.2354737.

[36] D. P. Chatterjee and A. K. Nandi, "A review on the recent advances in hybrid supercapacitors," *Journal of Materials Chemistry A*, vol. 9 no. 29, pp. 15880-15918, 2021.

[37] Gogotsi, Yury, and Reginald M. Penner. "Energy storage in nanomaterials–capacitive, pseudocapacitive, or battery-like." *ACS nano* 12.3 (2018): 2081-2083

[38] Edwards, Ian AS, Harry Marsh, and Rosa Menendez. "Introduction to carbon science". Butterworth-Heinemann, (2013).

[39] Zhang, Li Li, and X. S. Zhao. "Carbon-based materials as supercapacitor electrodes." *Chemical society reviews* 38.9 (2009): 2520-2531.

[40] Zhao, Jingyuan, and Andrew F. Burke. "Electrochemical capacitors: Materials, technologies and performance." *Energy Storage Materials* 36 (2021): 31-55.

[41] Halper, Marin S., and James C. Ellenbogen. "Supercapacitors: A brief overview." *The MITRE Corporation, McLean, Virginia, USA* 1 (2006).

[42] Kötz, Rüdiger, and M. J. E. A. Carlen. "Principles and applications of electrochemical capacitors." *Electrochimica acta* 45.15-16 (2000): 2483-2498.

[43] Cericola, Dario, and Rüdiger Kötz. "Hybridization of rechargeable batteries and electrochemical capacitors: Principles and limits." *Electrochimica acta* 72 (2012): 1-17.

[44] Pell, Wendy G., and Brian E. Conway. "Peculiarities and requirements of asymmetric capacitor devices based on combination of capacitor and battery-type electrodes." *Journal of Power Sources* 136.2 (2004): 334-345.

[45] Low, Wei Hau, et al. "Facile synthesis of graphene-Zn3V2O8 nanocomposite as a high-performance electrode material for symmetric supercapacitor." *Journal of Alloys and Compounds* 784 (2019): 847-858.

[46] Zhu, Yirong, et al. "3D interconnected ultrathin cobalt selenide nanosheets as cathode materials for hybrid supercapacitors." *Electrochimica Acta* 269 (2018): 30-37.

[47] Saikia, Binoy K., et al. "A brief review on supercapacitor energy storage devices and utilization of natural carbon resources as their electrode materials." *Fuel* 282 (2020): 118796.

[48] A. Berrueta, A. Ursua, I. S. Martin, A. Eftekhari, and P. Sanchis, “Supercapacitors: Electrical Characteristics, Modeling, Applications, and Future Trends,” *IEEE Access*, vol. 7, pp. 50869– 50896, (2019), Doi: 10.1109/ACCESS.2019.2908558.

[49] Srinivasan, Shiva Srenivasan, et al. "BLDC drive for EV application." *Journal of Physics: Conference Series*. Vol. 2007. No. 1. IOP Publishing, (2021).

[50] Mirzaeian, Mojtaba, et al. "Electrode and electrolyte materials for electrochemical capacitors." *international journal of hydrogen energy* 42.40 (2017): 25565-25587.

[51] Sharma, Priyanka, and Vinod Kumar. "Study of electrode and electrolyte material of supercapacitor." *Materials today: proceedings* 33 (2020): 1573-1578.

[52] Miller, Elizabeth Esther, Ye Hua, and F. Handan Tezel. "Materials for energy storage: Review of electrode materials and methods of increasing capacitance for supercapacitors." *Journal of Energy Storage* 20 (2018): 30-40.

[53] Shuja, Ahmed, et al. "Supercapacitors for energy storage applications: Materials, devices and future directions: A comprehensive review." *Journal of Alloys and Compounds* (2024): 176924.

[54] Forouzandeh, Parnia, and Suresh C. Pillai. "Two-dimensional (2D) electrode materials for supercapacitors." *Materials Today: Proceedings* 41 (2021): 498-505.

[55] Forouzandeh, Parnia, Vignesh Kumaravel, and Suresh C. Pillai. "Electrode materials for supercapacitors: a review of recent advances." *Catalysts* 10.9 (2020): 969.

[56] Patel, Karan Kamleshbhai, et al. "Evolution and recent developments of high performance electrode material for supercapacitors: A review." *Journal of Energy Storage* 44 (2021): 103366.

[57] Simon, Patrice, and Andrew Burke. "Nanostructured carbons: double-layer capacitance and more." *The electrochemical society interface* 17.1 (2008): 38.

[58] Béguin, François, et al. "Carbons and electrolytes for advanced supercapacitors." *Advanced materials* 26.14 (2014): 2219-2251.

[59] Simon, Patrice, and Yury Gogotsi. "Materials for electrochemical capacitors." *Nature materials* 7.11 (2008): 845-854.

[60] Miao, Ling, et al. "Recent advances in carbon-based supercapacitors." *Materials Advances* 1.5 (2020): 945-966.

[61] Liu, Chenguang, et al. "Graphene-based supercapacitor with an ultrahigh energy density." *Nano letters* 10.12 (2010): 4863-4868.

[62] Huang, Xiao, et al. "Graphene-based composites." *Chemical Society Reviews* 41.2 (2012): 666-686.

[63] Ke, Qingqing, and John Wang. "Graphene-based materials for supercapacitor electrodes–A review." *Journal of Materiomics* 2.1 (2016): 37-54.

[64] Arasi, S. Ezhil, et al. "Studies on electrochemical mechanism of nanostructured cobalt vanadate electrode material for pseudocapacitors." *Journal of Energy Storage* 41 (2021): 102986.

[65] Pramitha, A., and Y. Raviprakash. "Recent developments and viable approaches for high-performance supercapacitors using transition metal-based electrode materials." *Journal of Energy Storage* 49 (2022): 104120.

[66] Theerthagiri, Jayaraman, et al. "Recent progress and emerging challenges of transition metal sulfides based composite electrodes for electrochemical supercapacitive energy storage." *Ceramics international* 46.10 (2020): 14317-14345.

[67] Najib, Sumaiyah, and Emre Erdem. "Current progress achieved in novel materials for supercapacitor electrodes: mini review." *Nanoscale Advances* 1.8 (2019): 2817-2827.

[68] Zhong, Cheng, et al. "A review of electrolyte materials and compositions for electrochemical supercapacitors." *Chemical Society Reviews* 44.21 (2015): 7484-7539. A review of electrolyte materials and compositions for electrochemical supercapacitors - Chemical Society Reviews (RSC Publishing) DOI:10.1039/C5CS00303B

[69] Lokhande, Prasad Eknath, Umesh S. Chavan, and Abhishek Pandey. "Materials and fabrication methods for electrochemical supercapacitors: overview." *Electrochemical Energy Reviews* 3 (2020): 155-186.

[70] L. Zhang, X. Hu, Z. Wang, F. Sun, J. Deng, and D. G. Dorrell, "Multi-objective Optimal Sizing of Hybrid Energy Storage System for Electric Vehicles," *IEEE Transactions on Vehicular Technology*, (2017) vol. 67, no. 2, pp. 1027-1035, Feb. 2018, DOI: 10.1109/TVT.2017.2762368.

[71] IEC62391-1, “Fixed electric double-layer capacitors for use in electric and electronic equipment- Part 1: Generic specification”.

[72] IEC62391-2, “Fixed electric double-layer capacitors for use in electric and electronic equipment- Part 2: Sectional specification- Electric double/layer capacitors for power application”.

[73] 2018, IEC 62576, “Electric double-layer capacitors for use in hybrid electric vehicles- test methods for electrical characteristics”.

[74] Technical datasheet of Eaton TV series supercapacitors: https://www.eaton.com/content/dam/eaton/products/electronic-components/resources/data-sheet/eaton-tv-supercapacitors-cylindrical-cells-data-sheet.pdf

[75] Pholauyphon, Wasinee, et al. "Guidelines for supercapacitor electrochemical analysis: A comprehensive review of methodologies for finding charge storage mechanisms." *Journal of Energy Storage* 98 (2024): 112833.

[76] R-Smith, Nawfal Al-Zubaidi, et al. "Fast method for calibrated self-discharge measurement of lithium-ion batteries including temperature effects and comparison to modelling." *Energy Reports* 10 (2023): 3394-3401.

[77] Muzaffar, Aqib, M. Basheer Ahamed, and Chaudhery Mustansar Hussain. "Testing and measurement techniques for supercapacitors." *Smart Supercapacitors*. Elsevier, (2023(. 651-672.

[78] Laschuk, Nadia O., E. Bradley Easton, and Olena V. Zenkina. "Reducing the resistance for the use of electrochemical impedance spectroscopy analysis in materials chemistry." *RSC advances* 11.45 (2021): 27925-27936.

[79] Yang, Peihua, and Wenjie Mai. "Flexible solid-state electrochemical supercapacitors." *Nano Energy* 8 (2014): 274-290.

[80] Technical datasheet of Eaton 1 F SC: https://www.eaton.com/content/dam/eaton/products/electronic-components/resources/data-sheet/eaton-hv-supercapacitors-cylindrical-cells-data-sheet.pdf.

[81] Technical specifications of Bio-Logic: ttps://my.biologic.net/products/bcs-800-superseded/.

[82] Technical datasheet of LEM IT_65-S Ultrastab current transducer: https://4donline.ihs.com/images/VipMasterIC/IC/LEMH/LEMH-S-

A0013467573/LEMH-S-A0013795721-1.pdf?hkey=6D3A4C79FDBF58556ACFDE234799DDF0.

[83] National Instruments (NI) PXI-4461 board specification: https://docs-be.ni.com/bundle/ni-4461-4462-specs/raw/resource/enus/373770k.pdf

[84] Technical datasheet of Keysight 34470 A multimeters: https://www.keysight.com/it/en/assets/7018-03846/data-sheets/5991-1983.pdf.

[85] Technical datasheet of ITECH bidirectional programmable DC power supply IT-6000C series: https://eur.itechate.com/en/product/dc-power-supply/IT6000C.html.

[86] Technical datasheet of ITECH bidirectional programmable DC power supply IT-M3400 series: https://www.itechate.com/uploadfiles/catalogue/IT-M3400-en.pdf.

[87] Technical specification of Fluke 8588A multimeter: https://www.fluke.com/en/product/calibration-tools/electrical-calibration/bench-multimeters/8588a.

[88] Technical specification of Fluke 5730A multi-function calibrator https://www.fluke.com/en/product/calibration-tools/electrical-calibration/electrical-calibrators/5730a

[89] Technical datasheet of Eaton 400 F SC: https://www.eaton.com/content/dam/eaton/products/electronic-components/resources/data-sheet/eaton-xv%20supercapacitor-cylindrical-snap-in-data-sheet.pdf.

[90] Technical datasheet of SPSCAP SCP-STA series SC:https://spscap.de/fileadmin/Webdata/public/datenblaetter/Zellen_2_7-Volt_Technologie/SCP_STA_2.7V650-5000_20160725.pdf.

[91] D. Torregrossa, M. Bahramipanah, E. Namor, R. Cherkaoui and M. Paolone, "Improvement of Dynamic Modeling of Supercapacitor by Residual Charge Effect Estimation," *IEEE Transactions on Industrial Electronics*, vol. 61, no. 3, pp. 1345-1354, (2014), DOI: residual10.1109/TIE.2013.2259780.

[92] International Vocabulary of Metrology (VIM): JCGM 200:2012 International vocabulary of metrology - Basic and general concepts and associated terms (VIPM)

[93] Joint Committee for Guides in Metrology. (2008). Evaluation of measurement data—Guide to the expression of uncertainty in measurement. *JCGM*, *100*(2008), 1-116.

[94] Drummond, Ross, David A. Howey, and Stephen R. Duncan. "Parameter estimation of an electrochemical supercapacitor model." *2016 European Control Conference (ECC)*. IEEE, 2016.

[95] N. Ma, D. Yang, S. Riaz, L. Wang, and K. Wang "Aging Mechanism and Models of Supercapacitors: A Review," *Technologies*, (2023), vol. 11, no. 2: 38, DOI: 10.3390/technologies11020038.

[96] Zhang, Jiawei, and Minghua Chen. "Supercapacitors." *Towards Next Generation Energy Storage Technologies: From Fundamentals to Commercial Applications* (2024): 331-368.

[97] Cabrane, Zineb, and Soo Hyoung Lee. "Electrical and mathematical modeling of supercapacitors: comparison." *Energies* 15.3 (2022): 693.

[98] Mehra, Pranathi, Sahaj Saxena, and Suman Bhullar. "A Comprehensive Analysis of Supercapacitors and Their Equivalent Circuits—A Review." *World Electric Vehicle Journal* 15.8 (2024): 332.

[99] Miniguano, Henry, et al. "A general parameter identification procedure used for the comparative study of supercapacitors models." *Energies* 12.9 (2019): 1776.

[100] Zhang, Lei, et al. "A review of supercapacitor modeling, estimation, and applications: A control/management perspective." *Renewable and Sustainable Energy Reviews* 81 (2018): 1868-1878., DOI: 10.1016/j.rser.2017.05.283.

[101] Parvini, Yasha, et al. "Supercapacitor electrical and thermal modeling, identification, and validation for a wide range of temperature and power applications." *IEEE Transactions on Industrial Electronics* 63.3 (2015): 1574-1585., DOI: 10.1109/TIE.2015.2494868.

[102] Freeborn, Todd J., Brent Maundy, and Ahmed S. Elwakil., "Measurement of Supercapacitor Fractional-Order Model Parameters from Voltage-Excited Step Response*", IEEE Journal on Emerging and Selected Topics in Circuits and Systems*, vol. 3, no. 3, pp. 367-376, Sept. 2013, DOI: 10.1109/JETCAS.2013.2271433.

[103] Zhang, Lei, et al, “Fractional-order modeling and State-of-Charge estimation for ultracapacitors,” *Journal of Power Sources*, vol. 314, pp. 28-34, 2016 DOI:10.1016/j.jpowsour.2016.01.066.

[104] Prasad, Ravneel, Kajal Kothari, and Utkal Mehta. "Flexible fractional supercapacitor model analyzed in time domain." *IEEE Access* 7 (2019): 122626-122633., DOI: 10.1109/ACCESS.2019.2938543.

[105] Kumar, Mano Ranjan, Subhojit Ghosh, and Shantanu Das. "Charge-discharge energy efficiency analysis of ultracapacitor with fractional-order dynamics using hybrid optimization and its experimental validation." *AEU-International Journal of Electronics and Communications* 78 (2017): 274-280., DOI: 10.1016/j.aeue.2017.05.011.

[106] Wang, Yujie, et al. "A fractional-order model-based state estimation approach for lithium-ion battery and ultra-capacitor hybrid power source system considering load trajectory." *Journal of Power Sources* 449 (2020): 227543. vol. 449, 227543, 2020.

[107] N. Bertrand, J. Sabatier, O. Briat and J. -M. Vinassa, "Embedded Fractional Nonlinear Supercapacitor Model and Its Parametric Estimation Method," *IEEE Transactions on Industrial Electronics*, (2010) vol. 57, no. 12, pp. 3991-4000, 2010, DOI: 10.1109/TIE.2010.2076307.

[108] Dzieliński, Andrzej, Grzegorz Sarwas, and Dominik Sierociuk. "Comparison and validation of integer and fractional order ultracapacitor models." *Advances in Difference Equations* 2011 (2011): 1-15., DOI: 10.1186/1687-1847-2011-11

[109] Nelms, R. M., D. R. Cahela, and Bruce J. Tatarchuk. "Modeling double-layer capacitor behavior using ladder circuits." *IEEE Transactions on Aerospace and Electronic Systems* 39.2 (2003): 430-438., DOI: 10.1109/TAES.2003.1207255.

[110] Devillers, Nathalie, et al. "Review of characterization methods for supercapacitor modelling." *Journal of Power Sources* 246 (2014): 596-608., DOI: 10.1016/j.jpowsour.2013.07.116.

[111] Zhang, Lei, et al. "A comparative study of equivalent circuit models of ultracapacitors for electric vehicles." *Journal of Power Sources* 274 (2015): 274, pp. 899-906, 2015, DOI 10.1016/j.jpowsour.2014.10.170.

[112] Xu, Dan, et al. "Modeling of supercapacitor behavior with an improved two-branch equivalent circuit." *IEEE Access* 7 (2019): 26379-26390., DOI: 10.1109/ACCESS.2019.2901377.

[113] Faranda, Roberto. "A new parameters identification procedure for simplified double layer capacitor two-branch model." *Electric Power Systems Research* 80.4 (2010): 363-371, DOI: 10.1016/j.epsr.2009.10.024.

[114] Marín-Coca, Sergio, et al. "New parameter identification method for supercapacitor model." *IEEE Access* 11 (2023): vol. 11, pp. 21771-21782, , DOI: 10.1109/ACCESS.2023.3250965.

[115] Belachemi, F. "Modeling and characterization of electric double-layer supercapacitors used in power electronic." *Electrical Engineering, L'Institut National Polytechnique de Lorraine: France* (2000).

[116] Musolino, Vincenzo, Luigi Piegari, and Enrico Tironi. "New full-frequency-range supercapacitor model with easy identification procedure." *IEEE transactions on industrial electronics* 60.1 (2012): 112-120., DOI: 10.1109/TIE.2012.2187412.

[117] Zubieta, Luis, and Richard Bonert. "Characterization of double-layer capacitors for power electronics applications." *IEEE Transactions on industry applications* 36.1 (2000): 199-205. vol. 36 no. 1, pp. 199-205,. 2000, DOI: 10.1109/28.821816.

[118] De Carne, Giovanni, Antonio Morandi, and Shahab Karrari. "Supercapacitor modeling for real-time simulation applications." *IEEE Journal of Emerging and Selected Topics in Industrial Electronics* 3.3 (2022): 509-518., DOI: 10.1109/JESTIE.2022.3165985.

[119] Yang, Hengzhao, and Ying Zhang. "Self-discharge analysis and characterization of supercapacitors for environmentally powered wireless sensor network applications." *Journal of Power Sources* 196.20 (2011): 8866-8873.

[120] Liu, Kai, et al. "Improved study of temperature dependence equivalent circuit model for supercapacitors." *IEEE Transactions on Plasma Science* 41.5 (2013)., vol. 41, no. 5, pp. 1267-1271, May 2013, DOI: 10.1109/TPS.2013.2251363.

[121] Nikkhoo, M., E. Farjah, and T. Ghanbari. "A simple method for parameters identification of three branches model of supercapacitors." *2016 24th Iranian Conference on Electrical Engineering*

(ICEE). IEEE, 2016., pp. 1586-1590, DOI: 10.1109/IranianCEE.2016.7585774.

[122] A. R. Conn, N. I. M. Gould, P. L. Toint 'Trust region methods', *MOS-SIAM Series on Optimization*, vol. MP01, Philadelphia (USA), 2000 – Society for Industrial and Applied Mathematics (SIAM).

[123] Prasad, Ravneel, et al. "Supercapacitor parameter identification using grey wolf optimization and its comparison to conventional trust region reflection optimization." *2019 International Aegean Conference on Electrical Machines and Power Electronics (ACEMP) & 2019 International Conference on Optimization of Electrical and Electronic Equipment (OPTIM)*. IEEE, 2019.

[124] M. Zucca, M. Hassanzadeh, D. Signorino and U. Pogliano, "Measurement Repeatability of a Supercapacitor Equivalent Circuit Parameters," 2024 *Conference on Precision Electromagnetic Measurements* (CPEM), Denver, CO, USA, (2024), pp. 1-2.

[125] M. Zucca, M. Hassanzadeh, D. Signorino and U. Pogliano, "Uncertainty Evaluation of a Supercapacitor Equivalent Circuit Parameters," in *IEEE Transactions on Instrumentation and Measurement*, DOI: 10.1109/TIM.2025.3544362.

[126] M. L. Johnson, L. M. Faunt, "Parameter estimation by least-squares methods," *Methods in Enzymology*, *Academic Press*, vol. 210, pp. 1-37, 1992

[127] Deng, Zhongguang, et al. "Scale factor calibration for a rotating accelerometer gravity gradiometer." *Sensors* 18.12 (2018): 4386. vol. XVIII, no. 12, 2018.

[128] P. Castle, "Mensor Calibration Blog," [Online]. Available: https://blog.mensor.com/blog/what-does-k2-mean-in-accuracy-specification